Generating a climatology of surface solar radiation over the UK with application to wheat yield prediction

THEODOROS GKOUSAROV

A thesis submitted to the School of Environmental Sciences of the University of East Anglia in partial fulfilment of the requirements for the degree of Master in Science by Research.

University of East Anglia, School of Environmental Sciences

June 2014

Abstract

A UK climatology of daily mean Surface Incoming Shortwave (SIS) solar radiation was generated for the period 1983-2010 using a combination of satellite based data from the Climate Data Record (CDR) of SIS provided by the Climate Monitoring Satellite Applications Facility (CMSAF) and by MeteoSwiss. The combined version of these datasets has a 3km spatial resolution and it is currently the best available, long-term homogeneous satellite-based climate data record of daily surface solar radiation.

The SIS climatology enabled an investigation of UK inter-annual variability and long term trends. The impact of synoptic scale weather typing on SIS accumulations was analysed using a combination of daily satellite based data from CMSAF and daily weather types from the GrossWetterLagen classification (GWL).

Solar radiation drives photosynthesis in crops, highlighting the importance of knowing the spatial and temporal distribution of this valuable resource. Harnessing both state-of-the-art satellite based SIS estimates and model based temperature records enabled an investigation of the contributory effect of the variable radiation climate to the UK 'yield plateau' in wheat which has been widely observed over the last twenty years. Trend analyses do not support the theory that the observed yield plateau may be completely explained by solar radiation variability, since the main wheat growing area of England exhibits a general 3-5% increase of SIS accumulations during a fixed grain fill window over the 1994-2010 period. However, analysis performed to quantify the statistical relationship between SIS recorded during grain fill and actual yields from the HGCA Recommended Lists (RL) trial sites reveals encouraging results when controlling for soil type and previous crop.

Table of Contents

Abstract 3

List of Tables 7

List of Figures 8

Acknowledgements 15

List of Acronyms 17

Introduction 21

Context and motivation 21

Background - Solar radiation 22

The importance of solar radiation climate 24

Methods for estimating Surface Incoming Shortwave (SIS) solar radiation- Surface solar radiation network 27

1.1.4 Other methods for estimating surface solar radiation 28

1.1.5 Trends in Surface Incoming Shortwave (SIS) solar radiation 30

1.2 Literature review on the observed wheat yield plateau. 37

1.2.1 Wheat grain fill - background 39

1.2.2 The effect of temperature and solar radiation on grain fill 41

1.3 Hypotheses 43

1.4 Aims & Objectives 44

1.5 Thesis outline 45

2 Materials and Methods 46

2.1 Sources and data selection 46

2.2 The CMSAF Climate Data Record (CDR) data set 51

2.2.1 MVIRI Climate Data Record (CDR) SIS retrieval method 53

2.2.2 MVIRI Climate Data Record (CDR) accuracy 54
2.2.3 Stability and homogeneity of the MVIRI data set 55
2.3 The CMSAF Operational data set 57
2.4 METEOSWISS - SEVIRI Solar Surface Radiation dataset 59
2.5 CMSAF Surface Incoming Shortwave (SIS) CLARA 60
2.6 The Weather Research and Forecasting (WRF) numerical model 61
2.7 Analysis tools 63
2.7.1 CDO 63
2.7.2 McIDAS-V 63
2.8 Wheat grain yield data - Recommended Lists (RL) 64
2.8.1 Limitations 65
2.9 Weather pattern classification - GrossWetterLagen (GWL) 65
2.10 Methodology 66
3 Results and Discussion 67
3.1 Solar radiation data verification 68
3.1.1 Case study – Comparing model derived SIS against satellite based SIS total accumulations 74
3.2 Model temperature data verification 78
3.3 Satellite-based Surface Incoming Shortwave (SIS) solar radiation climatology over the UK 78
3.3 Comparisons with existing climatologies 81
3.5 Testing Hypotheses & Objectives 85
3.5.1 Inter-annual variability (1983-2010) 85
3.5.2 Trends 87
3.6 The impact of weather typing 90
3.6.1 GrossWetterLagen (GWL) 90

3.6.2 Case study - The impact of synoptic-scale weather variability on surface radiation accumulation 90

4 Grain fill climatology and wheat grain yield correlation 95

4.1 A climatology of SIS over the UK during the ‘standard’ grain fill period 96

4.2 Trends of Surface Incoming Shortwave (SIS) solar radiation during the ‘standard’ UK grain fill period. 101

4.3 The effect of temperature on grain fill duration -WRF simulations 105

4.4 Site-specific analysis of yields against grain-fill Surface Incoming Shortwave solar radiation (unadjusted and temperature-adjusted) using RL trials data 107

5 Conclusions and Recommendations 116

5.1 SIS datasets performance 116

5.2 SIS climatology over the UK 116

5.3 Synoptic weather typing and potential applications 116

5.4 Trends on SIS accumulations - quantifying the impact on yield plateau 117

5.5 Grain fill climatology - Simulating the grain fill period length. 118

5.6 SIS - Yields correlations analysis. 118

6 References 121

List of Tables

Table 2.1 Operational periods of Meteosat satellites [adapted from Posselt et al., 2013].....52

Table 2.2 Locations of BSRN stations used in the Posselt et al. (2012) validation study. [Taken from Posselt et al., 2012].....54

Table 2.3 Statistics for the comparison of daily mean SIS between the mean of all BSRN stations and CMSAF as well as ERA-Interim, GEWEX and ISCCP. From left to right columns indicate SIS source, number of days taken into account for the analysis period (nday), overall Bias (W/m^2), Mean Absolute Bias (MAB) expressed in W/m^2, Standard Deviation (SD) expressed in W/m^2 [Taken from Posselt et al., 2012].....55

Table 3.2 Comparison of the generated CLIMASIS dataset against other solar data sources. [Source: http://solargis.info/doc/119 accessed and modified 28th August 2013].....85

Table 4.2 Number of entries for fungicide treated Claire variety based on different soil types and previous crops. Green cells highlight those combinations which have more than 4 entries. The following Figures 4.10-4.13 refer to the data presented in this Table.....108

Table 4.3 Summary of the data used to correlate total SIS (MJ/m2) with yields for both 'adjusted' and 'standard' grain fill period. 113

List of Figures

Figure 1.1 a) The solar radiation spectrum at the top of the atmosphere and at the surface (Wikipedia 2013); **b**) A record of solar constant intensity based on satellite data collected since 1978 (NASA 2003). 22

Figure 1.2 a Global mean energy balance (W/m^2) of the Earth. Numbers indicate best estimates for the magnitudes of the globally averaged energy balance components together with their uncertainty ranges, representing present day climate conditions at the beginning of the twenty first century. [Figure provided by Wild et al. (2013)]; **b** The electromagnetic spectrum. 23

Figure 1.3 The process of photosynthesis in plants. The plant uses water and carbon dioxide and with the help of visible radiation creates carbohydrates (sugars) and releases oxygen. 25

Figure 1.4 Long-term monthly variability of direct and diffuse contribution to the sum of SIS throughout the year for Aberdeen, UK (**a**) and Upington, ZA (**b**). [Solargis (2013)]..... 26

Figure 1.5 a) Locations of Surface Synoptic and Metar Stations as of 20 March 2007 (NOAA 2007); **b)** Locations of Synoptic stations over the United Kingdom which record SIS as of 15 June 2012. 27

Figure 1.6 Mean daily global irradiation in MJ/m^2 for January (left) and July (right) over the averaging period 1993-2007, based on interpolation of surface station observations (Met Office 2013a)..... 28

Figure 1.7 a) Example of a Meteosat coverage area using the SEVIRI (Spinning Enhanced Visible and InfraRed Imager) radiometer. Image taken on November 03, 2013 at 11:42 UTC using the visible channel (ch01) (Weatherquest 2013); **b**) Monthly mean cloud fractional coverage for the 1982-2009 period, based on AVHRR instruments aboard polar orbiting satellites [Karlsson et al., 2013]..... 29

Figure 1.8 Linear trends (W/m^2 per decade) of the satellite-derived SIS based on the annual series from the CMSAF over Europe during the period 1994-2005.[Figure kindly provided by Sanchez-Lorenzo and Wild (2012)] 33

Figure 1.9 Linear trends (W/m^2 per decade) of the satellite-derived SIS annual series from the CMSAF over Europe during the period 1994-2005 for winter (a), spring (b), summer (c) and autumn (d) series. [Sanchez-Lorenzo and Wild (2012)] 34

Figure 1.10 Linear trends of the mean monthly series (W/m^2/decade) obtained using the 47 CMSAF and GEBA series over Europe during the period 1994-2005. [Figure provided by Sanchez-Lorenzo and Wild (2012)] 36

Figure 1.11 Wheat yields (tonnes/hectare) in Europe over the period 1961-2005 (**a**) (Clark 2013) and in the UK between 1982 and 2012 (**b**) [Knight et al., 2012] 38

Figure 1.12 Sum of surface solar radiation during 2012 expressed as a percentage of 1983-2005 average. Satellite-based data provided by CMSAF [Gkousarov et al., 2013] 39

Figure 1.13 Winter wheat crop growth stages according to the Zadoks and Feekes scales [adapted from Large (1954)] 40

Figure 2.1 The UK land surface synoptic station observation network operated by the Met Office in May 2010. [Reproduced from Met Office 2013 © Crown copyright] 48

Figure 2.2 Locations of synoptic stations over the United Kingdom which record SIS as of 15 June 2012. 49

Figure 2.3 Locations of the Baseline Surface Radiation Network (BSRN) stations. Red: operational; Blue: planned [Figure provided by MeteoSwiss (2013a)] 50

Figure 2.4 Pyranometer for measuring global radiation (MetOffice 2013b) 51

Figure 2.5 Schematic of the Magicsol retrieval algorithm [MeteoSwiss (2013b)] 53

Figure 2.6 Example of **s**triping effect as a result of the data processed from Meteosat 2 and 3. Left figure shows affected SIS data (horizontal lines) while right figure shows unaffected data. 56

Figure 2.7 Simple difference (W/m^2) for MVIRI CDR SIS minus operational SEVIRI SIS for the sum of the last four months of 2005. [Taken from Kniffka, 2012] 58

Figure 2.8 a) Map of simple difference (%) between the total sum of daily means from operational SEVIRI based SIS minus the total sum of daily means from the polar orbiting dataset CLARA for the month of June 2013. **b)** Spatial coverage of SIS retrieval from polar orbiting satellites on the 24th June 2013 (Karlsson et al. 2013). 60

Figure 2.9 WRF model domains used in simulations. The horizontal resolutions for 27,9 and 3km domains are denoted by d01, d02 and d03 respectively (Steele 2013). 62

Figure 2.10 Windows based version (1.5.5) of CDO running in a command line environment. 63

Figure 2.11 Main graphical user interface of McIDAS-V (V 1.4) in the Windows environment. 64

Figure 3.1 Correlation between the satellite retrieval method (Y axis) and surface based observations (X axis). The data are for Holbeach (52.48N 0.0E) from January 1st to December 31st 2011. Data are expressed in kJ/ m^2 /day. 68

Figure 3.2 Correlation between the WRF based model output (Y axis) and surface based observations (X axis). The data are for Holbeach (52.48N 0.0E) from January 1st to December 31st 2011. Data are expressed in kJ/m^2/day. 69

Figure 3.3 Correlation between the satellite retrieval method (Y axis) and surface based observations (X axis). The data are for Church Lawford, (52.35N 1.32W) from January 1st to December 31st 2011. Data are expressed in kJ/ m^2 /day. 69

Figure 3.4 Correlation between the WRF based output (Y axis) and surface based observations (X axis). The data are for Church Lawford, (52.35N 1.32W) from January 1st to December 31st 2011. Data are expressed in kJ/m^2/day. 70

Figure 3.5 2011 daily time series of BIAS for WRF model (blue line) and satellite estimate (red line). The data are for Church Lawford (52.35N 1.32W) for January 1st to December 31st 2011. Bias expressed in kJ/m^2/day 71

Figure 3.6 Correlation between the satellite retrieval method (Y axis) and surface based observations (X axis). The data are for Leconfield (53.52N 0.27E) from January 1st to December 31st 2003-2007. Data are expressed in kJ/ m^2 /day. 71

Figure 3.7 Total incoming shortwave solar radiation (MJ/m^2) for the period 10th June – 21st July 2012 (top left WRF model output, top right satellite based SIS). Total incoming shortwave solar radiation (MJ/m^2) for the period 10th June – 21st July 2006 (bottom left WRF model output, bottom right satellite based SIS). 75

Figure 3.8 a) Site not representative for grid cell as it contains high sub-1°-grid variability. **b**) Site representative of the 1°-grid as the spatial variability inside the grid is low. **[**Taken from Hakuba et al., (2013)**]** 76

Figure 3.9 Total accumulations of SIS for the first ten days of June 2013. Blue triangles indicate the locations of the surface based stations and the total accumulations over these ten days in these locations expressed in MJ/m^2. Values inside the grid squares indicate the total accumulations using satellite-based estimates of SIS (MJ/m^2). 77

Figure 3.10 a) Mean annual sum of SIS (MJ/m^2) based on MVIRI+SEVIRI (1983-2010) **b**) UK terrain [Taken from Withnature.co.uk (2014)] 79

Figure 3.11 Annual sum of SIS (MJ/m^2) for each year since 1983 up to 2010, based on MVIRI+SEVIRI. 80

Figure 3.12 Mean SIS daily global irradiation (MJ/m^2) for the months of January and July based on the averaging period 1983-2010. 81

Figure 3.13 Mean daily global irradiation in MJ/m^2 for January (left) and July (right) over the averaging period 1993-2007, based on interpolation of surface station observations [Met Office, 2013] 82

Figure 3.14 Average annual sum of SIS (1998-2011) on horizontal and optimally inclined surface. The map is generated by JRC including as input satellite data from CMSAF. Data values are given as kWh/m^2, but the same colour scale also represents potential solar electricity [kWh/kWp] generated by a 1 kWp system per year with photovoltaic modules

mounted at an optimum inclination and assuming system performance ratio 0.75. [Taken from PVGIS (2013); Suri et al., (2007); Huld et al., (2012)] 83

Figure 3.15 Average annual sum of SIS in kWh/m^2 (4/2004 - 3/2010) generated by Solargis including as input satellite data from CMSAF [Taken from Solargis, 2013] 84

Figure 3.16 a) P90 of the mean annual sum of SIS averaged over the period 1983-2010. **b**) Relative standard deviation of the annual sum expressed as a percentage of average over the 1983-2010 period. 86

Figure 3.17 Linear trends (W/m^2/decade) of the satellite-derived SIS based on the annual series from the CMSAF over Europe during the period 1994-2010. 87

Figure 3.18 Linear trends (W/m^2/decade) of the satellite-derived SIS annual series from the CMSAF over Europe during the period 1994-2010 for winter (**a**), spring (**b**), summer (**c**) and autumn (**d**) series. 89

Figure 3.19 a) Average daily March SIS based on 1983-2010 data; **b**) the average March SIS for all those March days (48) over the 1983-2010 record classified as experiencing the HM GWL weather type; **c**) HM GWL weather type mean sea level pressure; **d**) HM GWL weather type mean 500hPa circulation) 91

Figure 3.20 a) Average daily June SIS based on 1983-2010 data; **b**) the average June SIS for all those June days (8) classified as experiencing the WS GWL weather type; **c**) WS GWL weather type mean sea level pressure; **d**) HM GWL weather type mean 500hPa circulation. 93

Figure 3.21 Solar radiation anomalies for the weather type HM during the month of March, expressed as a percentage of average, based on the 1983-2005 period over Europe. 94

Figure 4.1 Wheat growing regions coloured by the percentage of the total region area occupied by wheat crops. [Source: Spectrumcommodities.com (2014)] 95

Figure 4.2 a) Mean sum of SIS during the 'standard' grain fill period (MJ/m^2) based on MVIRI+SEVIRI (1983-2010) **b**) UK terrain [Source: www.withnature.co.uk, 2014] 96

Figure 4.3 Mean sea level pressure pattern from ECMWF ERA Interim reanalysis data, over the June 10th – July 21st 1983-2010 period valid for 1200GMT. Contours are shown in millibars. 98

Figure 4.4 Standard deviation of SIS during the 'standard' grain fill period based on the total accumulations each individual year over the period 1983-2010. 99

Figure 4.5 Total accumulated SIS (MJ/m^2) during the 'standard' grain fill season, for each year in the period 2002-2013, based on MVIRI+SEVIRI. 100

Figure 4.6 Linear trends (W/m^2/decade) of the satellite-derived SIS based on the CMSAF dataset during **a**) the 'standard' grain fill period; **b**) the summer season (JJA) for the years 1994-2010. 102

Figure 4.7 Relative trend of SIS (%) during the grain fill season over the 1994-2010 period. 104

Figure 4.8 The duration of grain fill (days) starting on the 10th June for each year. The length of the period is estimated using 660 degree day accumulations at each individual grid point. 106

Figure 4.9 RL sites where fungicide-treated Claire winter wheat variety is grown. 108

Figure 4.10 Correlation of wheat yields (t/ha) against daily mean SIS (MJ/m^2/day) during the 'standard' grain fill period at all trial locations in the UK where Previous Crop was Winter wheat and Soil Type was Medium (n=43). R^2 = 6% and correlation coefficient = 0.25 109

Figure 4.11 Correlation of wheat yields (t/ha) against daily mean SIS (MJ/m^2/day) during the 'standard' grain fill period at all trial locations in the UK where Previous Crop is Winter rape and Soil Type is Medium (n=55). R^2 = 22% and correlation coefficient = 0.47 110

Figure 4.12 Correlation of wheat yields (t/ha) against daily mean SIS (MJ/m^2/day) during the 'standard' grain fill period at all trial locations in the UK where Previous Crop was Winter wheat and Soil Type was Deep clay (n=36). R^2 = 4.5% and correlation coefficient = 0.21 .. 110

Figure 4.13 Correlation of wheat yields (t/ha) against daily mean SIS (MJ/m^2/day) during the standard grain fill period at all trial locations in the UK where Previous Crop was Winter rape and Soil Type was Deep clay (n=37). R^2 = 17.5% and correlation coefficient = 0.42 111

Figure 4.14 Correlation of wheat yields (t/ha) against total SIS (MJ/m^2) during the 'standard' (blue) and also during the 'temperature adjusted' (red) grain fill period in Fowlmere (52.9N 0.06E) where Previous Crop was Winter rape and Soil Type was Medium (n=3). R^2 = 77% and correlation coefficient = 0.87, R^2 = 69% and correlation coefficient = 0.83.....113

Figure 4.15 Correlation of wheat yields (t/ha) against total SIS (MJ/m^2) during the 'standard' (blue) and also during the 'temperature adjusted' (red) grain fill period in Ragnall (53.25N 0.79W) where Previous Crop was Winter rape and Soil Type was Medium (n=3). R^2 = 4.6% and correlation coefficient = -0.21, R^2 = 9.3% and correlation coefficient = 0.30. 114

Acknowledgements

Thanks to Steve Dorling and Andrew Lovett for supervising this project. The utmost gratitude goes to Steve, my primary supervisor, for his continuous educational and motivational support throughout the whole study period of this project. His strong belief in my abilities was the driving force of this research, despite my own doubts at times. He managed to cover most of my questions, but most interestingly, he created many more new and for this I really owe him a lot. This Master's research would not have started due to financial barriers if it wasn't for Weatherquest Ltd who sponsored this project and provided me with employment throughout, the duration of this research for which I express my gratitude. A big thanks is also going to all my colleagues and friends at Weatherquest Ltd (Jim Bacon, Phil Garner, Chris Bell, and Steve Western) who supported emotionally and to Dan Holley and Ian Goouch for showing me the basics in NCL scripting and data visualization respectively. Thanks again to Chris Bell for arranging the catering during the development meetings where I had the chance to present some research results. Special thanks going to Christopher Steele for running the WRF simulations and providing the data used for calculating the grain fill period length. Help and support with NCL script building and debugging was also provided by Chris. He devoted time not only to help me with the scripts but also to understand how these work in every single detail.

A big thanks to Jorg Trentmann from the Climate Monitoring Satellite Applications Facility (CMSAF) for providing all the help regarding the satellite based SIS data documentation and advice on how to best use these data. Thank you also for enjoying a couple of drinks with me at the CMSAF users Workshop. Thanks to Rebekka Posselt and Reto Stockli from MeteoSwiss for providing the MSG SIS data for research purposes. Also thanks to DWD and CMSAF for supporting my trip in the Alps (Grainau) to attend the CMSAF users workshop in March 2014. Thanks goes to Paul James from DWD for kindly providing the daily GWL weather types utilized in this project. Thanks also to NIAB-TAG and HGCA for providing the RL trial data and to Haidee Philpott, Stuart Knight and Paul Gosling for helping me to understand the structure and the characteristics of the RL data. Thanks to Jim Orson for providing useful information regarding the yield plateau.

Arturo Sanchez-Lorenzo assisted by discussing his findings with me and allowing me to reproduce his figures.

All these data would be useless without the necessary hardware and software to handle it. For this I want to thank the UEA High Performance Computing Centre (HPCC) for providing access to cluster computers to store 1TB of data and the facility to run my scripts. Thanks also to Susan Jickells for teaching the module improving writing which allowed me to improve my English and my writing style. Thanks to my friends Olof Olafardotirr for proof reading the draft of the first chapter and Wildalis Carmona Marquez for inspiration. Big thanks to George Giannopoulos for teaching me the Endnote software.

Many other friends helped me to take some time to relax and enjoy this unique experience. Thanks to the UEA Hellenic Society for organizing nice Greek events to make me feel at home away from home. Thanks to the International Student Society for providing the best events in Norwich, especially the house parties. It was really great meeting you all!

I wouldn’t be here now writing this if my parents weren’t supportive of my choices. Through continuous support they spent their last savings to provide me with the opportunity to study something I always wanted. Therefore, I dedicate this thesis to my parents, and in particularly to my mom.

List of Acronyms

AVHRR	Advanced Very High Resolution Radiometer
BADC	British atmospheric Data Centre
BSRN	Baseline Solar Radiation Network
CDO	Climate Data Operators
CDR	Climate Data Record
CLARA	Cloud, Albedo and Radiation dataset (based on AVHRR instrument)
CMSAF	Climate Monitoring Satellite Applications Facility of EUMETSAT
CSP	Concentrated Solar Power plant
DEFRA	Department for Environment, Food and Rural Affairs
DJF	December, January and February calendar months
DWD	DeutchWetterDienst (German Met Service)
ECMWF	European Centre for Medium range Weather Forecasts
ERA-Interim	ECMWF ReAnalysis
EUMETSAT	European Organizations for the Exploitation of Meteorological Satellites

FAA	Flight Aviation Administration
FAPAR	Fraction of Absorbed Photosynthetically Active Radiation
GCOS	Global Climate Observing System
GEBA	Global Energy Balance Archive
GEWEX	Global Energy and Water Exchanges project
GHI	Global Horizontal Irradiance/Irradiation
GRIB	Gridded Binary
GWL	Gross Wetter Lagen synoptic pattern classification
HGCA	Home Grown Cereals Authority
HPCC	High Performance Computer Cluster at UEA
ISCCP	International Satellite Cloud Climatology Project
JJA	June, July and August calendar months
JRC	Joint Research Centre
MAB	Mean Absolute Bias
MAGIC	Mesoscale Atmosphere Global Irradiance Code
MAM	March, April and May calendar months
MFG	Meteosat First Generation
MIDAS	Met Office Integrated Data Archive System
MODIS	Moderate resolution Imaging Spectroradiometer
MSG	Meteosat Second Generation
MSLP	Mean Sea Level Pressure

MVIRI	Meteosat Visible and Infrared Imager
NAO	North Atlantic Oscillation
NCAR	National Centre for Atmospheric Research
NetCDF	Network Common Data Form
NIR	Near-Infrared wavelength
NOAA	National Oceanic and Atmospheric Administration
NRL	Naval Research Laboratory
NWP	Numerical Weather Prediction
PAR	Photosynthetically Active Radiation
PV	Photovoltaic
RL	Recommended List from HGCA
SD	Standard Deviation
SEVIRI	Spinning Enhanced Visible and Infrared Imager
SIS	Surface Incoming Shortwave solar radiation
SON	September, October and November calendar months
SSR	Surface Solar Radiation
SYNOP	Surface Synoptic Observations
TOA	Top Of the Atmosphere
UCAR	University Corporation for Atmospheric research
UEA	University of East Anglia
UKMO	UK Met Office

UV	Ultra-Violet wavelength
VIS	Visible wavelength
WMO	World Meteorological Organization
WRF	Weather Research & Forecasting model

Introduction

Context and motivation

This Masters thesis focuses on generating a climatology of Surface Incoming Shortwave (SIS) solar radiation over the British Isles using satellite and model based estimates as an input source. Daily estimates of SIS enable an investigation of the climatology of SIS during different user-specific periods in order to help understand the variability of this valuable energy resource. While alternatively using in-situ measurement data from hourly reporting surface stations might allow a more site-specific research with higher temporal granularity of measurements, the relatively sparse network density and occasional missing or corrupt data would result in a biased and incomplete SIS climatology. Therefore, the preferred approach is the use of model reanalysis data, and space-borne estimates of SIS which are interpolated over equally-spaced grid points. This ensures data availability even during periods of missing station observations resulting in a more complete climatology.

The main motivation for this study is the fact that the year 2012 exhibited much below average SIS over the United Kingdom during crucial crop growth stages. Serious concerns have been raised in the agricultural community about security of supply and price volatility, as the wheat yields from the 2012 harvest were the worst farmers have seen over the past twenty five years across the UK (Farmers Weekly 2012, Knight et al. 2012, Orson 2013). This research will build upon some of the findings from a recent desk study by Knight et al. (2012) funded by HGCA, combining winter wheat grain yields from trial sites with the total SIS intercepted during the UK grain fill period (early-mid summer).

Although the primary focus of this research has an agricultural application, the generation of a SIS climatology will inevitably also reveal valuable results for the renewable energy sector and for solar energy power plant planning in particular. Due to time constrains, this study will not however expand greatly on the various photovoltaic (PV) and concentrated solar power (CSP) technologies available.

Background - Solar radiation

The radiation density incident on a unit area at the top of Earth's atmosphere (TOA) on surface perpendicular to the sunrays is defined as the solar constant and it includes the whole range of the electromagnetic spectrum (**Figure 1.1 a**). Advanced terrestrial and satellite-based instruments have determined the annual average solar constant to be 1366.1 W/m^2 (Gueymard 2004). The World Meteorological Organization (WMO) also promotes 1367 W/m^2 as an acceptable value. The solar constant varies temporally by about 7% throughout the year, depending on the season (from 1412.0 W/m^2 in January to 1321 W/m^2 in July) as a result of variability in the Earth - Sun distance. The solar constant also varies during the eleven year sunspot cycle from 1368 W/m^2 when sunspot activity is low to 1363 W/m^2 when it is high (**Figure 1.1 b**). Variations in total solar radiation were so small that they were practically not measureable before the launch of meteorological satellites, hence the reason for the term 'solar constant'.

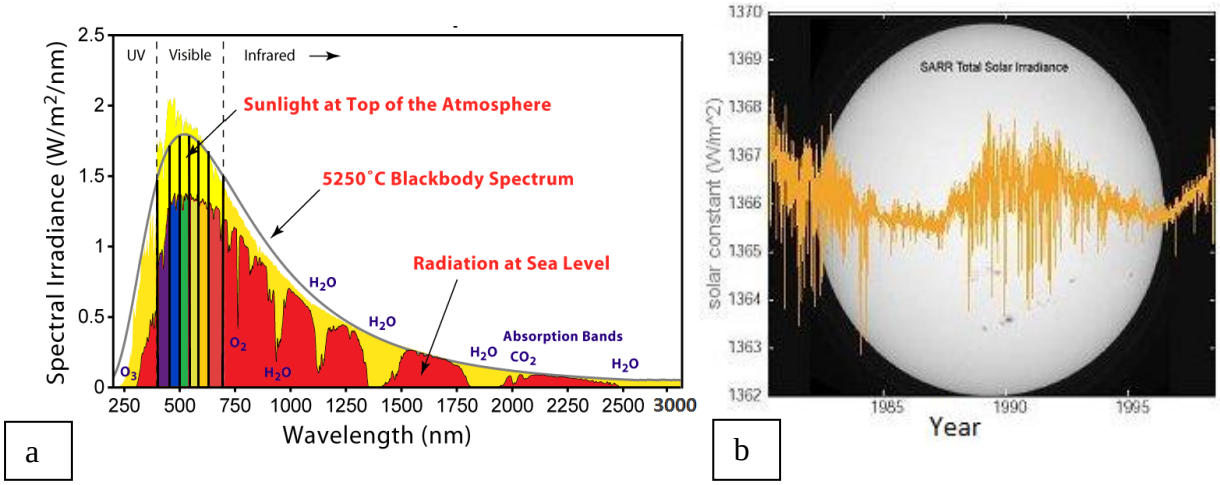

Figure 1.1 a) The solar radiation spectrum at the top of the atmosphere and at the surface (Wikipedia 2013); **b**) A record of solar constant intensity based on satellite data collected since 1978 (NASA 2003).

Out of the 1366 W/m^2 incident solar radiation energy at the top of the atmosphere (NASA, 2003), only 340 W/m^2 are in the form of visible light (wavelengths of 390 to 750 nm) and due to attenuation effects only 161 W/m^2 of visible light reaches Earth's surface on a complete clear-sky day [Wild et al. (2013); **Figure 1.2 a**]. Clouds and Earth's surface absorb this energy and because these surfaces are cooler than the sun and contain less energy, the re-emission peaks in the infrared (700 nm to 1 mm).

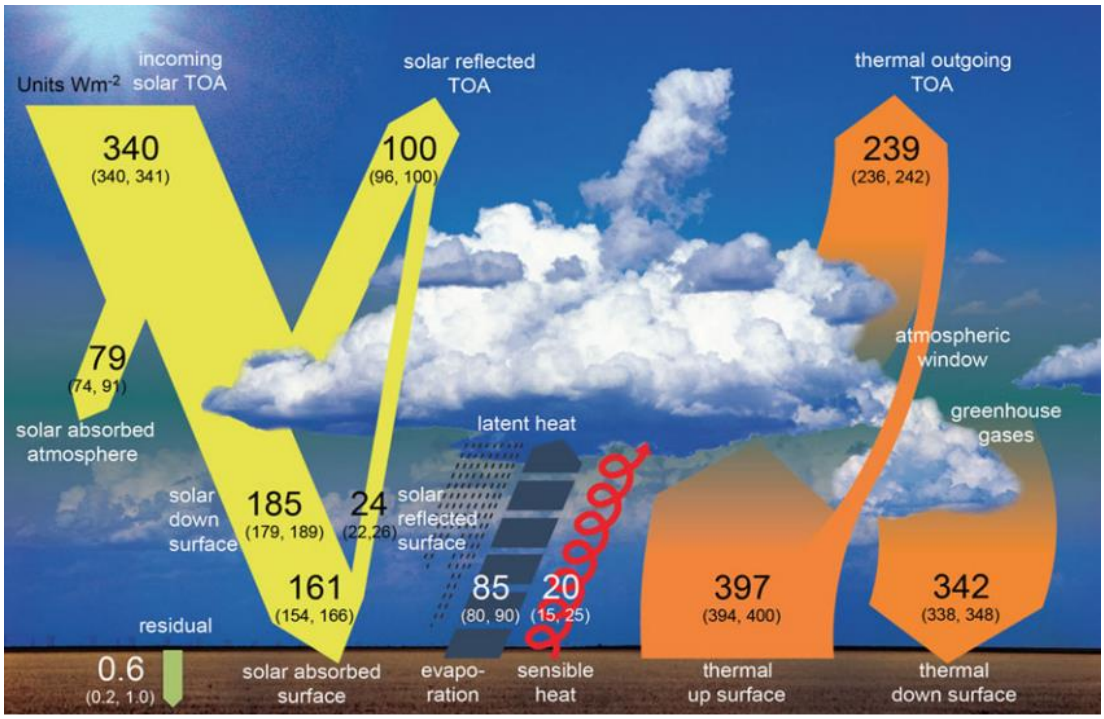

a

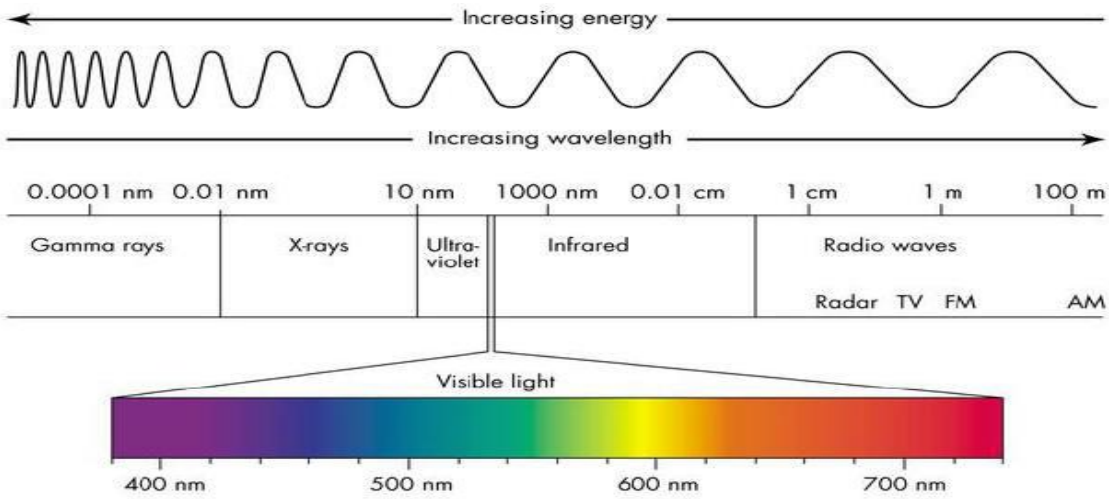

b

Figure 1.2 a Global mean energy balance (W/m^2) of the Earth. Numbers indicate best estimates for the magnitudes of the globally averaged energy balance components together with their uncertainty ranges, representing present day climate conditions at the beginning of the twenty first century. [Figure provided by Wild et al. (2013)]; **b** The electromagnetic spectrum.

The shortwave incoming solar radiation (SIS) is the radiation flux density reaching a horizontal unit area of the Earth's surface in the 200-4000 nm near-ultraviolet (UV), visible (VIS) and near-infrared (NIR) wavelength range (**Figure 1.2 b**). It is usually defined as Global Horizontal Irradiance (GHI) or Surface Solar Radiation (SSR) or Surface Incoming Shortwave (SIS) solar radiation and it is expressed in W/m^2. For the purposes of this study it is referred as SIS. The standard unit used in this research to express energy received on a unit surface per unit per time (insolation) is Mega Joules per square metre per day ($MJ/ m^2/$ day).

SIS consists of the sum of direct and diffuse components. Direct or beam radiation is the radiation directly reaching the Earth's surface from the sun. Meanwhile diffuse radiation is the radiation flux density reaching Earth's surface from various directions after it has been scattered in the atmosphere. During clear sky (cloudy) days, the direct component is higher (lower) than the diffuse. In overcast conditions the diffuse component is equal to the total global radiation.

The importance of solar radiation climate

The ultimate source of energy and life in our planetary system is solar radiation. On Earth it drives important chemical processes all the way through the atmosphere and down to the surface. The amount of radiation incident on Earth's surface is an important variable for climate monitoring (Posselt et al. 2012). The global radiation energy balance depends on the amount of incoming shortwave and outgoing longwave radiation, therefore it is important to have a robust quantitative understanding of the radiation fluxes in our system.

Estimates of the incoming and outgoing radiation fluxes are used in the model assimilation processes. A solar radiation climatology is useful in order to assess and understand past and current climate systems, examine possible trends and changes (Wild 2009), support the development of climate monitoring and forecasting models (Perez et al. 1990). The assessment of climate variability and the potential impacts can provide a basis for political decisions and infrastructure planning. Furthermore the energy from the sun strongly impacts evapotranspiration from soil and plants and has a unique impact on vegetation through all the stages of development.

Solar radiation significantly influences plants development through photosynthesis, a photochemical process which converts water and carbon dioxide into essential organic compounds (carbohydrates) using sunlight absorbed by the chlorophyll and which releases oxygen as a waste product (**Figure 1.3**). The visible portion of the solar radiation reaching Earth's surface is the most critical as it relates to photosynthetically active radiation (PAR). Plants absorb both direct beam and diffuse radiation. Usually, the upper parts of a plant receive higher contribution from the direct component, while the lower parts are subject to shading from underlying leaves therefore the direct beam is intercepted to a lower extent and rely more on the diffuse component. Of the total energy received by a crop canopy only 5% is converted into carbohydrates for biomass production (Reddy 2008). The rest are losses of energy by non-absorbed wavelengths (60%), reflection and transmission (8%), heat dissipation (8%) and metabolism (19%) part of the energy received during this stage is used during the transpiration process inside the different parts of the plant [Reddy, 2008].

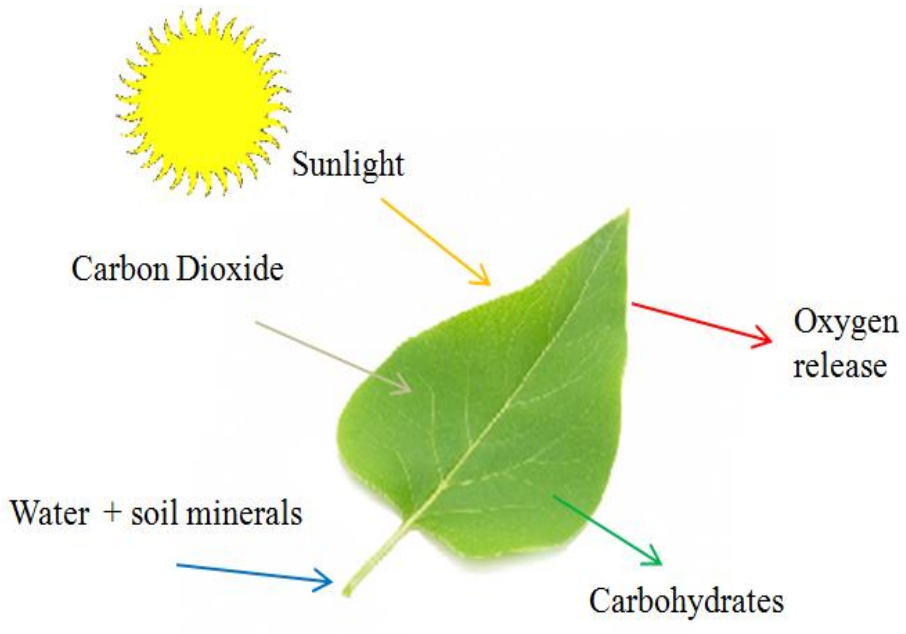

Figure 1.3 The process of photosynthesis in plants. The plant uses water and carbon dioxide and with the help of visible radiation creates carbohydrates (sugars) and releases oxygen.

Solar radiation is a well-known source of energy and has in fact been harnessed since ancient times. People build their residencies with a sun facing orientation to benefit from this free source of light and warmth. The benefits from this energy reaching the Earth's surface are numerous and many applications have been designed to take advantage of it.

The ratio between direct and diffuse radiation varies spatiotemporally and mostly depends on the location and the climatology of the area. In general, places nearer to the equator (poles) receive a higher (lower) contribution to the total sum in SIS from the direct component. For example, Aberdeen is located in the northern hemisphere (57.15^{o} N, 2.11^{o} W) and experiences an oceanic climate which leads to increased cloud cover (more scattering effect) therefore seeing a higher contribution from the diffuse part of SIS (**Figure 1.4 a**). The opposite is observed in the south African city Upington, (28.45 S, 21.24 E) which has a desert climate and experiences more clear sky days than Aberdeen leading to higher contribution from the direct portion of SIS (**Figure 1.4 b**).

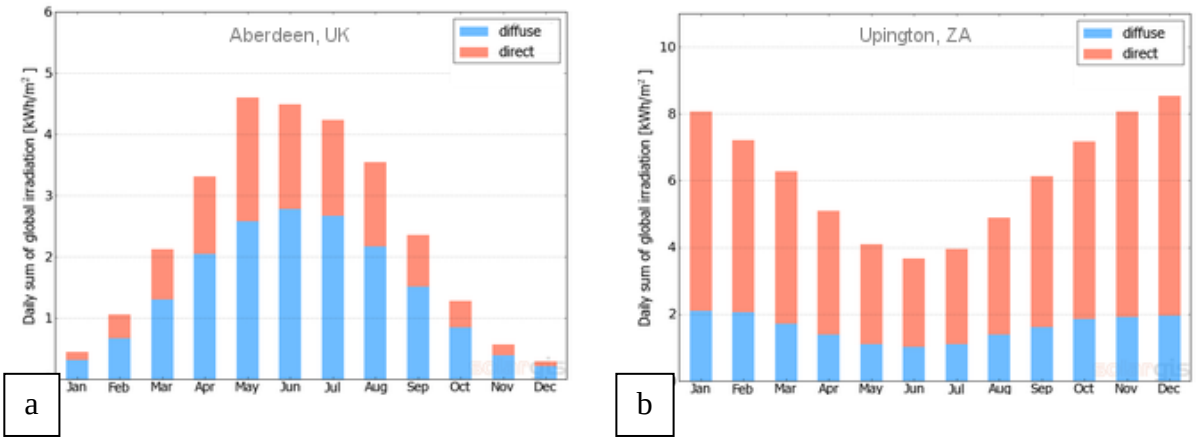

Figure 1.4 Long-term monthly variability of direct and diffuse contribution to the sum of SIS throughout the year for Aberdeen, UK (**a**) and Upington, ZA (**b**). [Solargis (2013)].

As solar radiation drives photosynthesis in plants, accurate measurements are required in order to understand the resource potential.

Methods for estimating Surface Incoming Shortwave (SIS) solar radiation- Surface solar radiation network

Despite the need for high quality homogeneous surface solar radiation data, measurements from the surface meteorological station network are not always available at each location of interest (**Figure 1.5 a**) or the network is sparse and with uneven distribution (Wild 2009). One common reason for this incompleteness in surface based measurements is the high cost of maintenance and operation [Wild, 2009]. Another issue is that even within the same network of stations utilizing the same sensors, inhomogeneities are present due to the lack of regular calibration and general maintenance (Trentmann 2013)

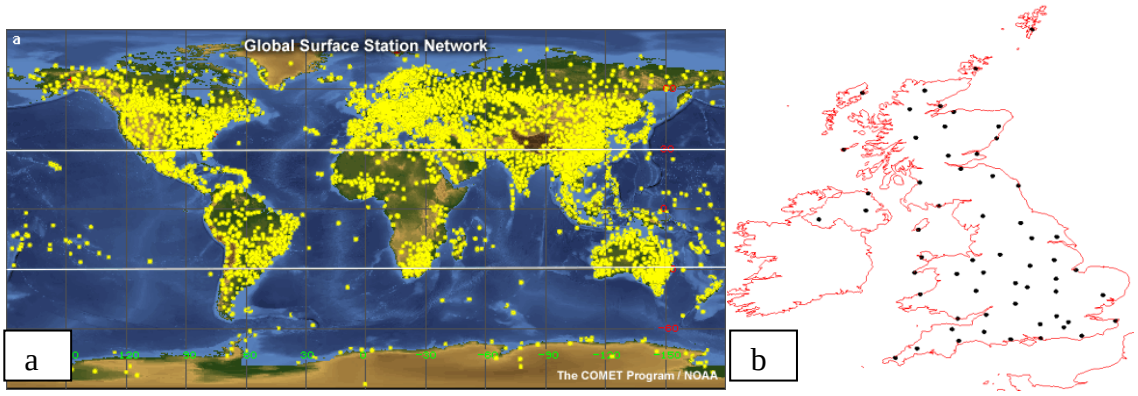

Figure 1.5 a) Locations of Surface Synoptic and Metar Stations as of 20 March 2007 (NOAA 2007); **b)** Locations of Synoptic stations over the United Kingdom which record SIS as of 15 June 2012.

According to the standards set by the World Meteorological Organization (WMO 2003), in order to derive a satisfactory climatological average of a particular climate element, there is a need for a sufficient period of record. For solar radiation, the required record of observations is ten years and preferably thirty years. The density requirements for monthly surface climatological data suggest that at least one station should be present over an area of 250 000 square kilometres [WMO, 2003] which implies a maximum distance of 500 km between each station. This actually varies according to the climate variable of interest. Some parts of the world do not however comply with the density requirements such as Africa, Antarctica, and large oceanic areas (**Figure 1.5 a**) which are sparsely populated with observation stations. For much of Europe and the UK in particular (**Figure 1.5 b**), spatial requirements are met for the majority of the land-based stations, however the measurements available are not always

homogeneous and are unevenly distributed (Wild 2009). Climatological maps of SIS can be derived by using interpolation between the station based observations (**Figure 1.6**).

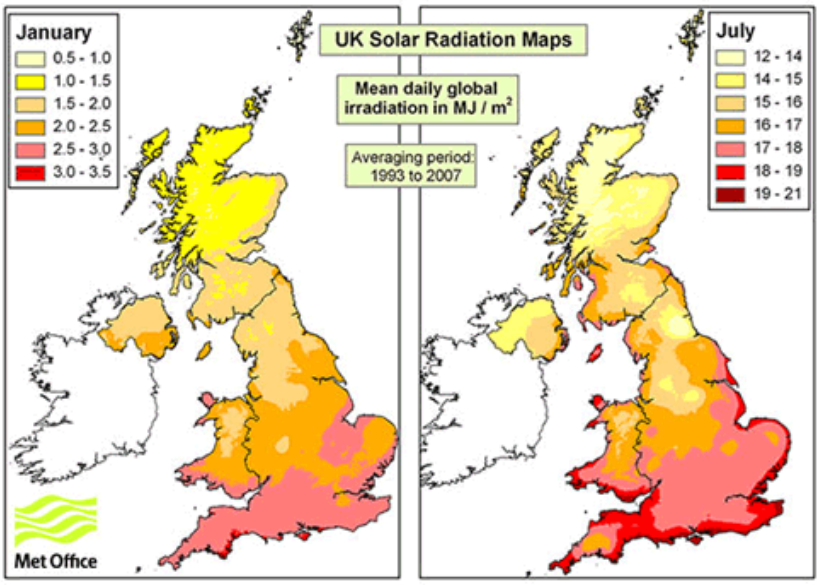

Figure 1.6 Mean daily global irradiation in MJ/m^2 for January (left) and July (right) over the averaging period 1993-2007, based on interpolation of surface station observations (Met Office 2013a)

This method, however, often creates errors due to the uneven spatial representation of measurements while occasional gaps in the records due to missing or corrupt data are also evident. Satellite and model based estimates of SIS provide higher spatial resolution and are therefore used for the purposes of this study.

1.1.4 Other methods for estimating surface solar radiation

To overcome the limitations of the surface based station network of observations, several alternative methods have been established for the estimation of surface solar radiation. These include atmospheric, empirical and stochastic models (Pandey and Katiyar 2013). An alternative way to retrieve surface radiation is to use the indirect estimates of SIS with the help of extraterrestrial instruments aboard weather and environmental satellites by means of remote sensing. Such satellites are located at the altitude of 36000 km above the equator providing continuous high temporal resolution over a fixed location (geostationary). The European domain which also includes the United Kingdom is covered by the Meteosat geostationary satellites (**Figure 1.7 a**). The European Organization for the Exploitation of

Meteorological Satellites (EUMETSAT) is responsible for the operation of Meteosat First and Second generation (MFG and MSG) meteorological satellites. The MFG and MSG satellites are equipped with the Meteosat Visible and Infrared Imager (MVIRI) and the Spinning Enhanced Visible and Infrared Imager (SEVIRI) aboard MFG and MSG, respectively (more details in **Section 2.2** of this Thesis). The data collected from these instruments (as well as others) are processed by the Satellite Applications Facility on Climate Monitoring (CMSAF) which was developed to provide high quality records for climate research applications.

Geostationary satellites provide a continuous coverage with the highest spatial resolution nearer the equator and directly below the nadir point of the satellite, however due to the nature of the orbit, there is no coverage over the poles. Weather and climate monitoring polar orbiting satellites have an orbiting track around the Earth at an altitude of about 800 km above Earth's surface providing a global coverage (**Figure 1.7 b**) usually with a higher spatial yet lower temporal resolution when compared to the geostationary coverage. Polar orbiting satellites have a significant limitation when operating for climate monitoring purposes which is the sparse temporal coverage.

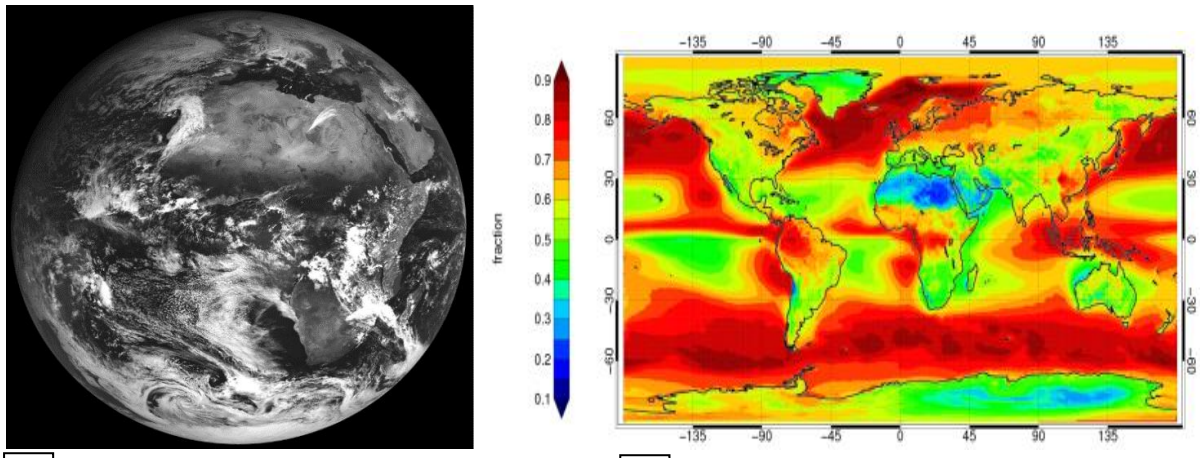

a b

Figure 1.7 a) Example of a Meteosat coverage area using the SEVIRI (Spinning Enhanced Visible and InfraRed Imager) radiometer. Image taken on November 03, 2013 at 11:42 UTC using the visible channel (ch01) (Weatherquest 2013); **b**) Monthly mean cloud fractional coverage for the 1982-2009 period, based on AVHRR instruments aboard polar orbiting satellites [Karlsson et al., 2013].

Satellite-sensed records go back to 1980, and therefore can be used for climate studies. Satellite-based estimates of SIS from the Climate Data Record (CDR) of the CMSAF have been used in several climate research and station validation studies due to a better performance for climate monitoring when compared against other available data sets of SIS (Posselt et al. 2012). Further information about the characteristics of the CMSAF data sets and the retrieval methodology are described in **Section 2.2** of this thesis.

The high temporal and spatial resolution of satellite-based estimates of SIS allowed several studies to focus on the trends of SIS at a global scale. The following section will discuss some insights concerning surface solar radiation trends on a global scale.

1.1.5 Trends in Surface Incoming Shortwave (SIS) solar radiation

According to several studies [e.g Russak (1990); Stanhill, 1995] based on analyses of in-situ measurements of SIS , there is evidence for surface radiation not being constant over time. Long term surface based records indicate that there was a widespread decrease in SIS across much of the world, including Europe, between the 1950s and the late 1980s, a phenomenon which is described as 'global dimming' (Stanhill and Cohen 2001). Ohmura and Lang (1989) showed that there was a decrease in SIS over several European sites, including Zurich, which over a 20-year period (1950s-1970s) revealed a decrease in the order of 10 W/m^2/decade absolute trend and 7% per decade as a relative trend. Meanwhile, Russak (1990) determined a reduction of 2.5% relative trend or 2.2 W/m^2/decade in terms of absolute decadal trend in SIS over the period 1955-1986 at Toravere in Estonia. Helsinki, Stockholm and Kaunas over the Baltic region experienced a reduction of about 5.5 W/m^2/decade or 5% relative trend over the 1964-1986 period [Russak, 1990].

The geographical extent of the dimming phenomenon was also reported as far afield as Hong Kong and New Zealand. According to Stanhill and Kalma (1995) the decrease in SIS over Hong Kong for the period 1958–1992 was 18 W/m^2/decade absolute trend with a relative trend of 10.6% per decade or 30% over the whole period, however it was based only on the measurements from one location. Evidence of dimming has also been observed over the Polar regions as examined by Stanhill (1995) who quantified this decrease in SIS over twenty-two

sites located in the Arctic region to have a magnitude of 3.6 W/m^2/decade absolute trend or -4 % per decade relative trend over the period 1950-1993. Stanhill and Cohen (1997) examined twelve sites across Antarctica and found a decrease of 2.8 W/m2/decade or 2.3% per decade for the period 1957-1994.

All these studies and many more, as suggested by Wild (2009), based on surface based observations up to around 1990, confirmed that global dimming was evident across much of the world. All these studies highlighted that the observed global dimming was a result most likely due to an increase in concentration of atmospheric aerosols caused by human activities.

However, more recent studies focusing on the post-1990 period have revealed an increasing trend in SIS (global brightening) [Stanhill and Cohen, 2001; Wild et al., 2005]. Wild et al. (2005) first demonstrated that the majority of the observational sites across the world revealed an increasing trend when more recent records were analysed. The increasing trends were particularly evident at a majority of three-hundred sites in Europe, and forty-five sites in Japan, and at the majority of the sites in Australia [Wild et al., 2005]. Based on surface observations from the Baseline Surface Radiation Network (BSRN), Wild et al. (2005) calculated an average increase of 6.6 W/m^2/decade absolute trend or about 3.6 % per decade relative trend based on the period 1992 to 2002. The brightening was also evident over China during the 1990s despite the significant dimming observed during the earlier decades. According to Wild (2009), several other studies focusing on the post-1980s period, including data up to 2002, present similar brightening results.

1.1.6 Causes of dimming and brightening

The word "global" in terms of dimming and brightening trends, does not imply spatial representation, but refers to the global radiation as the sum of direct and diffuse components [Wild, 2009]. These variations in SIS on a decadal scale have a terrestrial cause rather than externally forced, such as due to solar variability [Wild, 2009]. Variations in SIS are not only related to variations in cloud cover, they are also obvious under clear-sky conditions, indicating an anthropogenic influence through changes in aerosol properties and concentrations [Wild, 2009]. The period when global dimming was mainly observed coincides with the industrial development during the second half of the 20th century. Man-

made primary aerosol emissions from industrial sites, coupled with emissions associated with the burning of fossil fuels for electricity production and transportation impacted on the down-welling solar radiation through the processes of absorption and scattering. Higher than normal concentrations of aerosols can reduce the amount of solar radiation penetrating through the atmosphere leading to lower radiation fluxes incident at the surface. However, such changes in aerosols can also be of a natural origin such as from major volcanic eruptions (e.g. Krakatoa 1883; Pinatubo 1991). Aerosol particles have the ability to act as condensation nuclei during the process of cloud formation leading to change in cloud physical/optical properties. However, the impact of aerosols in the cloud formation process is quite complex and can't be analysed easily. According to Wild (2009), most of the previously cited early studies still contain some degree of uncertainty regarding the spatial representativeness of the observed trends due to the lack of adequate observations over the oceans and remote land areas. Satellite technology on the other hand allows monitoring of solar radiation and cloud cover at a global scale with high spatial and temporal resolution.

Sanchez-Lorenzo and Wild (2012) using MFG satellite based data from CMSAF, showed that there is a general increase of 3.1 W/m^2/decade in SIS for the whole of the domain presented in **Figure 1.8** for the period 1994-2005. However, in some regions, such as eastern parts of Iberia, the Balkans, England and particularly in the Mediterranean, there is a decrease in SIS between 1994 and 2005.

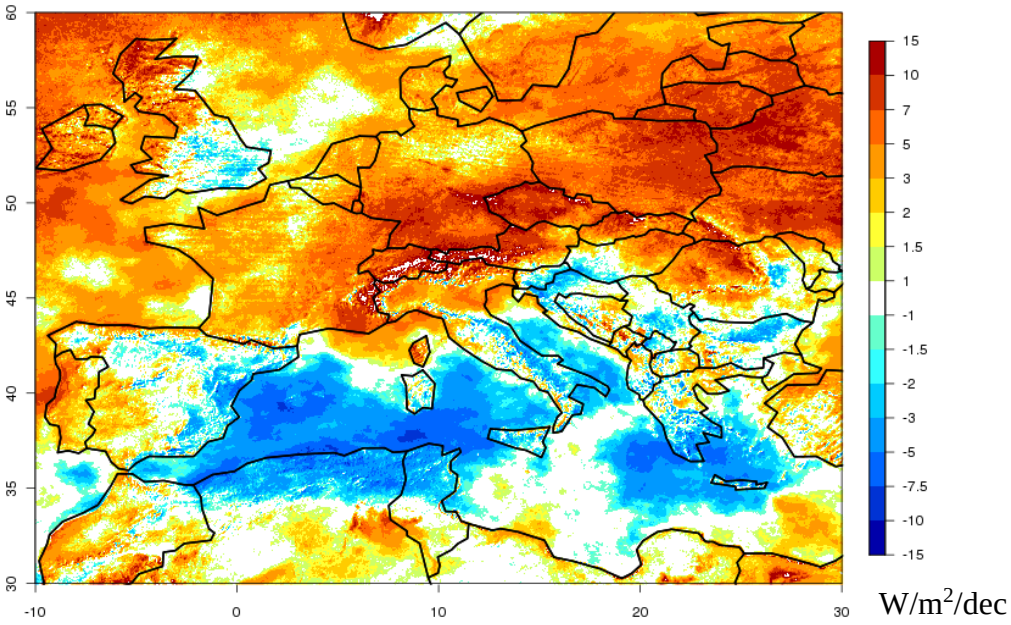

Figure 1.8 Linear trends (W/m^2 per decade) of the satellite-derived SIS based on the annual series from the CMSAF over Europe during the period 1994-2005. [Figure kindly provided by Sanchez-Lorenzo and Wild (2012)]

According to (Sanchez-Lorenzo and Wild 2012) Sanchez-Lorenzo and Wild (2012), SIS trends vary both spatially and between seasons (**Figure 1.9**). The seasons in this case and also for the purposes of this research are defined as spring (MAM), summer (JJA), autumn (SON), and winter (DJF).

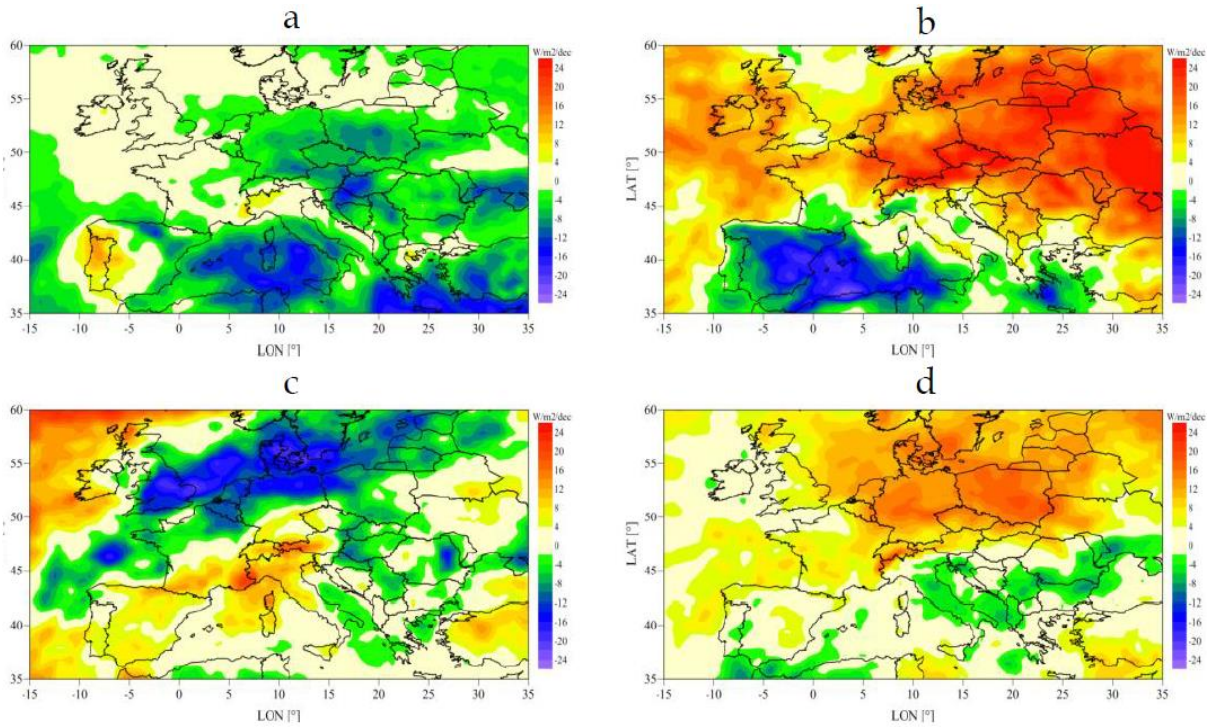

Figure 1.9 Linear trends (W/m^2 per decade) of the satellite-derived SIS annual series from the CMSAF over Europe during the period 1994-2005 for winter (a), spring (b), summer (c) and autumn (d) series. [Sanchez-Lorenzo and Wild (2012)]

Figure 1.9 a exhibits a 1994-2005 winter season average negative trend of -3.5 W/m^2/decade over the European domain as a whole with a decrease of 4 to 10 W/m^2/decade across much of Europe (apart from Portugal which has positive trends of about +4 to +8 W/m^2/decade) according to Sanchez-Lorenzo and Wild (2012).

An observed strong brightening (about +15 to +24 W/m^2/decade) is evident for the spring season (**Figure 1.9 b**) over Central and Eastern parts of Europe, but a negative trend over southern Europe (-4 to -8 W/m^2/decade) and in particular the western Mediterranean and Iberia (-10 to -22 W/m^2/decade). The mean trend over the domain is of +7.8 W/m^2/decade [Sanchez-Lorenzo and Wild (2012)]. **Figure 1.9 b** also has a lot of similarities in spatial characteristics when compared to the decadal trends (**Figure 1.8**).

Figure 1.9 c presents a completely different spatial variation of trends across much of Europe during the summer season with northern Germany, England, the Low Countries and Denmark presenting a strong negative trend (about -14 to -20 W/m^2/decade) while a positive trend is evident over western Mediterranean. The mean trend for this period over the whole domain is

-0.2 W/m^2/decade [Sanchez-Lorenzo and Wild (2012)]. The summer season is the time when the maximum amount of daily SIS is reached, therefore any significant trends during this time will have a significant offset in the total annual SIS. Trends in the magnitude of SIS during the summer season can have an impact on the stability and profitability of a PV investment since this season contributes greatly to the annual SIS totals. Trends can also have an impact in agriculture, when coinciding with some of the most critical stages of crop development occurring in summertime.

Autumnal trends are illustrated in **Figure 1.9 d** and present a general increasing trend over central and northern parts of Europe of about 12-14 W/m^2/decade, but slight negative of about 2-4 W/m^2/decade around the Mediterranean basin.

Sanchez-Lorenzo and Wild (2012) in their study also compared the satellite-sensed SIS time series from CMSAF against 47 surface-based measurement stations in the form of monthly means derived from the Global Energy Balance Archive (GEBA). GEBA [Gilgen et al., 1998] is developed and maintained at ETH in Zurich and holds data from surface based instrumental measurements from more than 2000 stations across the world (as of October 2013) with 250,000 monthly means of surface radiation fluxes [ETH, 2013]. The trends and values derived from the 47 CMSAF and GEBA time series are similar apart from during winter months of January and February (**Figure 1.10**). The comparison in terms of monthly time series increasing the confidence in the satellite-derived trends, and the opposite trends observed could possibly be due to a higher bias in the CMSAF data during the winter months [Trentmann, personal communication, 2012). Sanchez-Lorenzo and Wild (2012) concluded that further research is needed in order to understand the possible causes of this opposite trend. It is further shown that June exhibits positive trends of 13 to 18 W/m^2/decade, while July presents negative trends of 15 to 18 W/m^2/decade (**Figure 1.10**).

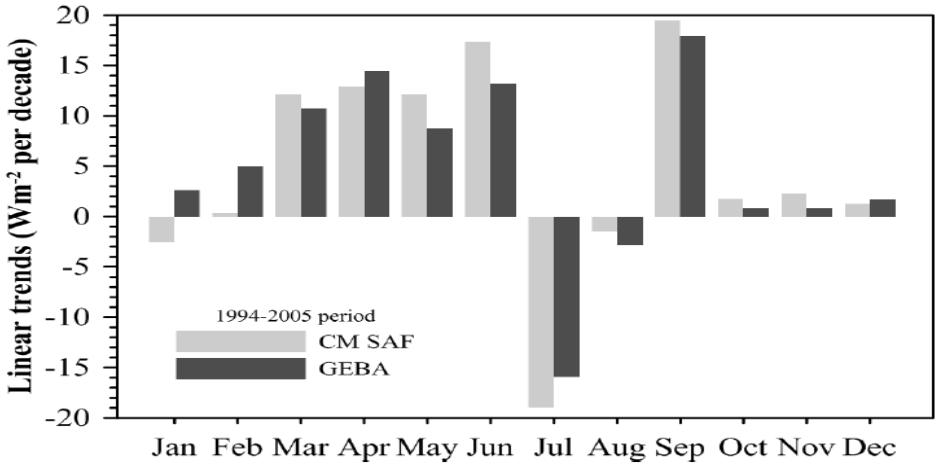

Figure 1.10 Linear trends of the mean monthly series (W/m^2/decade) obtained using the 47 CMSAF and GEBA series over Europe during the period 1994-2005. [Figure provided by Sanchez-Lorenzo and Wild (2012)]

Sanchez-Lorenzo and Wild (2012) concluded that the widespread annual brightening observed across much of Europe is a large-scale phenomenon and not an effect of urbanization. It is noteworthy that only monthly-varying climatological aerosol information has been used as an input to the satellite-estimates of SIS and the trends can therefore be attributed to changes in cloud properties (fraction and/or optical thickness). Since the time series in the report only covers 12 years, the change is probably, at least partly, due to internal variability, maybe related to the North Atlantic Oscillation (NAO) [Trentmann, personal communication, 2013]. Thus, an increase or decrease in cloud cover/thickness during this 1994-2005 period is possibly the main reason of these variations. The variability of weather on all timescales has implications for the output, viability and penetration of a wide range of renewable energy technologies, ranging across wind, wave, hydro, solar and bioenergy systems.

The high spatial variability of the temporal change highlights the usefulness of satellite-derived data for climate analysis purposes. The analysis needs to be brought up to date and the choice of whole seasons or months is not necessarily ideal for particular applications. One of the main applications which will be examined in this study giving value to the importance and the usefulness of the satellite based data is the investigation of the SIS trends during the wheat grain filling period over the United Kingdom (early-mid summer), as discussed below.

1.2 Literature review on the observed wheat yield plateau.

Wheat is a rich source of carbohydrate in the diet of a majority of countries and is consumed by billions of people. Wheat biomass and grain is also a popular source of animal feed, particularly in years when harvests are adversely affected by rain and significant quantities of the grain are of low quality and nutrients, rendering them unsuitable for human food use.

Since the Second World War, wheat yields and quality have been improving as a result of newer technologies, better understanding of varieties, genetic improvements, fertilization, and disease treatment. For example, wheat grain yields from 1980 to 1996 increased rapidly, by an average of 0.10 t/ha per year over the UK (Knight et al. 2012). Unfortunately, this positive trend has not been sustained post-1996. The impact of an uncontrollable factor like the weather, contributed to yields in 2012 being the lowest in the last 25 years across the UK [Farmers Weekly, 2012; Knight et al., 2012]. Recent global climate fluctuations have been sufficient in some countries to significantly offset increases in average grain yields. Over the last two decades, a crop yield plateau has been observed across most European countries, including the United Kingdom (**Figure 1.11 a)** (Ahmed et al. 2011); (Brisson et al. 2010, Finger 2010, Lobell et al. 2011, Knight et al. 2012). Specifically, Lobell et al. (2011) estimated that, between 1980 and 2008, global wheat production declined by 5.5% due to observed climate variability, clearly an important contribution to the yield plateau effect observed in many countries.

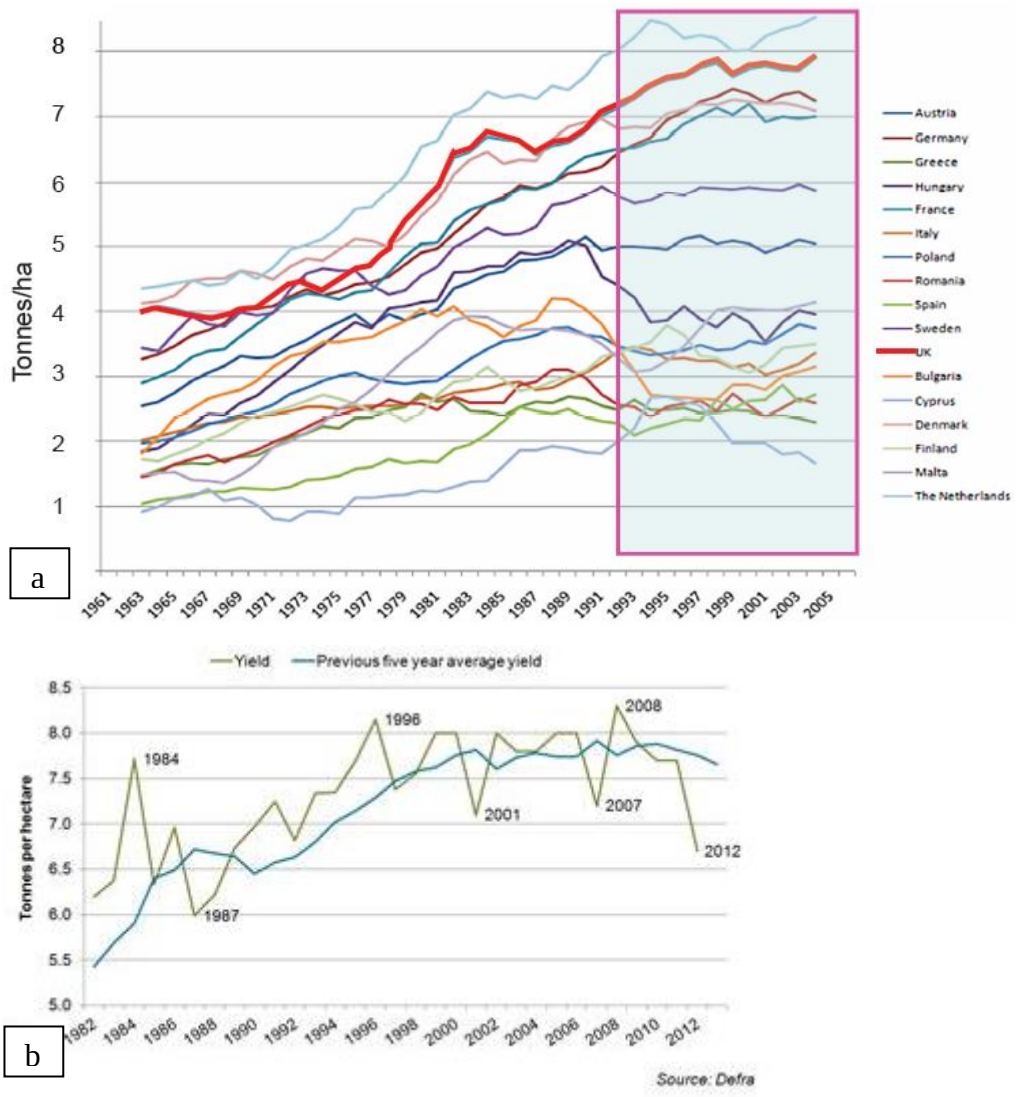

Figure 1.11 Wheat yields (tonnes/hectare) in Europe over the period 1961-2005 (**a**) (Clark 2013) and in the UK between 1982 and 2012 (**b**) [Knight et al., 2012]

Yields have plateaued despite the potential of new varieties increasing by 0.05 t/ha per year (**Figure 1.11 b**; Knight et al., 2012]. In 2012, some of the worst yields and quality of wheat grain were reported in the UK at the end of the harvest period [Farmers Weekly (2012); Clark, 2013], coinciding with the second wettest year across the UK since records began in 1910 [Met Office (2012)], and one of the dullest of the last 30 years (**Figure 1.12**; Gkousarov et al. (2013)].

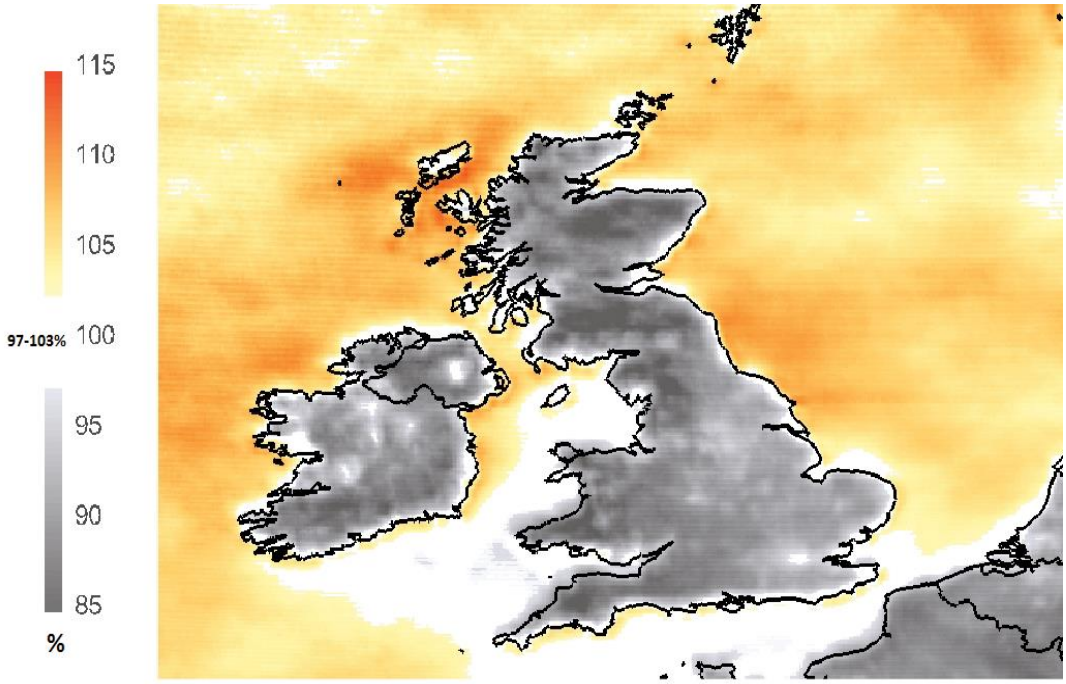

Figure 1.12 Sum of surface solar radiation during 2012 expressed as a percentage of 1983-2005 average. Satellite-based data provided by CMSAF [Gkousarov et al., 2013]

In order to quantify the possible impact of variable solar radiation in agriculture, this study focuses mainly on the impact of solar radiation on wheat grain yields during the grain fill period, building on the recent yield plateau study from Knight et al. (2012). Previous studies have generally been undertaken at regional-national resolution, using coarse scale station weather information representative of whole calendar months. What is needed is higher spatial resolution and the ability to focus on key crop development periods which do not necessarily adhere to this simple calendar. The difference between these two data sources is explained in **Section 1.2.2** of this thesis.

1.2.1 Wheat grain fill - background

Grain filling is the stage starting after pollination and following anthesis during which the kernel matures or ripens (Herbek and Chad 2009). Wheat crop stages are described by the Feekes and Zadoks scale systems, which were specifically designed for monitoring cereal crop development (Travis 1992). The main wheat crop growth stages are illustrated in **Figure 1.13**.

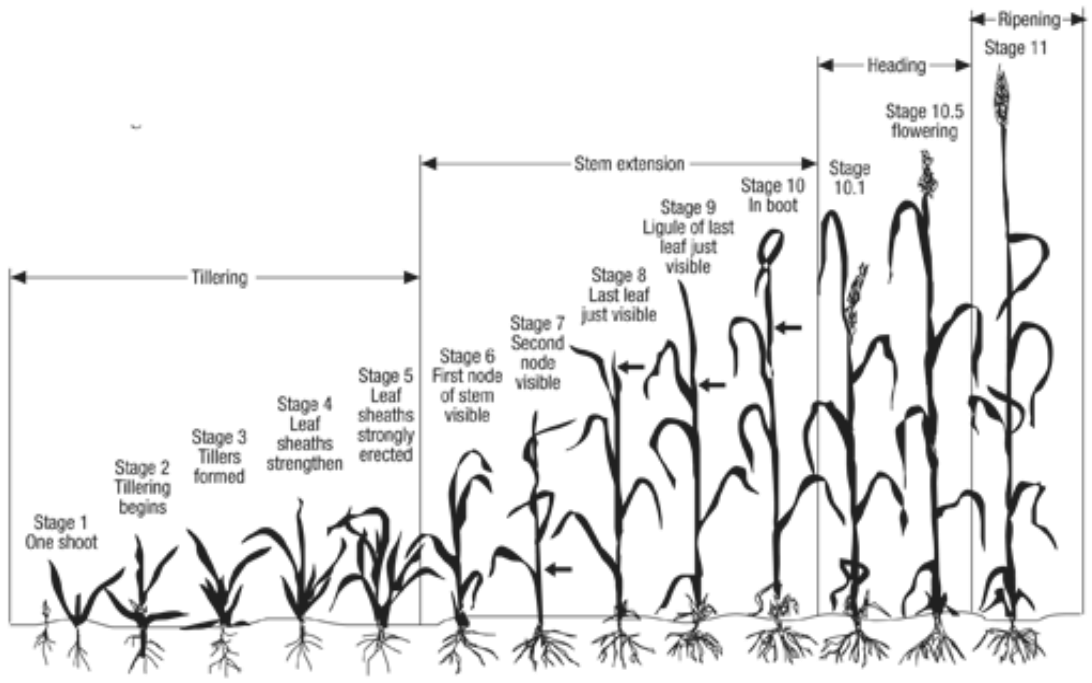

Feekes	1	2	3	4	5	6	7	8	9	10	10.1	10.5	11
Zadoks	10	21	26	30	30	31	32	37	39	45	50	60	90

Figure 1.13 Winter wheat crop growth stages according to the Zadoks and Feekes scales [adapted from Large (1954)]

A few hours after pollination (Feekes 10.51 to 10.53; Zadoks 60 crop development stages) the embryo and the endosperm begin to form and products of photosynthesis (glucose, sucrose) are transported to the developing grain from the flag leaf [Herbek and Lee., 2009]. The energy stored in the stems, leaves and roots prior to grain filling is critical to the grain as it is used as a supply in case of a crop stressing environment during the first key growth stages of the grain development. Archbold (1945) concluded that the pre-anthesis assimilate contribution to the grain yield expressed as a percentage of yield was no more than 20% . Meanwhile, Bidinger et al. (1977) determined that the pre-anthesis assimilate reserve contributes from 12% for watered crops to 22% on average for droughted crops to the total yield. According to Herbek

and Lee. (2009) the impact of the stress is higher when it occurs during the grain filling. The duration of the grain filling period (Feekes 10.54 to 11.4; Zadoks 70 to 92 crop development stages) is critical for the final grain yield since during this stage, kernel size and weight are determined [Herbek and Lee., 2009]. The longer the duration of the grain fill the greater the potential for higher yields according to various studies, including Herbek and Lee. (2009). Any crop stress during grain filling can limit the number of days of this process and therefore reduce the absorption of key nutrients, leading to lower grain yields. Drought, extreme temperatures, low light levels, insufficient nitrogen in the soil as well as pests and diseases are all factors that can play an important role [Knight et al., 2012]. There is a strong link between solar radiation received during this grain fill period and final yield. However, there are other factors which also play an important role such as if the crop is well-established prior to this stage for the production of photosynthetic matter during grain fill. Sufficient earlier growth of the crop canopy is also essential for the effective interception of solar radiation, as is sufficient moisture in the soil. Waterlogging past anthesis and during grain fill can cause abnormal early ripening and lead to early leaf senescence and as a result can reduce grain yields due to lower grain weights [Araki et al. (2012)].

1.2.2 The effect of temperature and solar radiation on grain fill

The length of the wheat grain filling period is not constant, since it depends greatly on temperature and is measured as the time taken to accumulate 660 degree days over the period starting immediately after pollination [Knight et al., 2012]. This value was used by Knight et al. (2012) as an area average representative of Central England in order to calculate the length of the grain fill period, starting on the 10th of June for each year. According to these authors the duration of grain fill from 1980 to 2011 had a decreasing trend from about 45 to 42 days over this area (**Figure 1.14 a**) which seems counter-intuitive to an increase in observed yields (at least until the mid-nineties). However, these authors also showed that the total number of sunshine hours for the calendar month of June (which only includes part of the grain fill period) has increased from about 150 hours in 1980 to about 250 hours by 1990, plateaueing thereafter (**Figure 1.14 b**). Knight et al. (2012) in their study observed a positive correlation between the national average wheat yields and total sunshine duration in hours over England for the month of June as indicated in **Figure 1.14 b**. The increasing trend in sunshine hours over Central England during the 1980-1990 period also coincided with a widespread increase

in SIS (global brightening) during the 80s and up to the 90s over many parts of Europe according to several studies [Wild, 2009; Sanchez-Lorenzo and Wild (2012); Wild et al., 2012].

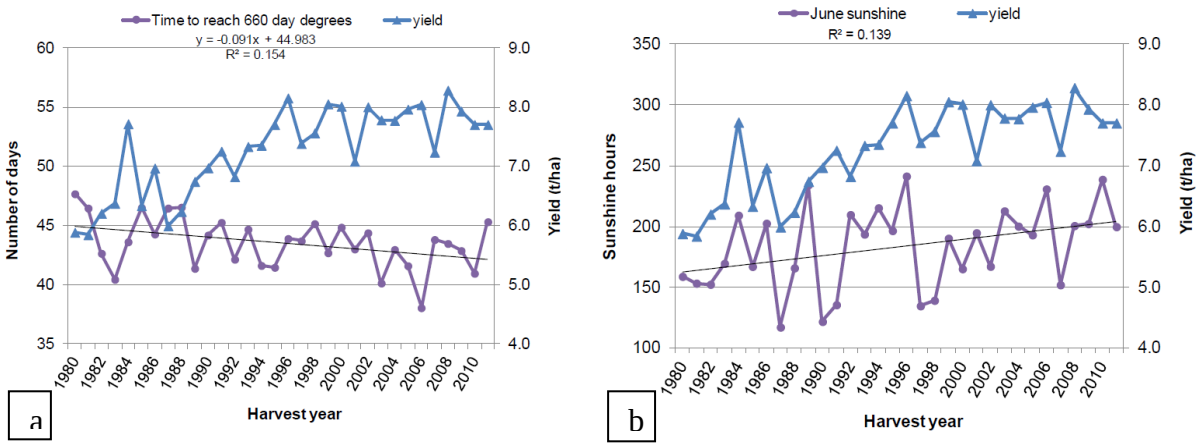

Figure 1.14 Trends of average wheat yield and number of days to reach 660 degree days (**a**) and average wheat yield and total sunshine hours for the month of June (**b**) for Central England [taken from Knight et al., 2012].

The limitation of the Knight et al. (2012) study is the fact that they used a single value as a large area average to determine the grain fill length, when in reality spatial variations in temperature can exist even on a small scale, leading to variation in the duration of grain fill. Furthermore, they determined the 10th of June as the regular starting point of grain fill. This however varies from year to year and place to place, and also depends broadly on the sown wheat variety [Clark, personal communication (2013)]. According to the Knight et al. (2012) study, the grain fill end date is determined as the 21st of July, however, this value is also temperature dependent and it is not constant over the different fields, years and varieties. For the purposes of this study and as described by Knight et al. (2012) the 'standard' grain fill period spans over the period of 10th June-21st July for each single year. For the purposes of this study a new concept will be applied which is the 'temperature adjusted' grain fill period and WRF model simulations will be used to generate a more idealistic approach for grain fill duration. Another limitation was the fact that they used "sunshine hours" instead of SIS. The difference is that plants absorb solar radiation in the form of visible light even with small intensities, while sunshine duration is defined by the WMO (2013) as the period during which the direct radiation received on a surface exceeds the 120 W/m^2 threshold. This practically means that during rather cloudy days when the mean hourly intensity of direct surface

irradiance is, for example, 80-90 W/m^2, this does not qualify as a 'sunshine hour'. Meanwhile the limitation of using SIS is that it includes a range of wavelengths which are not absorbed by the plants. Estimates of Fraction of Absorbed Photosynthetically Active Radiation (FAPAR) would be more indicative of the total solar radiation intercepted by the crop. As FAPAR depends on the state of each plant (plant health, growth stage, etc) significant spatial variations from field to field would not be resolved by the coarse spatial resolution of the current space-borne instruments which, ironically, provide high temporal resolution. Higher spatial resolution (1 km at sub-satellite point) FAPAR estimates are available from instruments (e.g. MODIS, AVHRR) aboard polar orbiting satellites, however these are obtained only twice a day or even once every eight or sixteen days, depending on the time taken by the satellite to perform an orbit over the same location.

Originally, the planned action was to seek long wheat yield records from individual farms, or from farm groupings through, for example, the Farm Business Survey. However due to the myriad of possible confounding factors relating to specific on-farm management decisions would led to a higher uncertainty on the impact of SIS during grain fill. Therefore, in this study, estimates of SIS during the grain fill over the UK are used to correlate against actual winter wheat grain yields from trials, which also follows the recommendation made by the Knight et al. (2012) project's stakeholder meeting following the release of their study. Annual yield data from trials of selected winter wheat varieties from the Recommended List (RL) of HGCA will be used for the purposes of this study in order to minimize the impact of the other important factors previously described (insufficient nitrogen in the soil, pests and diseases).

1.3 Hypotheses

This research study has three main hypotheses which can answer the following questions:

Is it possible to estimate wheat yields by assessing the amount of surface solar radiation intercepted by the crops during the UK wheat grain-fill period? Are yields stagnating due to reduction in SIS during grain-filling?

i) Since solar radiation drives photosynthesis, a positive relationship is expected between wheat grain yields and the amount of total SIS intercepted during the grain fill period, while acknowledging that this will be confounded by many other factors.

ii) The solar radiation intercepted during the grain fill period (early-mid summer) is expected to have a stable or even a negative trend during the ‘standard’grain fill period across the UK over the 1994-2010 record, which could also explain the wheat yield plateau trend observed since the late 1990's.

iiii) The relationship between the ‘temperature adjusted’ grain fill SIS accumulations and final yields from RL trials is expected to be stronger than that associated with the ‘standard’ grain fill period SIS accumulations.

1.4 Aims & Objectives

In order to fully test these hypotheses and to answer the research questions, it is necessary to also have a set of aims and objectives to construct the required underpinning UK SIS spatial fields and to interpret these as a function of both topography and the temporal variation in the frequency of different synoptic weather patterns.

Some of the expected findings derived as a by-product of this research should confirm or reject the following statements regarding the climatology of SIS over the UK:

1) The average annual sum of SIS is expected to be higher across southern parts of the UK due to the latitudinal gradient in solar radiation climate.

2) the average annual sum of SIS is expected to be higher nearer to the coasts and lower inland and over the hills, mainly due to enhanced in-land cloud cover associated with convection.

3) A change in the magnitude of period-specific total SIS accumulations is related to varying synoptic scale weather pattern sequences.

More specifically on the effect of SIS on wheat grain yields this research will also quantify the spatio-temporal variability of SIS during the UK grain-fill period by rejecting or confirming the following statements.

4) The average sum of SIS during the grain fill period (early-mid summer) is expected to be quite variable temporally and spatially, but still with a distinct zone separating coastal from inland areas and mountainous regions.

5) The duration of the 'temperature adjusted' grain fill period over the UK is expected to vary spatiotemporally.

6) The average sum of SIS during the 'temperature adjusted' and the 'standard' (10th June - 21st July) grain fill period should also vary both spatially and temporally as a function of grain fill duration.

1.5 Thesis outline

Chapter 2 covers several methods of retrieving SIS measurements and a more detailed explanation of the datasets and methods that are used in this study.

Chapter 3 deals with the comparison of satellite and model based solar radiation datasets with surface based observations and an example comparison of existing climatologies is made. Some of the hypotheses introduced in the first chapter, are tested to reveal the power of the approach adopted in this study.

Chapter 4 is also a results chapter introducing the climatology of surface solar radiation during the wheat grain fill period, including actual maps and trends for this specific period. Several sensitivity tests are carried out in order to determine which method provides higher correlation between the solar radiation intercepted by the crops during that period and the actual observed grain yields.

Chapter 5 presents important conclusions from each aspect of the research work leading to discussion and suggestions for further research and potential research improve makes.

2 Materials and Methods

2.1 Sources and data selection

This section provides an overview of the data used in this study and the methodology for deriving these data from land based stations, satellite instruments and Numerical Weather Prediction (NWP) models. SIS measurements at ground based SYNOP stations archived in the Met Office Integrated Data Archive System (MIDAS) [UKMO (2012)] and are used only as reference for verification purposes. In this study, SIS data from the Climate Monitoring Satellite Applications Facility (CMSAF) are used to generate the climatology. The motivation for selecting SIS data from CMSAF is due to a better performance for climate monitoring when compared against other data sets like ERA-reanalysis, GEWEX (Global Energy and Water Cycle Experiment) and ISCCP (International Satellite Cloud Climatology Project) [Posselt et al., 2012]. Another reason for choosing the CMSAF SIS dataset is the fact that it is available free of charge to download[1] in the form of daily and monthly means at a spatial resolution of 0.03^{o} regular latitude-longitude grid and can be used for all purposes. WRF model re-analysis of SIS and two metre temperature are also used in this study in order to determine the duration of the grain fill over the UK (results in **Section 4.3**). The WRF SIS will be tested against SYNOP station based observations (**Section 3.2)** to compare the performance against the generated dataset of satellite-based SIS. WRF model output of SIS could be used as a supplement to satellite-based estimates during periods when satellite sensors are not operating either due to a random error or a scheduled maintenance process of the instruments or satellites. The impact of different synoptic scale weather pattern sequences and the relationship between grain fill SIS and wheat grain yields are analysed by using a combination of several programs and scripts which are also discussed in this chapter.

[1] wui.cmsaf.eu

2.1.1 Surface based station observations from the Met Office Integrated Data Archive System (MIDAS)

As described in **Section 1.1**, land based observations are a convenient way to measure on-site meteorological parameters with higher accuracy and temporal frequency. However, due to their irregular spatial distribution, surface observations are only used here to verify the performance of the NWP models and satellite estimates. The source of station measurement SIS data is the UK Met Office SYNOP station network, archived in the Met Office Integrated Data Archive System (MIDAS) and acquired from the British Atmospheric Data Centre (BADC). The MIDAS Land and Marine surface station dataset (UKMO 2012) provides hourly and daily weather observation date reported by stations in the UK (**Figure 2.1**) and globally with records dating back to 1853 and available to date. Some of the variables recorded are wind speed and direction, air temperature, rainfall, soil temperature, sunshine duration and solar radiation accumulation (UKMO 2012).

Figure 2.1 The UK land surface synoptic station observation network operated by the Met Office in May 2010. [Reproduced from Met Office 2013 © Crown copyright]

The radiation components that are routinely measured by some of the stations are: global radiation, direct and diffuse radiation and long-wave radiation. Not all of the surface based stations which are archived in MIDAS report global radiation (SIS) and the spatial representation of the stations which do is much more sparse (**Figure 2.2**).

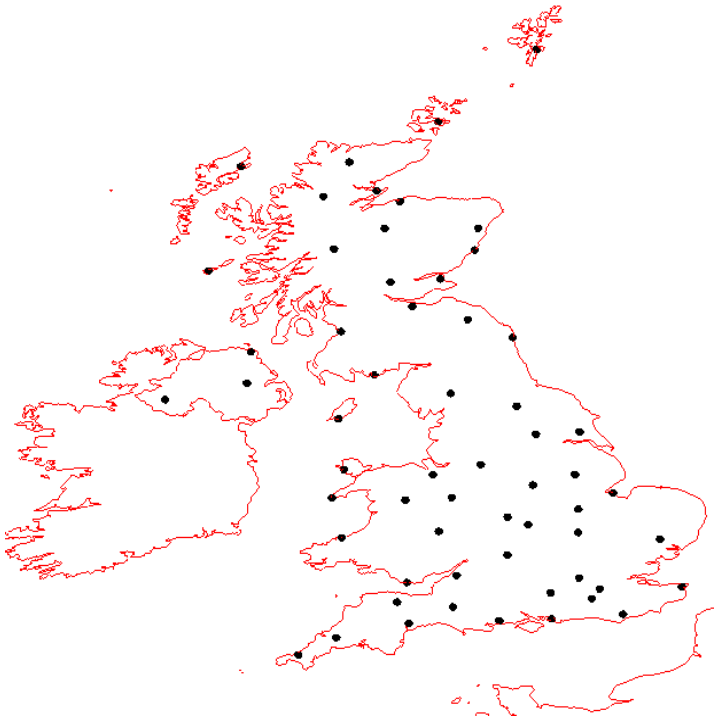

Figure 2.2 Locations of synoptic stations over the United Kingdom which record SIS as of 15 June 2012.

While other observation networks such as the Baseline Surface Radiation Network (BSRN) (**Figure 2.3**) would have a higher accuracy of SIS measurements, it's even sparser coverage network would not allow a proper verification procedure. There are currently only two operating BSRN stations in the UK (Lerwick and Camborne, **Figure 2.3**) while MIDAS contains land based surface measurements as reported by 154 stations in the UK (**Figure 2.1**) and across the world with an average distance between stations of about 40 km.

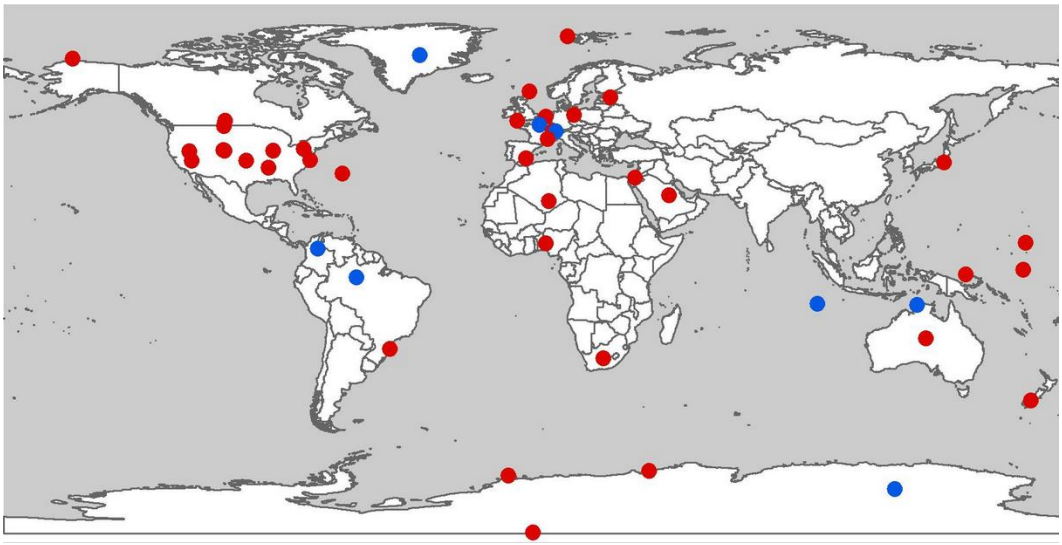

Figure 2.3 Locations of the Baseline Surface Radiation Network (BSRN) stations. Red: operational; Blue: planned [Figure provided by MeteoSwiss (2013a)]

Surface based global radiation is measured at surface stations using a pyranometer which has a sensor that is designed to measure incoming global radiation flux density (W/m^2) from a field view of 180 degrees [**Figure 2.4**; UKMO (2012)]. All pyranometers used by the Met Office synoptic observation network are calibrated using absolute cavity radiometers as reference, which are the standard radiation instruments maintained by the Met Office (UKMO 2012). Pyranometers are sensitive to the incoming radiation in the range of 305 to 2800 nm and this varies from the range of spectrum which is measured by the satellite based instruments (each instrument has different spectral response as explained in **Sections 2.21 & 2.22**) . The energy output of the pyranometers is then collected using Climate Data Loggers with a sampling frequency of five seconds and the output from the logger represents the accumulation of energy per unit area within each ten minute sample period [UKMO, 2006].

Figure 2.4 Pyranometer for measuring global radiation (MetOffice 2013b)

The SIS data from the SYNOP measurement network are archived in the BADC as hourly and daily totals of insolation (kJ/m^2). For the purposes of this study, only the daily total data are used and converted to MJ/m^2/day.

The advantages of using surface observations are the high accuracy at the point of measurement with high sampling frequency (seconds or minutes) and with high quality if the network is well maintained and the instruments are well calibrated. Some of the limitations present in ground based observations are the limited spatial coverage, limited record of continuous observations, missing data and external contamination of the pyranometer dome due to dust or snow cover. Meanwhile, space borne instruments and NWP model simulations can provide higher spatial density.

2.2 The CMSAF Climate Data Record (CDR) data set

The satellite-based data sets of SIS used in this study have been obtained from the EUMETSAT's Satellite Application Facility on Climate Monitoring (CMSAF). The Climate Data Record (CDR) SIS is derived from the first generation of Meteosat satellites (MFG) positioned in a geostationary orbit at a longitude of 0^o and an altitude of 36,000 km above the equator. MFG satellites started with the launch of the first Meteosat in 1977 and then 6 more series of similar type (Meteosat 2-7) were launched through to 1997 providing a continuous long period of coverage on which CMSAF CDR SIS is based (**Table 2.1**). The newly launched satellites have been operating alongside the existing operational satellite in order to

ensure an overlapping operational period for validation purposes. This explains why Meteosat 3 and 4 appear twice in **Table 2.1** [Posselt et al., 2012]

Table 2.1 Operational periods of Meteosat satellites [adapted from Posselt et al., 2012]

Satellite		From	To
Meteosat	2	16.08.1981	11.08.1988
Meteosat	3	11.08.1988	19.06.1989
Meteosat	4	19.06.1989	24.01.1990
Meteosat	3	24.01.1990	19.04.1990
Meteosat	4	19.04.1990	04.02.1994
Meteosat	5	04.02.1994	13.02.1997
Meteosat	6	13.02.1997	03.06.1998
Meteosat	7	03.06.1998	31.12.2005
Meteosat	8	31.12.2005	11.04.2007
Meteosat	9	11.04.2007	21.01.2013
Meteosat	10	01.01.2013	ongoing

The data were retrieved by the Meteosat Visible and Infrared Imager (MVIRI) which is a radiometer instrument aboard the Meteosat 2-7 satellites. MFG satellites are equipped with three different sensors capable of scanning the Meteosat full disk area (80N to 80S in latitude and 80E to 80W in Longitude every half-hour with a spatial resolution of 2.5 km at the nadir point in the visible band (5 km for the other channels) [Posselt et al. (2011)]. The visible band of MVIRI ranges from 450-1000 nm and only provides data during daytime. The water vapour channel (5700-7100 nm) is used to determine the amount of water content in a vertical column in the atmosphere. The thermal infrared band (10500-12500 nm) is used for mapping

the thermal emission of the Earth and clouds. Only the broadband visible channel of MVIRI has been used to derive the SIS, based on the original Heliosat method.

2.2.1 MVIRI Climate Data Record (CDR) SIS retrieval method

The Heliosat algorithm estimates the radiation at ground level using the effective cloud albedo at the top of the atmosphere (also known as cloud index) which is inversely related to the radiation reaching Earth's surface (Cano et al. 1986). This method then takes information from the look-up table of clear-sky irradiances based on the Mesoscale Atmospheric Global Irradiance Code (MAGIC) [Mueller et al., 2009]. MAGIC uses several variables such as water vapour, aerosol and ozone fields and information about the surface albedo as input data (MeteoSwiss 2013b). The combination of Heliosat and MAGIC makes up the MAGISOL method as illustrated in **Figure 2.5**. More detailed information about the insights of these methods can be found in Beyer et al. (1996), Cano et al., (1986), Hammer et al. (2003) and Posselt et al., (2011 & 2012).

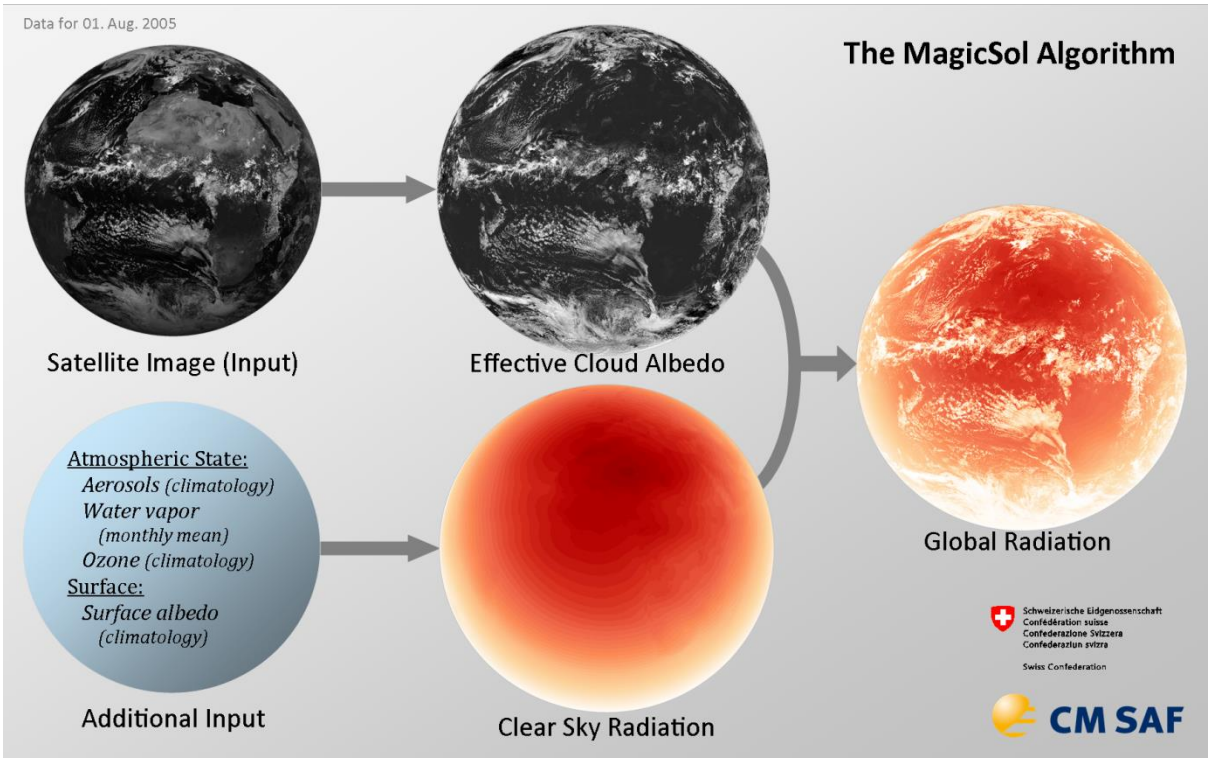

Figure 2.5 Schematic of the Magicsol retrieval algorithm [MeteoSwiss (2013b)]

2.2.2 MVIRI Climate Data Record (CDR) accuracy

This dataset has been validated by Posselt et al. (2012) using station observations from the BSRN as a reference (**Table 2.2**). The stations used in their study were only considered if the overlapping period of satellite estimates and station records was at least 12 months. Posselt et al. (2012) showed that the mean bias between the satellite-derived and surface-based observations for monthly and daily means is well below the target accuracy threshold set by the Global Climate Observing system (GCOS). More specifically, Posselt et al. (2012) quantified the CMSAF SIS Mean Absolute Bias (MAB) for daily means to be 15.52 W/m^2 while the threshold set by the GCOS is 25 W/m^2 (**Table 2.2**). CMSAF CDR SIS outperforms other surface radiation data sets such as those presented in **Table 2.3** (results of inter-comparison also presented in **Table 3.1**). The same data set has also been subjected to validation by several other researchers including Sanchez-Lorenzo and Wild (2012) and Journée et al. (2012) with similar results, falling within the accuracy targets set by the GCOS, confirming the high quality of the data set for climate monitoring applications.

Table 2.2 Locations of BSRN stations used in the Posselt et al. (2012) validation study. [Taken from Posselt et al., 2012].

Station	Country	Code	Latitude [°N]	Longitude [°E]	Elevation [m]	Data since
Bermuda	Bermuda	ber	32.27	−64.67	8	1.1.1992
Camborne	UK	cam	50.22	−5.32	88	1.1.2001
Carpentras	France	car	44.05	5.03	100	1.8.1996
De Aar	South Africa	daa	−30.67	23.99	1287	1.5.2000
Florianopolis	Brasil	flo	−27.53	−48.52	11	1.6.1994
Lerwick	UK	ler	60.13	−1.18	84	1.1.2001
Lindenberg	Germany	lin	52.21	14.12	125	1.9.1994
Payerne	Switzerland	pay	46.81	6.94	491	1.9.1992
Sede Boger	Israel	sbo	30.9	34.78	500	1.1.2003
Solar Village	Saudi Arabia	sov	24.91	46.41	650	1.8.1998
Tamanrasset	Algeria	tam	22.78	5.51	1385	1.3.2000
Toravere	Estonia	tor	58.25	26.46	70	1.1.1999

Table 2.3 Statistics for the comparison of daily mean SIS between the mean of all BSRN stations and CMSAF as well as ERA-Interim, GEWEX and ISCCP. From left to right columns indicate SIS source, number of days taken into account for the analysis period (nday), overall Bias (W/m^2), Mean Absolute Bias (MAB) expressed in W/m^2, Standard Deviation (SD) expressed in W/m^2 [Taken from Posselt et al., 2012]

SIS (daily mean)	n_{day}	Bias [W m^{-2}]	MAB [W m^{-2}]	SD [W m^{-2}]	AC	Frac$_{day}$ >25 W m^{-2} [%]
CM SAF–BSRN	28,674	4.58	15.52	23.73	0.92	17.08
HelioClim–BSRN	28,674	−17.94	34.89	43.13	0.74	50.09
ERAint–BSRN	28,674	5.64	26.86	39.14	0.74	36.62
GEWEX–BSRN	28,674	−2.81	22.90	31.31	0.85	32.89
ISCCP–BSRN	28,674	0.40	26.62	37.22	0.76	37.65

2.2.3 Stability and homogeneity of the MVIRI data set

The stability of the measurements is important for any trend analysis, especially over large areas indicative of a sparsely populated station network of observations, where the satellite estimates are the only reliable solution. Posselt et al. (2012) in their research investigated the homogeneity of the dataset for the Meteosat 2 to 7 operating period (1983-2005) and found that several step changes in the time series were obvious, especially around 1990. These step changes are indicative of potential inhomogeneities, mostly evident from the Equator to 40N latitude, covering the Sahara region and northern Africa [Posselt et al., 2012]. Sanchez-Lorenzo and Wild (2012) recently assessed the temporal stability of the CMSAF CDR SIS data set using observations from forty-seven stations from the Global Energy Balance Archive (GEBA) across Europe as a reference. The main finding of their study is that the CMSAF MVIRI surface radiation data set is temporally stable after 1994. The stability of the earlier data might be affected by changes in the satellite instruments used to generate the data set [Posselt et al., (2011 & 2012); Sanchez-Lorenzo and Wild (2012)].

Another issue also presented in the CMSAF CDR data sets is a striping feature (horizontal lines) obvious in the daily mean products before 1995 [Trentmann et al., 2010; Journe et al., 2012; Posselt et al., 2011 & 2012]. Data derived from the satellites Meteosat 2 and 3 exhibit a striping effect caused by uncorrected missing lines during nighttime (18:00-05:00UTC).

Daytime imagery from the visible channel contained data only every second line, while the rest of the lines contained the whole data information (Trentmann et al. 2010). These artificial features can be easily observed in **Figure 2.6**. According to Trentmann et al. (2010) the CDR SIS daily mean product has a mean amplitude of the stripes in the order of 5 W/m² and with a maximum in the order of 20 W/m². Meteosat 4 also exhibits stripping in some of the data, not only during early and late day hours, but also during the whole day, however the reason for this is not yet known [Trentmann et al., 2010].

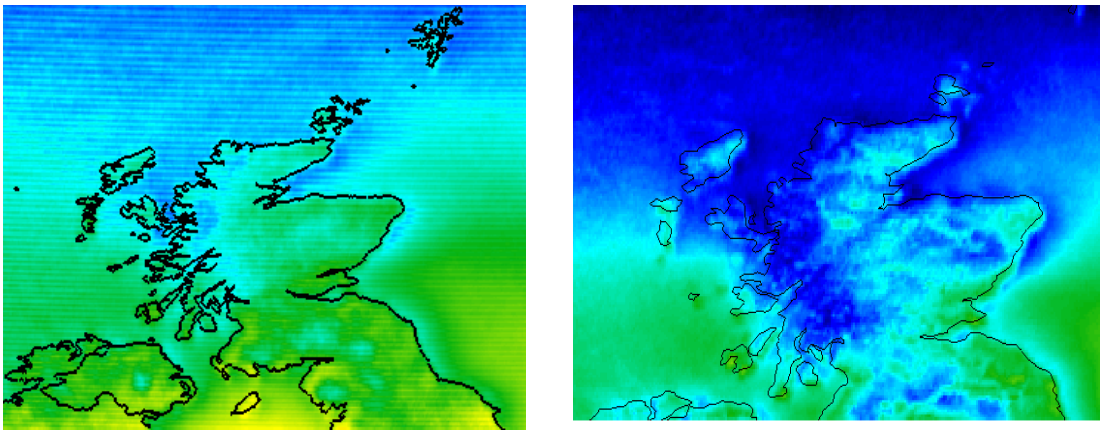

Figure 2.6 Example of **s**triping effect as a result of the data processed from Meteosat 2 and 3. Left figure shows affected SIS data (horizontal lines) while right figure shows unaffected data.

For mostly technical reasons, due to errors in the MVIRI instruments, there are some gaps in the CMSAF CDR data sets. 161 daily means of SIS are missing out of the whole daily record over the 1983-2005 period (MVIRI coverage) although most of the missing data are prior to 1994. Post-1994 there are only 24 missing daily means of SIS and these will be considered when applying calculations. For the complete list of missing data, Trentmann et al. (2010) provides more details.

The main advantage of the SIS CDR from CMSAF is the fact that the resulting time series are fully applicable for climate monitoring purposes, including trend estimation. However, due to the issues introduced previously concerning CMSAF CDR data before the 1994, for the

purposes of this study, only the CMSAF CDR SIS data covering the 1994-2005 period will be used for Trend analyses and will be merged with other data sets of climate quality. This was also the reason why Sanchez-Lorenzo and Wild (2012) investigated the trends in SIS over the European domain for the period 1994-2005. Journée et al. (2012) in their study also used the 1994-2005 sub-period to generate the climatology of SIS over Benelux, thereby avoiding the missing data problem. CMSAF will provide an updated data set covering 1983 to 2012 in 2016 which will also resolve some issues that are currently present in the MVIRI-based CDR data set, which has been found only to be homogeneous after 1994 [Trentmann, 2013]. One of the serious limitations of the SIS CDR is the fact that it is generated on an irregular basis, e.g. every 2 years, and this does not allow it to be used for operational applications where more recent data are required. The CDR SIS data and other radiation data are provided free of charge for every use in a CF-netcdf format from wui.cmsaf.eu. SIS from the CDR are available for the period of 01-01-1983 to 31-12-2005 as hourly, daily and monthly means (W/m^2) in a regular latitude longitude grid of 0.03^o (3 x 3 km) spatial resolution [Posselt et al., 2012]. For the purposes of this study only daily means are used and converted into daily insolation (MJ/m^2/day) as follows:

Daily means x 24 hours x 3600 seconds each hour divided by 10^6 in order to get the insolation in MJ/m^2/day which is the sum of the SIS incident on a horizontal surface received over the period of the whole day.

2.3 The CMSAF Operational data set

The MSG satellites (Meteosat 8–10, in operation since 2004; **Table 2.1**) are equipped with the Spinning Enhanced Visible and InfraRed Imager (SEVIRI) radiometer that measures in 12 different spectral bands with a higher temporal resolution compared to MVIRI (15 minutes). The imaging sampling distance is 3 km (at nadir) for the visible and infrared channels, although there is additionally a broadband high resolution visible (HRV) channel with a spatial resolution of around 1 km (at nadir). However, due to a satellite failure this channel does not cover the full Meteosat disk [EUMETSAT, 2013]. Only the two narrow-band visible channels of SEVIRI around 600 nm and 800 nm and data from the Geostationary Earth Radiation Budget (GERB) instrument aboard the MSG satellites have been used to derive the operational data set of SIS based on MSG provided by CMSAF. The operational SIS retrieval algorithm is using a different method to the CDR SIS, due to the fact that the SEVIRI

instrument is different in characteristics to its predecessor MVIRI and the MAGICSOL method could not be applied to extend the data sets based on SEVIRI (Trentmann et al. 2010). In brief, the operational data set of SIS is derived using cloud fraction information and based on this fraction, a clear-sky or a cloudy-sky retrieval algorithm is applied, but more detailed information can be found in Mueller et al. (2009).

For a short period of time (April-December 2005) MVIRI aboard Meteosat 7 and SEVIRI aboard Meteosat 8 were operating next to each other. This allowed a comparison to be developed between the two methods. Kniffka (2012) compared the monthly means of the CDR SIS with the operational product of SIS for the last four months of 2005 (September-December) and the main finding was that, in general, the CDR data set tends to overestimate surface radiation over the seas while the operational product tends to underestimate SIS, especially over land surfaces, in particular bright surfaces with regular cloud cover [Kniffka, 2012] (**Figure 2.7**).

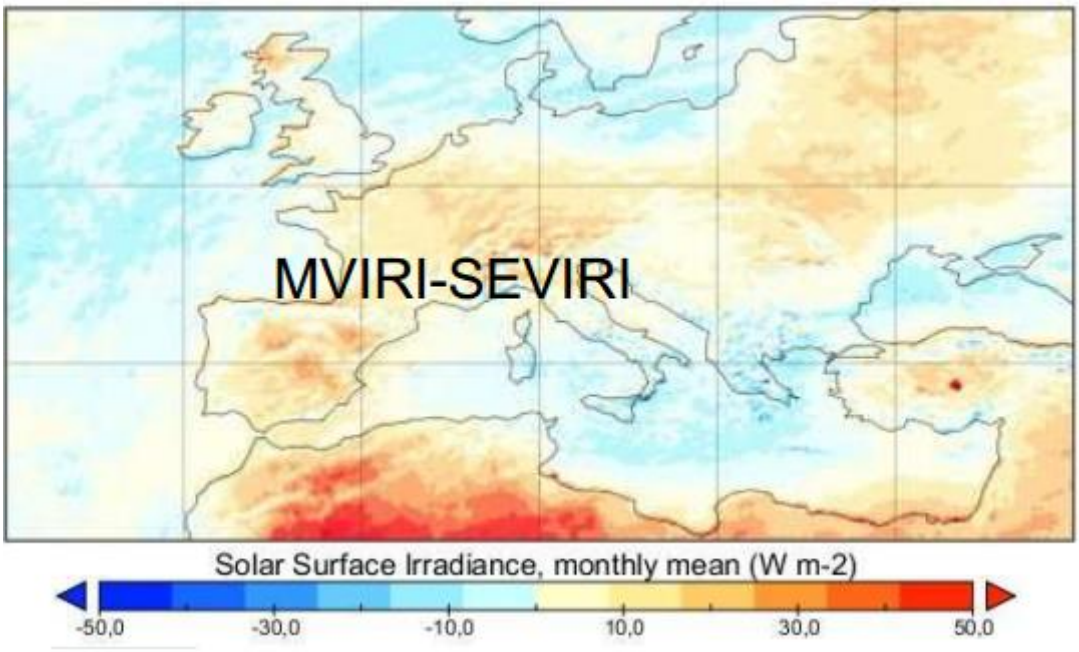

Figure 2.7 Simple difference (W/m^2) for MVIRI CDR SIS minus operational SEVIRI SIS for the sum of the last four months of 2005. [Taken from Kniffka, 2012]

The operational product of SIS is being retrieved using several different versions of the same algorithm, therefore each one is subjected to different biases. In general, the systematic maximum difference between the CDR and operational SIS is on the order of 10 to 20 W/m^2

(Trentmann 2013). Due to limited resources, CMSAF cannot monitor the performance of each version in an operational manner, and mostly rely on validation reports from CMSAF users, with the author of this thesis being one of them. Operational Products are generated on a weekly to monthly basis using algorithms and assimilated input data which are not homogeneous over time, resulting in them not being applicable for all climate monitoring purposes, e.g. trend estimation [Trentmann, 2013]. The operational SIS product comes on a 15 x 15 km sinusoidal grid and is available as daily and monthly means and monthly mean diurnal cycle from 2005 to date. For the purposes of this study the operational product of SIS has been regridded onto a regular longitude-latitude grid of 3 x 3 km using the Climate Data Operators (CDO) software routines to perform this process.

2.4 METEOSWISS - SEVIRI Solar Surface Radiation dataset

One of the CMSAF's missions is to develop a complete homogeneous CDR data set from 1983 to 2012 based on MFG and MSG, however this data set will not be available until the end of 2014 [Trentmann, 2013]. In the meantime, Posselt et al. (2012) from MeteoSwiss generated a climate quality surface solar radiation data set based on MSG satellites using the same algorithm as for the period 1983-2005 with the same aerosol information as for CMSAF CDR. The two narrowband visible channels of SEVIRI have been used to simulate MVIRI's broadband visible channel [Posselt et al., 2012]. Hereafter, for the purposes of this study, this data set is referred as MeteoSwiss CDR of SIS.

Posselt et al. (2013) performed a validation of the MeteoSwiss SIS CDR using forty-seven GEBA stations for the period 1983–2007 and four BSRN stations for the period 1990–2010 as ground-based reference over Europe. Results showed that the Mean Absolute BIAS (MAB) for the period 2006–2009 is well below the accuracy targets (<15 W/m^2) for monthly means. Specifically the MAB is 8.7 W/m^2 while the BIAS is 7.9 W/m^2. Posselt et al. (2013) in their study did not investigate the performance of daily means. More information about the statistics of the validation and the methodology which has been used are available from Posselt et al. (2012). The CDR SIS data set based on the MVIRI and SEVIRI instruments is currently (22 June 2013) the best available and homogeneous satellite-based long term climate data record of surface radiation [Trentmann, 2013]. CMSAF does not provide documentation for this data set therefore any enquiries should be addressed to the satellite climatology team of MeteoSwiss and any requests concerning the MeteoSwiss CDR SIS

should be sent to Rebekka Posselt[2] or Reto Stöckli[3] . The data are available as daily and monthly means for educational purposes only [MeteoSwiss, 2013].

2.5 CMSAF Surface Incoming Shortwave (SIS) CLARA

Although SIS based on geostationary satellites ensures continuous temporal coverage over a fixed area, occasionally, due to random instrument errors or scheduled maintenance processes, some gaps may also occur. For example, a scheduled maintenance took place from 1 to 9 July 2013 for the decontamination of the Meteosat 10 satellite [EUMETSAT (2013)]. This generated a discontinuity in the operational product of SIS for those days. To limit the impact of this occasional missing data, the use of polar-orbiting AVHRR instruments has been considered as an alternative. CMSAF in addition to the data sets and products described earlier (and many more) also recently released the Clouds, Albedo and Radiation dataset from AVHRR (CLARA) data set based on polar orbiting satellites (Karlsson et al. 2013). This data set extends from 01.01.1982-31.12.2009 (only the part after 1995 is homogeneous) and is available as daily and monthly means with a spatial resolution of 25 x 25 km SIS based on the geostationary Meteosat satellites has a higher accuracy, but in the case of missing data from geostationary satellites the CLARA data set might still be of use

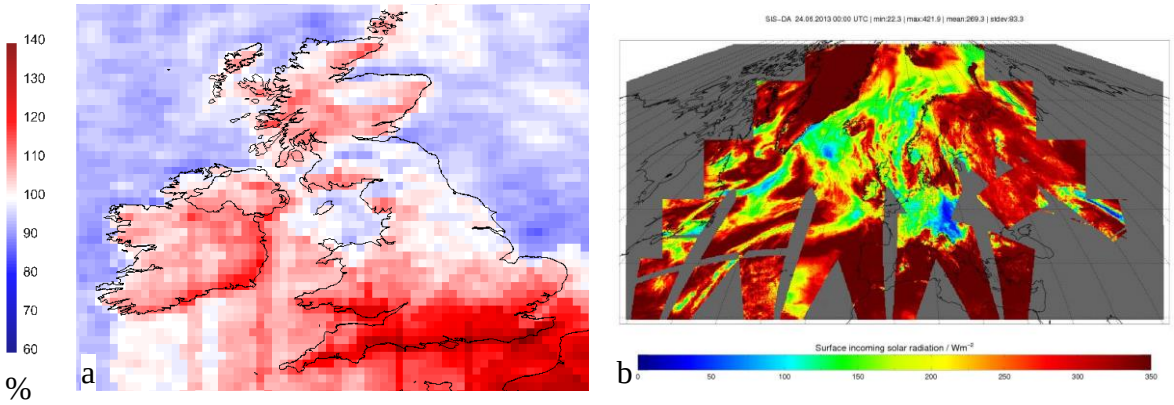

Figure 2.8 a) Map of simple difference (%) between the total sum of daily means from operational SEVIRI based SIS minus the total sum of daily means from the polar orbiting dataset CLARA for the month of June 2013. **b)** Spatial coverage of SIS retrieval from polar orbiting satellites on the 24th June 2013 (Karlsson et al. 2013).

[2] Rebekka.posselt@meteoswiss.ch
[3] reto.stoeckli@meteoswiss.ch

Through a comparison of the monthly means from AVHRR and SEVIRI for June 2013 (**Figure 2.8 a)** quantified relative differences are generally around 5 %, but the southern UK coastline experiences slightly larger differences (up to 15 %), which can be explained by the missing daily mean data due to the lower sampling frequency of the polar orbiting satellites compares to geostationary satellites. There are no daily means calculated, e.g. on 24 June 2013 (**Figure 2.8 b**). In general, northern latitudes get more frequent coverage while areas near the equator present more gaps between the swaths due to the nature of the polar orbiting track.

The satellite based datasets used for the purposes of this study are the CMSAF CDR SIS record 1983-2005 combined with the SEVIRI based record of SIS over the 2006-2010 period and where applicable and recommended by CMSAF the 2011-2012 operational dataset. To a lesser extend data for 2013 have been used from the operational SIS dataset based on a combination of geostationary and polar orbiting satellites.

2.6 The Weather Research and Forecasting (WRF) numerical model

The Weather Research and Forecasting (WRF) model is a mesoscale numerical weather prediction (NWP) system designed for atmospheric research and operational forecasting purposes and is used by more than 20000 users in more than 130 countries [UCAR, 2013]. The model has been developed through the joint efforts of National Centre for Atmospheric Research (NCAR), National Oceanic and Atmospheric Administration (NOAA), the Naval Research Laboratory (NRL), the Federal Aviation Administration (FAA), the University of Oklahoma and several other organizations in the United States and abroad [UCAR, 2013].

The WRF model used for the purposes of this study has been set and configured by Steele (2013). The model is hosted on the High Performance Computer Cluster (HPCC) at the University of East Anglia (UEA), Norwich. The simulations span over a twelve year period (01/01/2002 - 15/07/2013) and the domains covered in these simulations are illustrated in **Figure 2.9** and provided in three pre-set nested grid-spacing resolutions of 27 (d01), 9 (d02) and 3 km (d03).

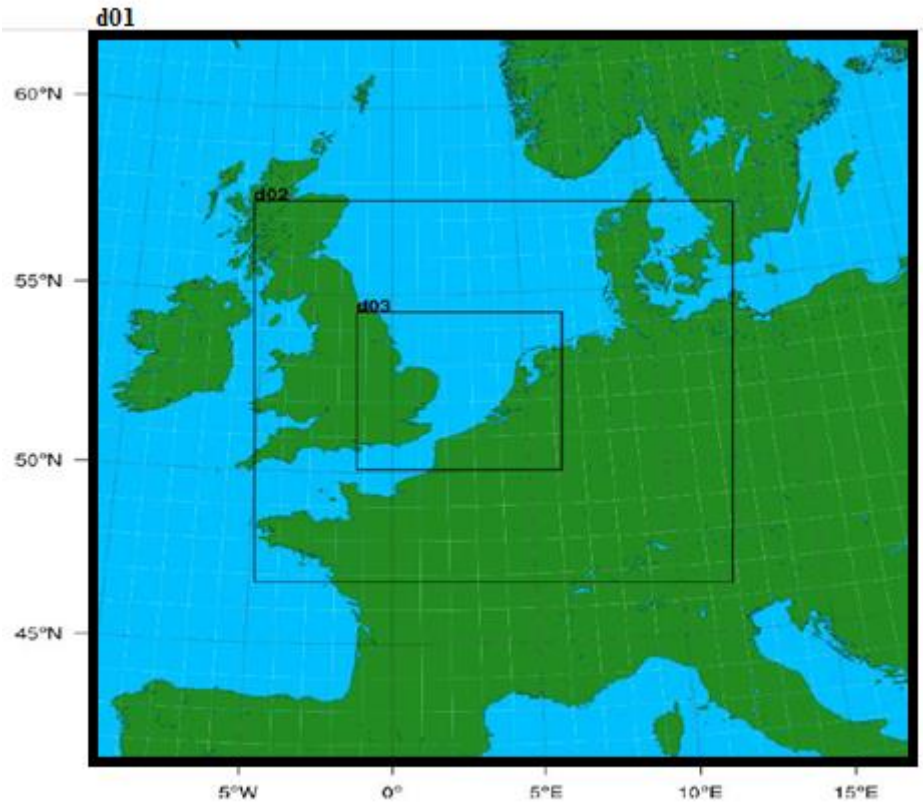

Figure 2.9 WRF model domains used in simulations. The horizontal resolutions for 27,9 and 3km domains are denoted by d01, d02 and d03 respectively (Steele 2013).

The output of these simulations has been used to derive two variables for the purposes of this study:

1) Model based SIS (variable listed as SWDOWN - Shortwave downward radiation at surface (W/m^2) in model output file repository). The model based SIS will be compared against SYNOP observations hosted in the MIDAS database and against satellite based SIS to determine which dataset (satellite-based or model-based) is more suitable to generate the climatology of SIS and more appropriate for the purposes of this study.

2) Model based two metre temperature (variable listed as T2 - Temperature at 2 metres (K) in model output file repository).

The location of the three domains was adopted from and pre-set by Steele (2013) and the d03 domain was selected for the purposes of this study since it provides higher spatial resolution compared to the other two options. One limitation of this domain (d03) however is the fact that it does not cover the whole of the UK (**Figure 2.9**). It would be preferred to use the d01

(27km) and d02 (9km) domains which include the whole of the UK, although this would significantly reduce the amount of detail available due to the coarser model grid spacing.

2.7 Analysis tools

This section describes a set of software tools which have been used largely for the manipulation, visualization and analysis of the data sets.

2.7.1 CDO

The Climate Data Operators (CDO) are command line (**Figure 2.10**) operators that were developed at the Max-Plank-Institute and were originally designed for manipulation and analysis of data produced by climate and numerical weather prediction models. There are more than 400 CDO operators which can perform simple file operations, simple statistics, arithmetic calculations, interpolation or the calculation of climate indices, regridding and other more complex file operations. CDO version 1.5.5 has been used for the manipulation of the satellite-derived data and this version supports NetCDF, GRIB and several binary formats. CDO is freely available at https://code.zmaw.de/projects/cdo and can run under UNIX/LINUX and Windows environments.

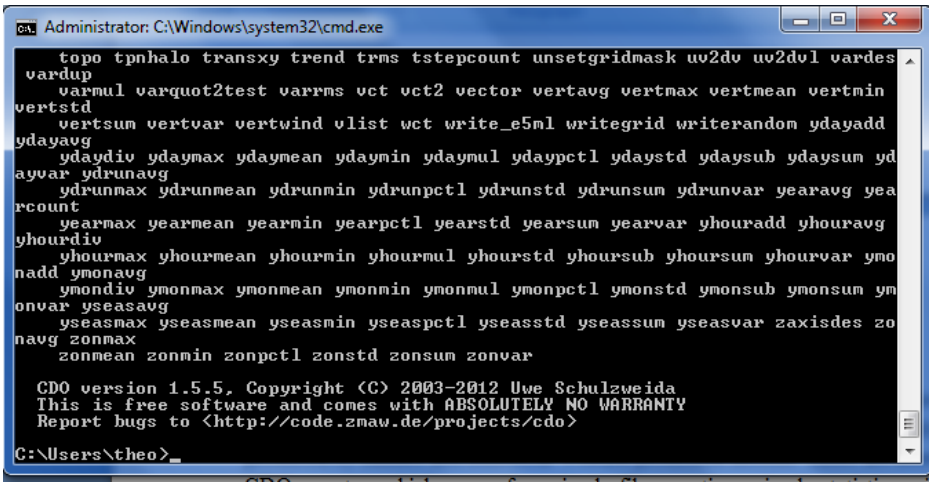

Figure 2.10 Windows based version (1.5.5) of CDO running in a command line environment.

2.7.2 McIDAS-V

The Man computer Interactive Data Access System (McIDAS; **Figure 2.11**) is a suite of sophisticated software packages that perform a wide variety of functions with satellite imagery, observational reports, numerical forecasts, and other geophysical data. In this study

version 1.4 of this program has been used for visualization purposes (e.g., **Figure 3.9**; **Figure 3.11**). McIDAS-V is freely available at http://www.ssec.wisc.edu/mcidas/software/.

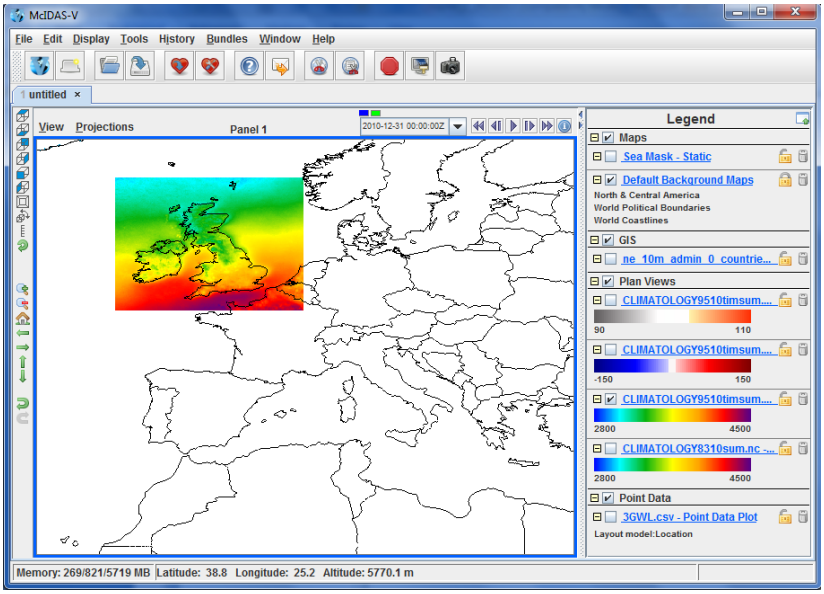

Figure 2.11 Main graphical user interface of McIDAS-V (V 1.4) in the Windows environment.

2.8 Wheat grain yield data - Recommended Lists (RL)

HGCA Recommended Lists (RL) provide information on yield and quality performance, as well as harvest results and trials information, agronomic features and market options for recommended varieties to assist growers with variety selection. RL trials are conducted under standard defined conditions that usually differ from those seen on a typical farm. Therefore any improvements in yield and quality in trials may not always be applicable to real on farm conditions due to limitations in farm management practices. [Knight et al., 2012]. When a variety enters official trials, it is allocated a unique reference number by the testing authority for this stage and it is forever associated with the variety whether or not the variety is actually still being grown and/or if the variety changes its name over the course of its life [Philpott, 2013]. A variety doesn't change its name due to an improvement; indeed while seed of a variety is being sold, tests are carried out to ensure that the variety remains the same as the original. Varieties can exist for many years but the seed may not be sold or, more likely, not selected for inclusion in RL trials as these represent the best of the varieties and not all of the varieties (Philpott 2013). For the purposes of this study, HGCA kindly provided data from RL trials extending from 1992 up to 2012, but excluding 1993.

2.8.1 Limitations

The trial data were provided in an excel spreadsheet without supporting documentation and with no coordinates. Assistance was kindly provided by Haidee Philpott and Stuart Knight from NIAB-TAG, and Paul Gosling from HGCA who supplied later the coordinates. Suggestions on the best methodology as far as correlating yields were discussed with Philpott (2013). After a thorough study, the most important information was selected. Some of the information extracted from the RL Excel file was: Wheat yields in tonnes per hectare, harvest years, variety, disease treatment, trial locations (coordinates and place names), previous crops and soil types. One desirable variable is flowering dates for each individual sites, however this information is not readily available in the provided Excel file. Due to the fact that the data from RL trials were received two months after the scheduled time, only a small part of it will be used, in order to demonstrate the power of approach (**Section 4.4**).

2.9 Weather pattern classification - GrossWetterLagen (GWL)

Grosswetterlagen (GWL) are a well-known set of European daily synoptic types developed originally by Hess and Brezowsky (1952) and maintained at the German national meteorological service or Deutsche WetterDienst (DWD) since the 1950's. Based on their method, James (2007) used mean sea level pressure (MSLP) charts and 500 hPa geopotential height fields from the ERA40 reanalyses to generate twenty-nine classification types for summer and for winter based on synoptic scale events lasting at least three days. One example of a GWL weather type (WA) is illustrated in **Figure 2.12**. GWL classification describes synoptic scale flow and subsequent effects on regional weather conditions with a focal point centred over Central Europe, as indicated in **Figure 2.13**. Although the GWL has been developed in reference to Germany, the GWL scale is closer to the true synoptic scale, encapsulating whole synoptic features, compared to Lamb weather type classification method (Briffa et al. 1990) which has a smaller scale impact . For the purposes of this study only two examples of different synoptic scale circulation regimes will be examined using the GWL types HM and WS for the months of March 2012 and July 2012, respectively.

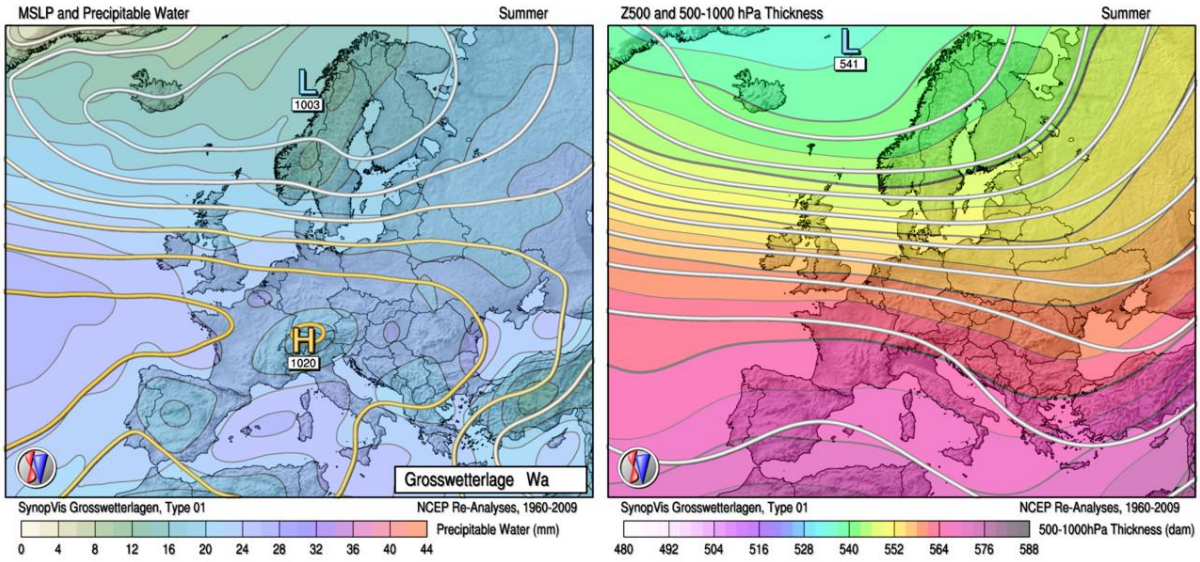

a b

Figure 2.12 a WA GWL weather type mean sea level pressure; b) WA GWL weather type mean 500hPa circulation [Taken from James, 2007].

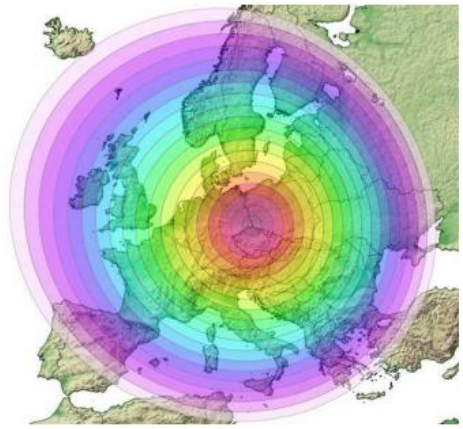

Figure 2.13 The focal point for the GWL classification method [Taken from James, 2007].

2.10 Methodology

In this Master's thesis, the adopted approach is to merge the homogeneous part of the CMSAF CDR of SIS (1994-2005) with the CDR SIS from MeteoSwiss (2005-2010) to generate a climatology of SIS over the United Kingdom and to perform trend analyses. The operational SIS cannot be used for trend analyses, but will be used to extend the analysis of SIS (actual and anomalies) for 2011, 2012 and 2013 for the grain fill season. Particular interest is focused

on 2012 as it is the year which resulted in some of the worst wheat yields of the last twenty-five years in the UK as described in **Section 1.2**. WRF model data (SW_down and 2 metre temperature) will also be used for parts of this study from 2002 onwards but the exact data will be defined according to the applications and explained later when encountered. This study will not take into account any data for 2013 for correlating yields, because a) RL data extend only up to 2012, b) WRF model climatology does not include some data for July 2013 and this will result in limitations in simulations, c) as described in **Section 2.6**, there is an eight-day gap in the operational data set of SIS. However some of the data will be used for particular applications using the polar orbiting dataset CLARA to cover carefully any gaps.

3 Results and Discussion

In order to use the WRF model output and the satellite-based data sources it is important to first verify their accuracy. The CMSAF data sets of SIS have been verified by several other users, including Posselt et al. (2011; 2012) against high accuracy surface based station observations from the GEBA and BSRN networks. Although there is no real need to repeat this process, both satellite and model based data are provided in gridded format and it is therefore relatively easy to perform a comparison in order to quantify the bias against surface station observations from the Met Office SYNOP network of observations. Time constraints meant only a limited amount of sites and years could be used for data validation. Additionally, data gaps in the daily SYNOP surface based observations are occasionally present; a manual task of locating the missing dates is applied in order to ensure more reliable comparison with satellite or model based data. Large biases in daily means can potentially imply that the data used as reference could contain missing hourly input, therefore it appears that satellite based data overestimate SIS. To demonstrate the accuracy of satellite based SIS, the year 2011 was selected due to the fact that it is based on the operational product of SIS and it is expected to have lower accuracy skills compared to the climate quality data sets of CDR SIS.

3.1 Solar radiation data verification

Satellite based SIS has been validated by comparison with surface based observations from three ground locations, Holbeach in Lincolnshire, Church Lawford in Warwickshire and Leconfield in east Yorkshire. The station observations of the first two examples have been quality checked for missing data, while the third example is presented to demonstrate that Met Office SYNOP data can contain missing or unreliable data and therefore it would take a lot of time and effort to perform verification for multiple stations and over longer periods. This also shows that any attempt to create a climatology or to use the land based SIS observations for critical applications would first require a thorough and time consuming filtering. However, all the details about the missing or unreliable data have been recorded by the Met Office in metadata and it is available for investigation if required. **Figures 3.1** to **3.4** and **3.6** show that both the satellite based data and model output present a very good correlation against station observations in the specified locations.

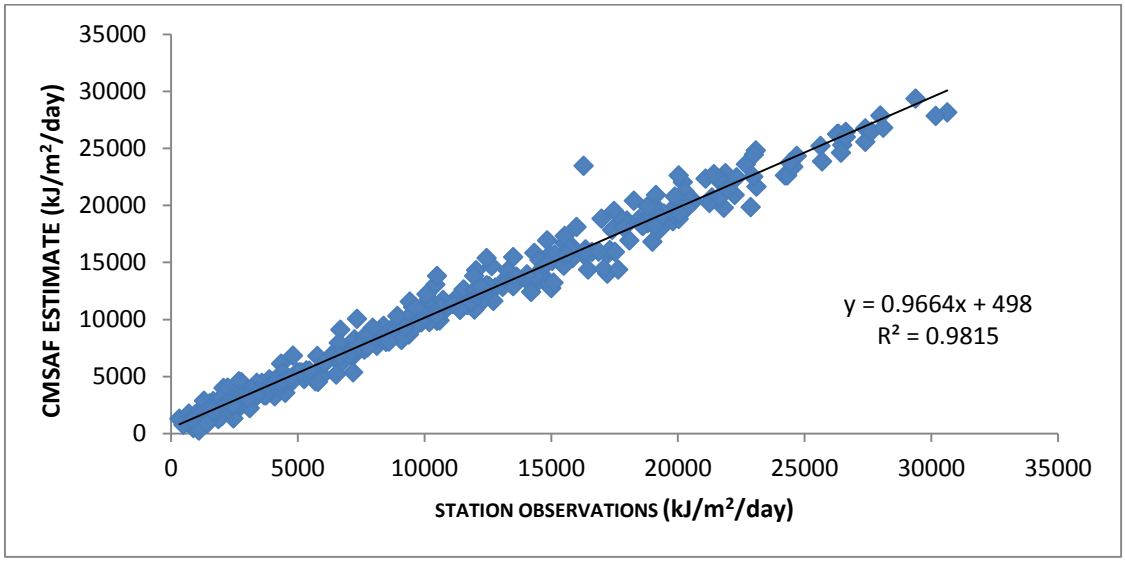

Figure 3.1 Correlation between the satellite retrieval method (Y axis) and surface based observations (X axis). The data are for Holbeach (52.48N 0.0E) from January 1st to December 31st 2011. Data are expressed in kJ/ m^2 /day.

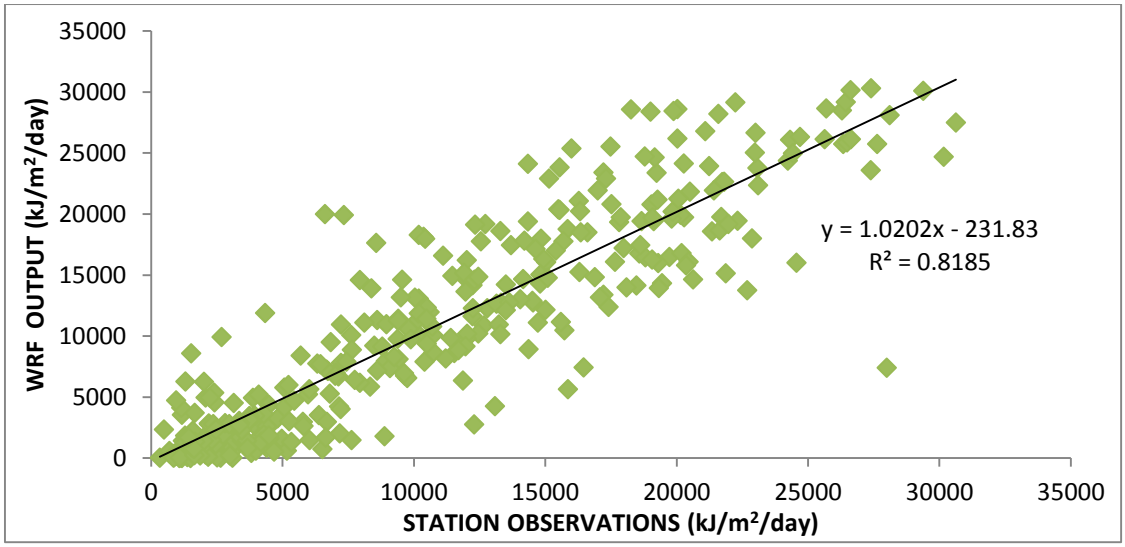

Figure 3.2 Correlation between the WRF based model output (Y axis) and surface based observations (X axis). The data are for Holbeach (52.48N 0.0E) from January 1st to December 31st 2011. Data are expressed in kJ/m^2/day.

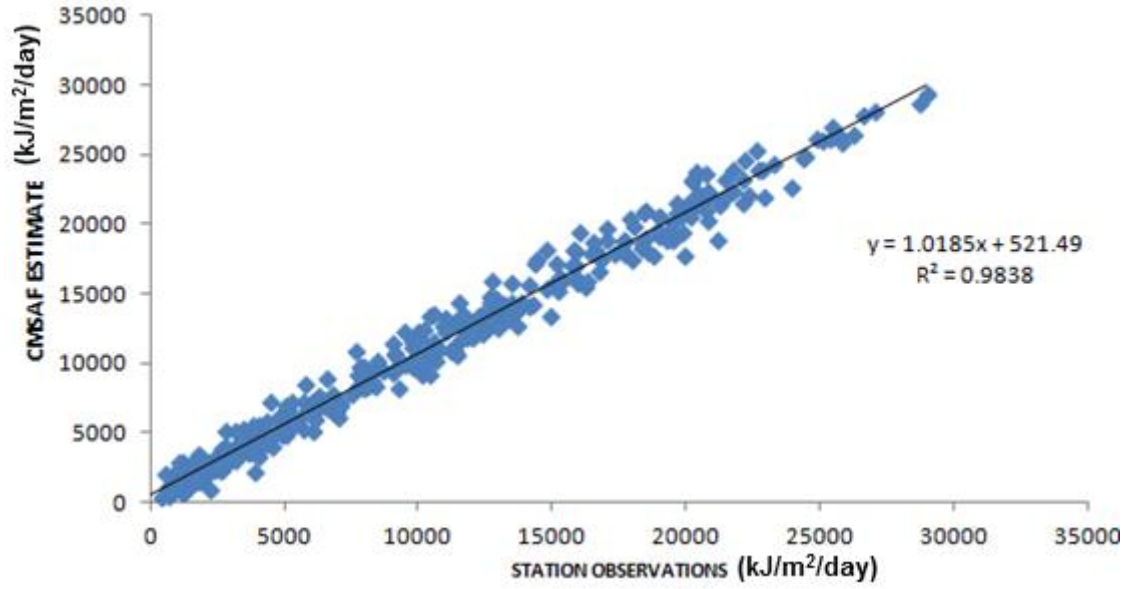

Figure 3.3 Correlation between the satellite retrieval method (Y axis) and surface based observations (X axis). The data are for Church Lawford, (52.35N 1.32W) from January 1st to December 31st 2011. Data are expressed in kJ/ m^2 /day.

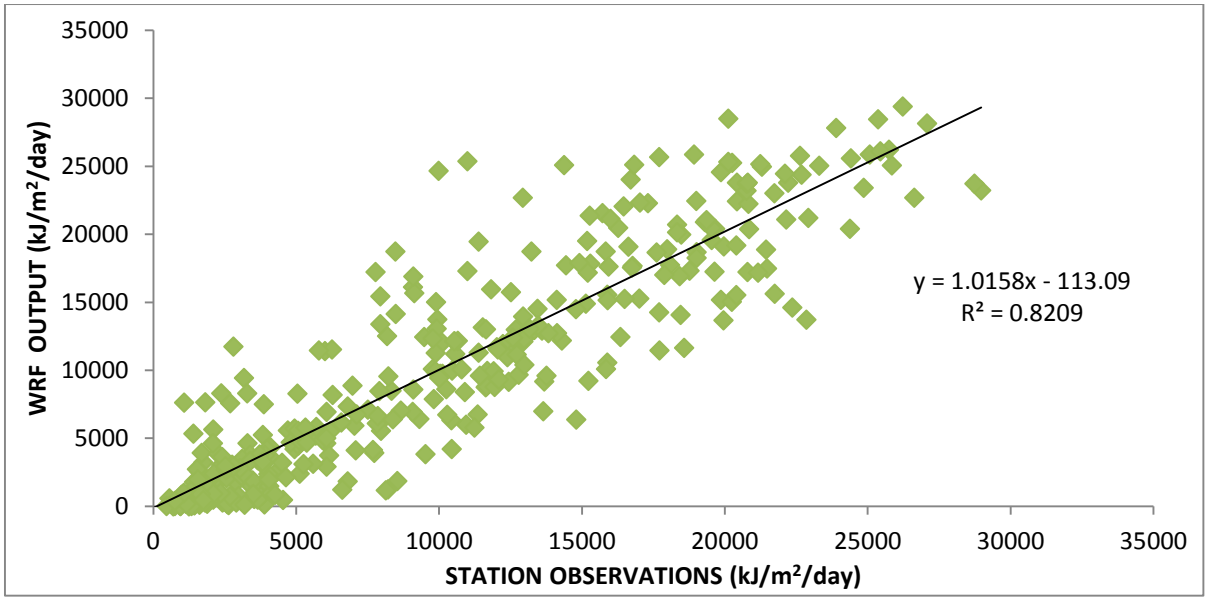

Figure 3.4 Correlation between the WRF based output (Y axis) and surface based observations (X axis). The data are for Church Lawford, (52.35N 1.32W) from January 1st to December 31st 2011. Data are expressed in kJ/m^2/day.

In **Figure 3.5** both the model and satellite based data biases are presented on a single graph extending over a period of a whole calendar year. Model based bias is much larger than that of the satellite estimate, especially during the period when land surface based convection is most active (middle of spring until the middle of autumn). This suggests that the model is having difficulty in forecasting accurately small scale atmospheric processes such as convection, due to insufficient parameterization of the atmospheric boundaries. As a result,an underestimated forecast of cloud cover can consequently lead to overestimated radiation reaching the surface.

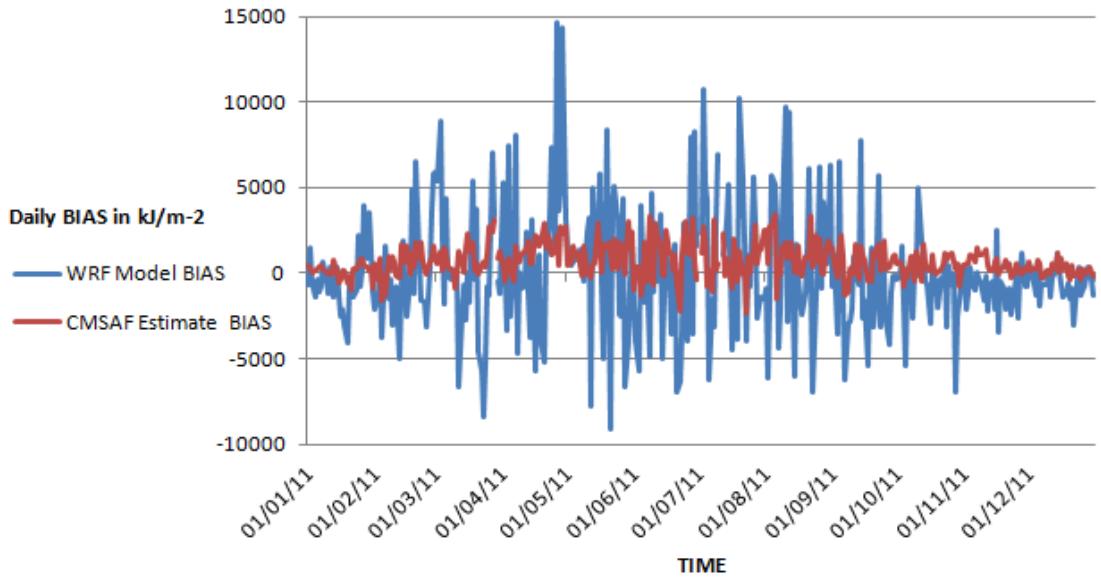

Figure 3.5 2011 daily time series of BIAS for WRF model (blue line) and satellite estimate (red line). The data are for Church Lawford (52.35N 1.32W) for January 1st to December 31st 2011. Bias expressed in kJ/m^2/day

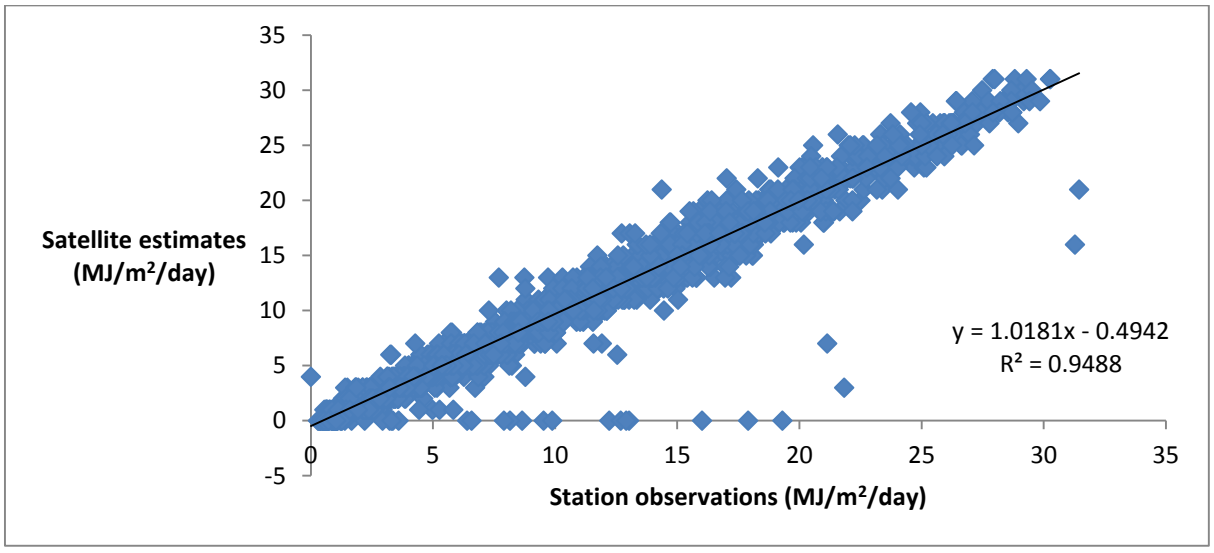

Figure 3.6 Correlation between the satellite retrieval method (Y axis) and surface based observations (X axis). The data are for Leconfield (53.52N 0.27E) from January 1st to December 31st 2003-2007. Data are expressed in kJ/ m^2 /day.

Although the correlation in **Figure 3.6** appears to be strong, several data points are presenting large deviation from the source in reference. This is due to the missing hourly data which consist the daily station based observations. The figures above indicate that the accuracy of satellite based estimates is superior to the model output, therefore only the satellite based SIS will be used for the purposes of this study (climatology, period-specific accumulations, etc.) A change in WRF model physics configuration could improve the accuracy of the output, however this would require the regeneration of the model climatology which is beyond the scope of this study.

The Mean Absolute Bias (MAB) of the daily means for the satellite based SIS (model output) is below (above) the threshold accuracy set by the Global Climate Observing System (GCOS) which is 25 W/m^2 or 2160 kJ/m^2 for the daily means. Quality metrics are presented in **Table 3.1** and compared against the results derived from the Posselt et al. (2012) study (their results are also presented in **Table 2.3** of this thesis). MAB is calculated by subtracting the mean errors of the daily satellite or model based estimates against a reference point, which in this case is a land based station (sourceA-sourceB). All the results have been converted into kJ/m^2.

Table 3.1 Statistics for the comparison of daily mean absolute bias (MAB) satellite and model based SIS compared to the results from the Posselt et al. (2012) report.

(SIS) Daily Mean	Number of days	Mean Absolute Bias (kJ/m^2)
CMSAF- Holbeach station	363	727
WRF_Model-Holbeach station	363	2641
CMSAF-Church_Lawford station	363	894
WRF_MODEL-Church_Lawford station	363	2465
CMSAF-BSRN	28674	1341
HelioClim-BSRN	28674	3014
ERAint-BSRN	28674	2321
GEWEX-BSRN	28674	1979
ISCCP_BSRN	28674	2300

The target accuracy is therefore achieved for daily means. Unfortunately the satellite-based MVIRI and SEVIRI instruments are sensing in slightly different wavelength bands compared to ground based pyranometers therefore the produced output of SIS from these sources are not necessarily comparing like-for-like variables as illustrated in the scatter plots above (**Figures 3.1; 3.3; 3.6**).

3.1.1 Case study – Comparing model derived SIS against satellite based SIS total accumulations

Both daily satellite and model based data are in a gridded format therefore a comparison can be performed for the assessment of performance. However as both data sources are in different formats and projections it was not possible to easily perform computational calculations in order to derive a single figure showing the bias, therefore the assessment is carried out using a visual approach.

The comparison is performed for a 42 day period starting on the 10th of June for both 2006 and 2012 (**Figure 3.7**), which approximates the average wheat 'grain fill' period and length. Both 2006 and 2012 were selected as these have been analysed as the most extreme periods within 2002-2012 record (available for both modelled and satellite based SIS) across England, representing the lowest and highest recorded SIS accumulations. The analysis is restricted to England as it the area for which the 3 km horizontal spatial resolution WRF model data are available for the purposes of this study. It appears that in both years, the model based estimate accumulates higher amounts of SIS compared to the satellite based estimate, although the spatial patterns are similar.

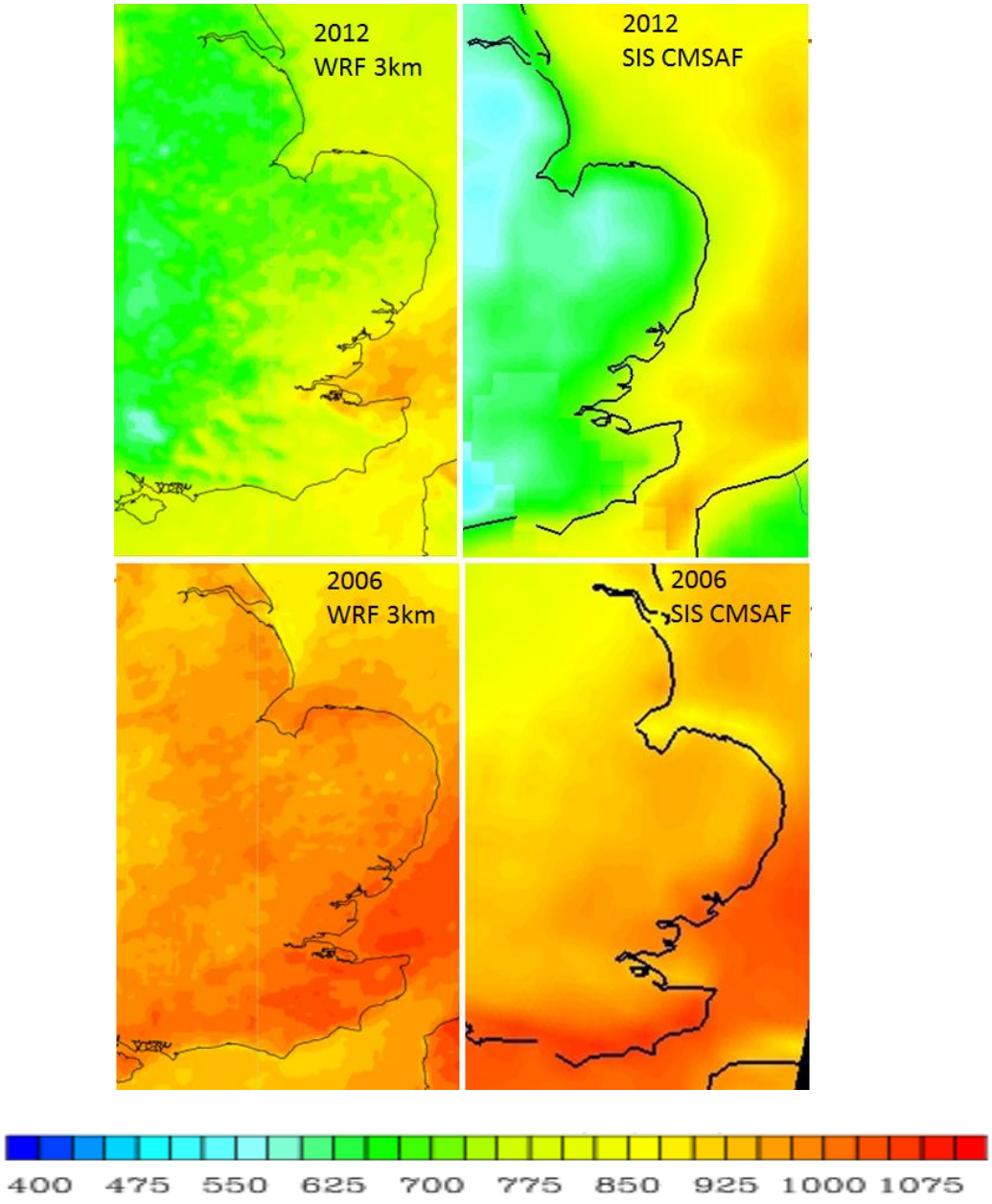

Figure 3.7 Total incoming shortwave solar radiation (MJ/m^2) for the period 10th June – 21st July 2012 (top left WRF model output, top right satellite based SIS). Total incoming shortwave solar radiation (MJ/m^2) for the period 10th June – 21st July 2006 (bottom left WRF model output, bottom right satellite based SIS).

The inter-comparison of model analysis and satellite based observations indicates that the latter present lower biases when compared against land based observations, therefore these are used for the purposes of this study with regard to SIS accumulations. However, model

based SIS has the distinct advantage of simulating on demand SIS for periods when satellite observations are not available. In this case, NWP model analysis provides a complete spatial and temporal data coverage, but lower accuracy as compared to in-situ observations and satellite estimates. Satellite estimates present a comparable accuracy to in-situ measurements, long data record, but occasional data gaps due to satellite maintenance. It is important to mention that it is not anticipated that the satellite retrievals or WRF hindcast must exactly fit observations, since spatial representations are distinct. Satellite and model based gridded data represent a broader area (pixel/domain resolution) while ground based observations are site-specific. However, results show a good agreement between retrievals from satellite, model output and observations (correlation greater than 0.9 for satellite and higher than 0.8 for model output).

Furthermore Hakuba et al. (2013) in their research, showed that site-specific station observations even from the high accuracy GEBA and BSRN station sites are not always representative of the area covered by the CMSAF datasets (**Figure 3.8**) and this can result in a higher bias when compared to spatially averaged satellite-based estimates. This is also one of the reasons why, for the purposes of this Master's research, the author decided not to perform a more extensive verification as this would require an examination of the Met Office SYNOP stations representativeness compared to the area covered by the satellite-based instruments or the WRF model output.

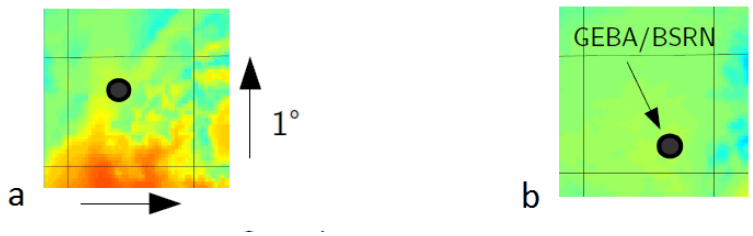

Figure 3.8 a) Site not representative for grid cell as it contains high sub-1°-grid variability. **b**) Site representative of the 1°-grid as the spatial variability inside the grid is low. **[**Taken from Hakuba et al., (2013)**]**

Since in this research, the interest is focused on the magnitude of total accumulations of SIS over user-specific periods, it is vital to compare the total amounts of SIS as estimated by the

satellite instruments against land based station observations. The quality of the CMSAF data sets of SIS is such that they are often used as reference to land based station observations [Trentmann, 2013]. A comparison of the sums of SIS over a user-specific period is illustrated in **Figure 3.9** and has been used as input in an experimental case study upon the request of Jim Orson of the National Institute for Agricultural Botany (NIAB) [Orson, 2013]. The request was to use a source of measurement which could verify the accuracy of the land-based station observations used in the agricultural industry. The request was made upon the assumption that one of the industry stations was constantly recording unrealistically low daily accumulations of SIS compared to others in the surrounding area. The knowledge gained from this research showed that all six stations (**Figure 3.9**) that are operated by the Met Office are quite close to the satellite estimates (deviation +/- 2%) while the NIAB-Cambridge station operated by WIN (Weather Innovations Consulting LP) present much lower values (165 MJ/m^2) with an error estimate of around 20-25%.

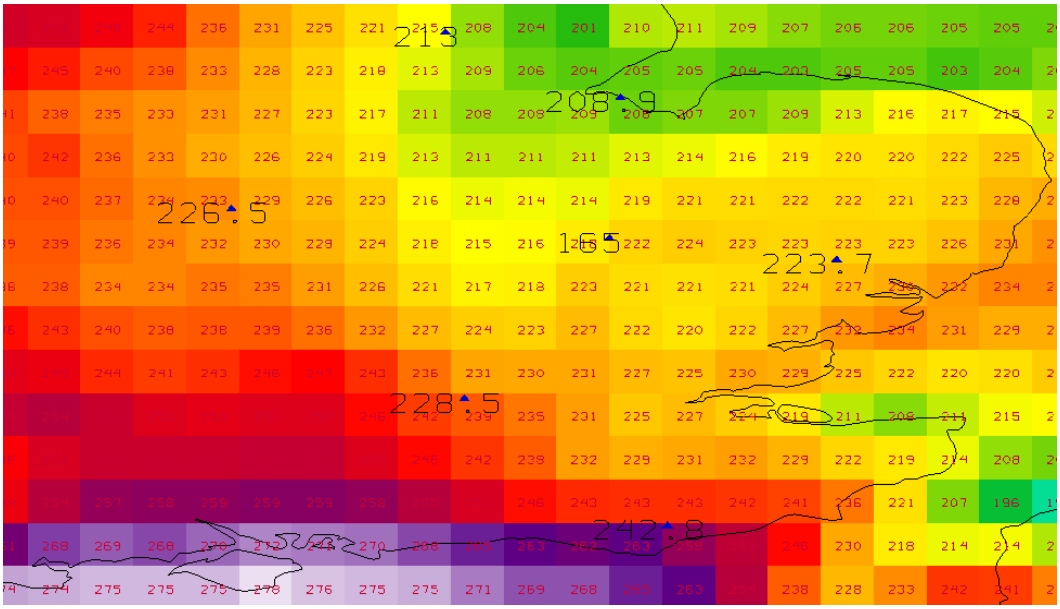

Figure 3.9 Total accumulations of SIS for the first ten days of June 2013. Blue triangles indicate the locations of the surface based stations and the total accumulations over these ten days in these locations expressed in MJ/m^2. Values inside the grid squares indicate the total accumulations using satellite-based estimates of SIS (MJ/m^2).

3.2 Model temperature data verification

The WRF model derived temperature data used for the purposes of this study in order to calculate the length of the grain fill period, have been verified by Steele (2013) in his PhD thesis (Chapter 4, pages 125-132) against the temperature observations from the Cabauw tower and the Egmond aan Zee meteorological mast located in the Netherlands. His main finding was that his configuration of the WRF model underestimated the temperature by about 1-2C. The overall temperature under-estimation will therefore lead to an over-estimation of the length of the grain fill period and this bias will be present in all years. However, in terms of overall performance these data are safe to use for the purposes of this research and therefore an independent validation is not repeated in this study.

3.3 Satellite-based Surface Incoming Shortwave (SIS) solar radiation climatology over the UK

As expected from the **Section 1.4** of this study, the mean annual sum of SIS, also known as global radiation, follows a south to north decreasing trend. An expected north to south increasing trend over the North Sea, uninterrupted by topographic features, while over the land the influence of topography is noticeable. Southern parts of the UK revealed a mean annual sum of SIS over the period 1983-2010 of about 4200 MJ/m^2/year with the Channel Islands taking the lead with about 4400 MJ/m^2/year. On the other hand, north-west Scotland was peaking at 3400 MJ/m^2/year while the Northern Isles had a mean annual sum of 3200 MJ/m^2/year. The southern parts of the UK normally receive higher annual total accumulations and the further north the lower it becomes (**Figure 3.10 a**). There is also a strong orographic influence depicted over the elevated areas of the UK (**Figure 3.10 b**). Topography plays an important role in the amount of SIS reaching the Earth as it contributes to the development of cloud (orographic lifting effect) and potentially to cloud reduction to the lee of the high ground. As a result, areas in the foothills of the Pennines and the Scottish Mountains receive lower SIS due to increased cloud extent, while the opposite happens to the east of these mountain ranges, taking into account that the predominant wind direction in the UK is from the west- southwest.

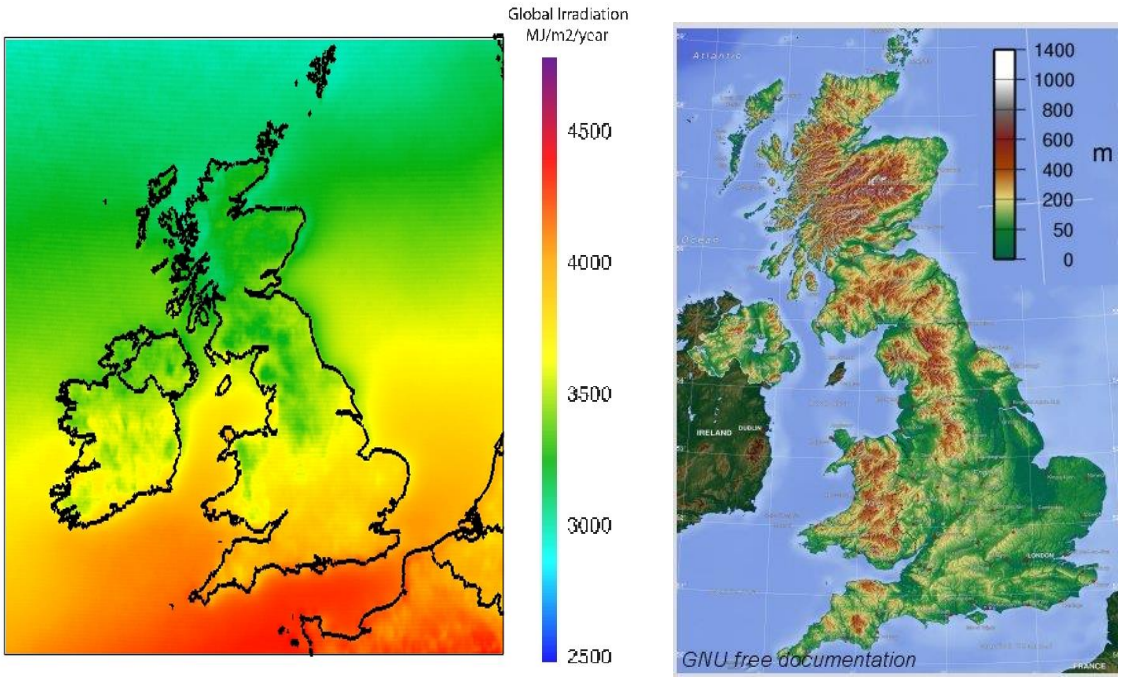

Figure 3.10 a) Mean annual sum of SIS (MJ/m^2) based on MVIRI+SEVIRI (1983-2010) **b**) UK terrain [Taken from Withnature.co.uk (2014)]

The satellite based climatology of SIS reveals that the mean annual sum of SIS follows a predictable north to south increasing trend over the North Sea, uninterrupted by topographic features. The analysis of spatio-temporal variability of SIS both over land and sea can also reveal the mean atmospheric circulation of large areas of the UK, based on the spatial distribution of SIS during specific periods. However, this concept becomes more obvious when the analysis is restricted to summer months when the daily mean SIS reaches a maximum and can contribute to larger diurnal temperature ranges between the sea and the land. **Figure 3.11** presents the inter-annual variability of the SIS sum for each year over the period 1983 to 2010 highlighting the magnitude of the spatial and temporal variability.

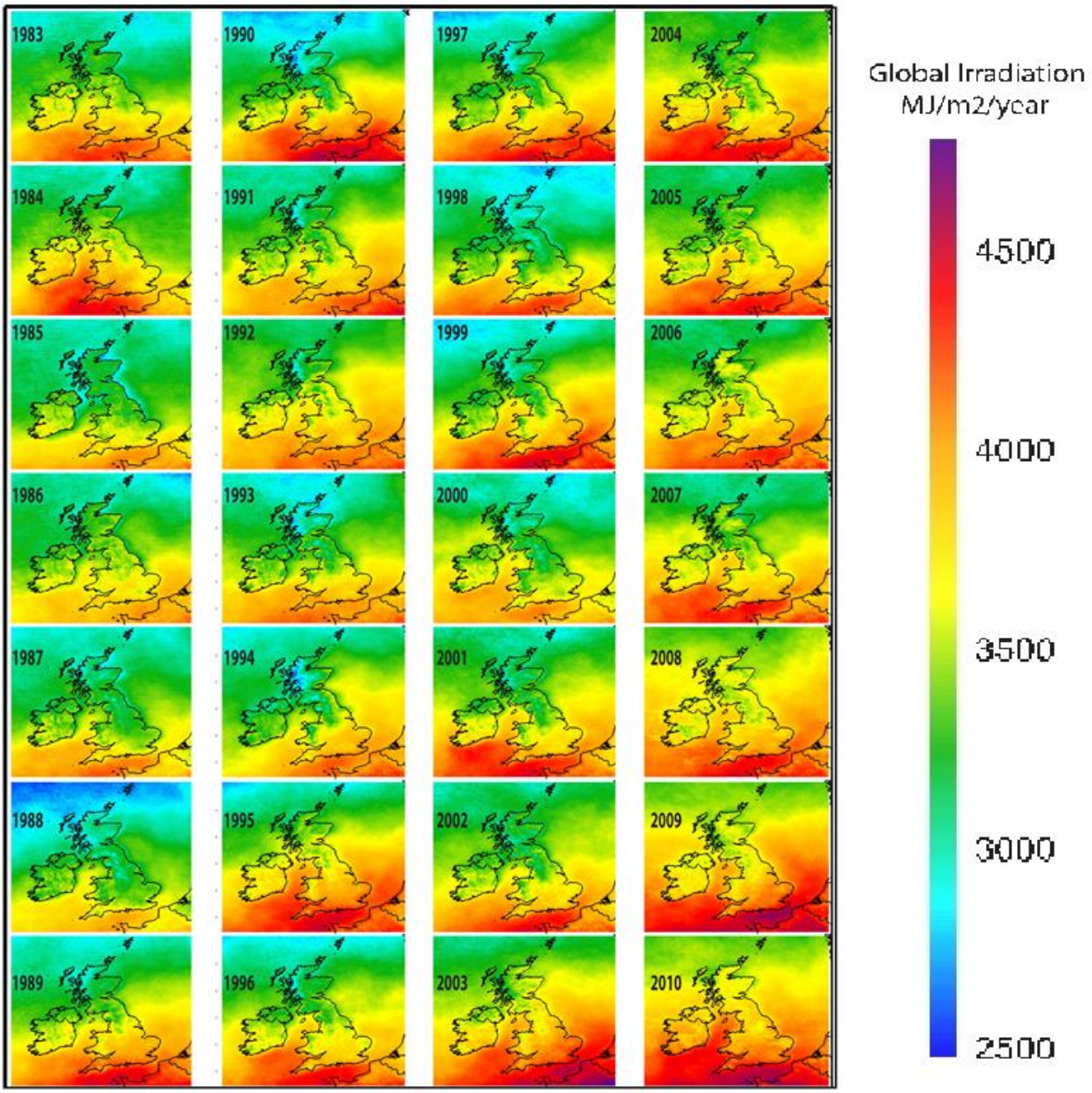

Figure 3.11 Annual sum of SIS (MJ/m^2) for each year since 1983 up to 2010, based on MVIRI+SEVIRI.

The inter-annual variability of SIS was visually assessed for each individual year over the 1983-2010 period and the results revealed that year 1988 yielded the lowest mean of SIS over the whole 28 years of record across far northern Scotland and the Northern Isles with Shetland yielding about 2600 MJ/m^2/year that particular year (**Figure 3.11**). Meanwhile, 2003 and 2009 were the years which led to a maximum annual sum of SIS across much of southern

England with the Channel Islands peaking at about 4600 MJ/m^2/year. These results (**Figure 3.11**) clearly demonstrate a significant spatio-temporal variability of the inter-annual SIS.

3.3 Comparisons with existing climatologies

The generated climatology of satellite-based SIS (**Figure 3.12)** is compared to the climatology of interpolated surface based observations from the UK Met Office (**Figure 3.13**). Although the length of the averaging period is different in between the methods, it appears that both methods present similar results in terms of magnitudes. The detailed color coding and the higher spatial resolution of the satellite-based data provide higher detail in terrain and coastal effects. Color scale ranges have been adapted to allow a better discrimination of the spatial characteristics of SIS distribution across the UK domain. Terrain features like mountains and coastal zones become noticeable due to the complete availability of information over both the land and across the sea, compared to the land based station network of observations. Satellite derived estimates over the seas allow the user to study the predominant weather pattern as a function of land-sea interactions in spatial distribution of the SIS during specific, user-defined periods. The effect of the weather pattern variability will be discussed in **Section 3.6** of this thesis.

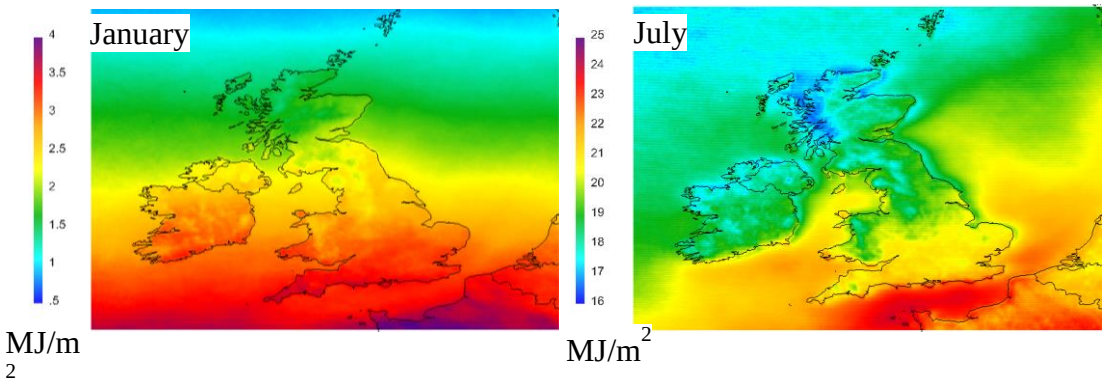

Figure 3.12 Mean SIS daily global irradiation (MJ/m^2) for the months of January and July based on the averaging period 1983-2010.

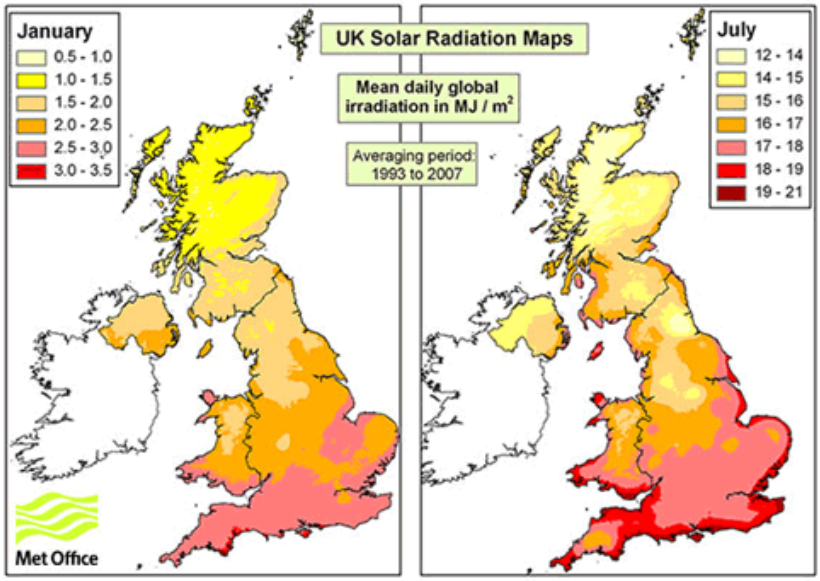

Figure 3.13 Mean daily global irradiation in MJ/m^2 for January (left) and July (right) over the averaging period 1993-2007, based on interpolation of surface station observations [Met Office, 2013]

Furthermore, the generated satellite based climatology (1983-2010) is compared against other datasets which are derived with a more sophisticated method using as input the same data as used in this study, but additionally applying terrain correction to account for potential shading, increasing the resolution to 1 km (PVGIS; **Figure 3.14**) and even up to 90m (Solargis; **Figure 3.15**). These datasets require enormous computational capabilities and storage therefore increasing the costs of generation and maintenance of these data/systems transferring the costs to the potential user/client. In the following examples it is shown that there are no significant differences in the magnitude or the spatial distribution orientation when compared to the combined MVIRI+SEVIRI (for the purposes of the comparison only, this dataset is referred as CLIMASIS).

Figure 3.14 Average annual sum of SIS (1998-2011) on horizontal and optimally inclined surface. The map is generated by JRC including as input satellite data from CMSAF. Data values are given as kWh/m^2, but the same colour scale also represents potential solar electricity [kWh/kWp] generated by a 1 kWp system per year with photovoltaic modules mounted at an optimum inclination and assuming system performance ratio 0.75. [Taken from PVGIS (2013); Suri et al., (2007); Huld et al., (2012)]

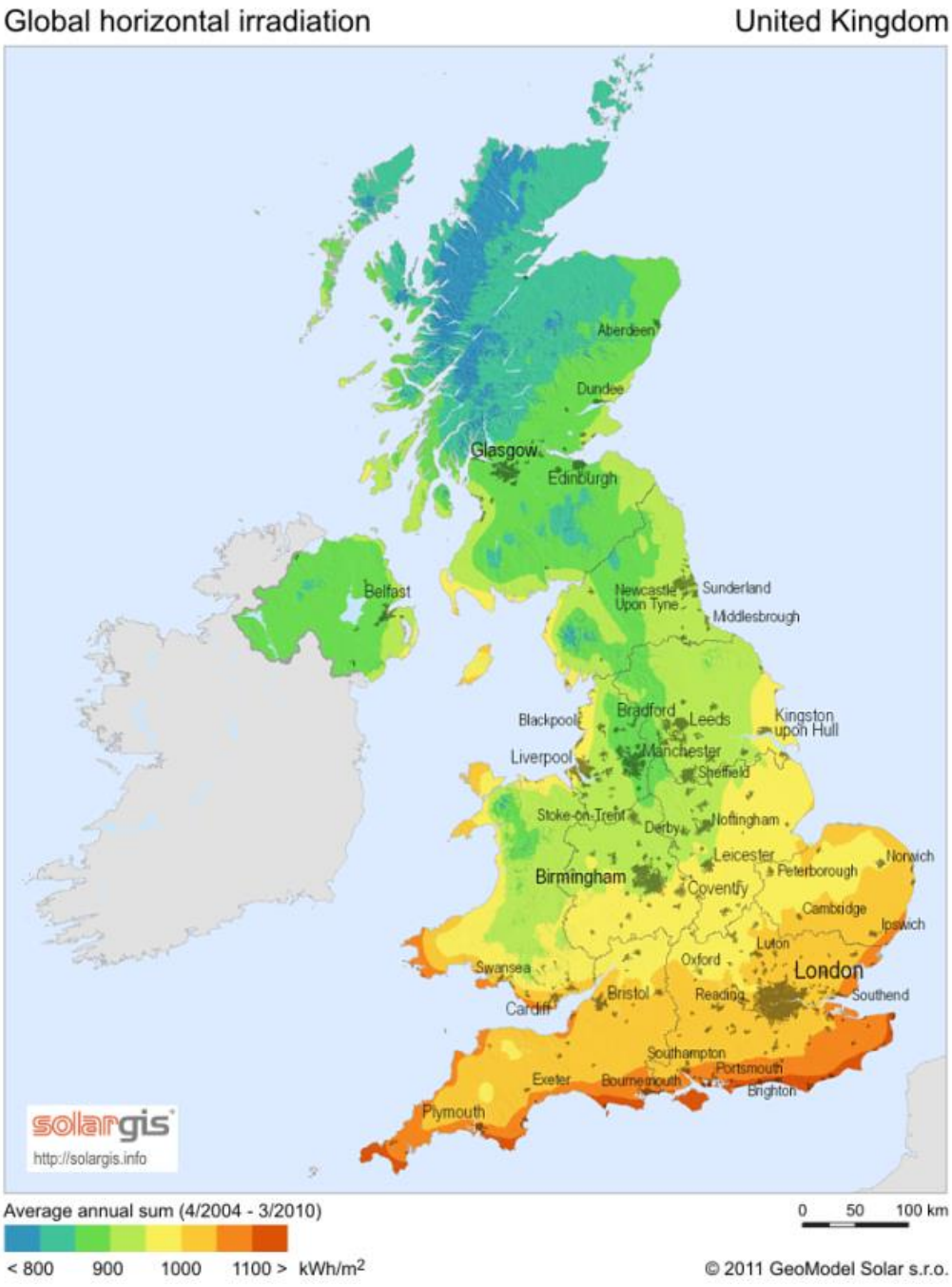

Figure 3.15 Average annual sum of SIS in kWh/m^2 (4/2004 - 3/2010) generated by Solargis including as input satellite data from CMSAF [Taken from Solargis, 2013]

The main advantage of the combined MVIRI+SEVIRI dataset is the long record of daily estimates dating back to 1983 with a large part of it (1994-2010) is currently the longest available, satellite-based homogeneous climate data record of surface solar irradiance and therefore suitable for any trend analysis [Trentmann, 2013]. **Table 3.2** presents the

specifications of other satellite based (some including additional input data) datasets. Solargis and Meteonorm are operating on a commercial basis while the others are freely available.

Table 3.2 Comparison of the generated CLIMASIS dataset against other solar data sources. [Source: http://solargis.info/doc/119 accessed and modified 28th August 2013]

	SolarGIS	Meteonorm	NASA	NREL	PVGIS-CMSAF	CLIMASIS (new)
Input Data Source	Satellite	Ground Stations (+ Satellite)	Satellite	Satellite	Satellite	Satellite
Geographical coverage	Global	Global	Global	Americas, Africa, South Asia and China	Europe, Middle East and Africa	Europe, Middle East and Africa (currently UK)
Uncertainty in annual GHI values	2 % to 7 %	2 % to 22 %	Unknown	Unknown	Not provided	Not provided
Spatial Resolution	up to 90 x 90 m	Interpolation	110 x 110 km	40 x 40 km	1 x 1km	3 x 3km
Time Resolution	15/30 minutes	Monthly	Monthly	Monthly	Monthly	Daily
Time Period	1994/1999 to Present	1960 to 1991	1983 to 1993	1985 to 1991	1998 to 2011	1983-2005 MVIRI (CMSAF 2013) + 2006-2010 SEVIRI [MeteoSwiss,2013] + to present (CMSAF)
	(18+/13+ years)	1995 to 2005 (32+10 years, irregularly distributed)	(10 years)	(6 years)	(14 years)	(28 years)
Availibility of recent data	Yes	No	No	No	No	Yes

3.5 Testing Hypotheses & Objectives

3.5.1 Inter-annual variability (1983-2010)

The year-to-year variability of the annual mean solar radiation is an important metric for estimating potential risks in predicting yields of solar radiation accumulations for use in specific applications and it is therefore included in this thesis. To evaluate the stability and the profitability of a photovoltaic (PV) investment, we first need to monitor the variability of the solar radiation both spatially and temporally to identify areas most suitable for a PV investment. P90 is the level of annual average daily SIS that occurs 90% of the time and is a popular metric in the solar energy industry for estimating expected solar PV project performance and associated revenues [Zempleni et al, 2010]. A P90 value of 3000 MJ/m^2 means that 90% percent of the time the annual SIS accumulations exceed 3000 MJ/m^2.

Similarly, a P10 value or the 10th percentile of probability of exceedance indicates that there is a ten percent chance of exceeding the values shown. The spatial distribution of the P90 values (**Figure 3.16**) looks very similar to the mean annual climatology (**Figure 3.10**), although quite reasonably as expected, with lower values when it comes to magnitude. 90% of the time, the annual solar radiation accumulation is higher than the values shown in **Figure 3.16 a**. **Figure 3.16 b** illustrates which areas experienced the lowest and the highest inter-annual variability of SIS over the 1983-2010 period. This result indicates how much the SIS accumulations can vary from year to year based on the 1983-2010 time record and derives useful results for the security and the stability of a PV power plant. The standard deviation of the mean annual sum of SIS over the 1983-2010 period (**Figure 3.16 b**) quantifies the variability to about 3-5% across the English Channel and much of south-western UK, while the rest of the UK ranges from about 5 % to 7% and with the Scottish Mountains peaking at about 9%.

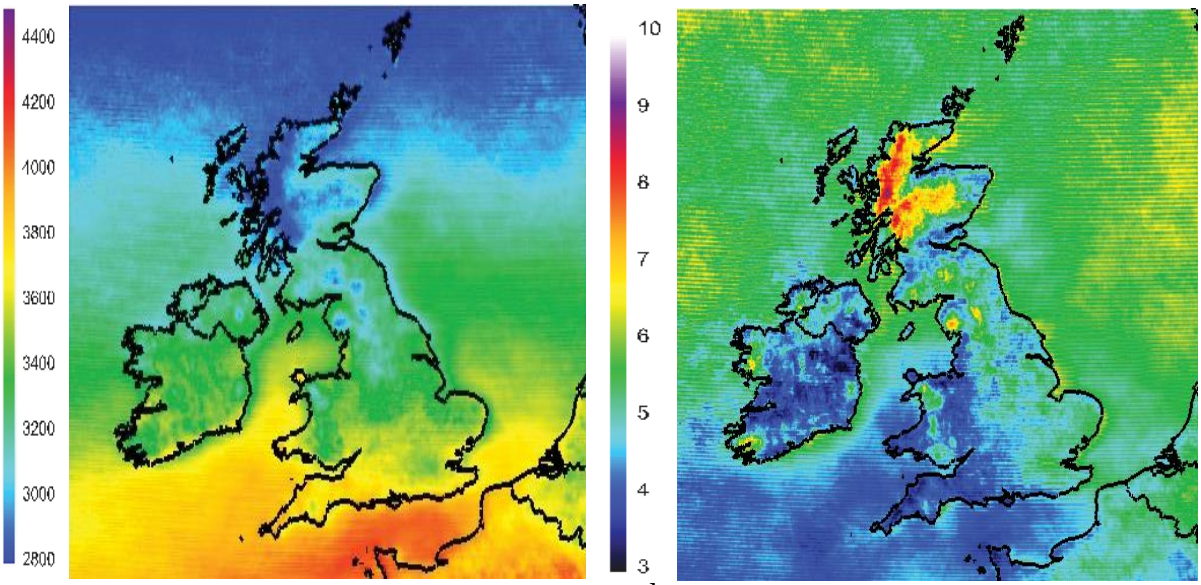

a b

SIS (MJ/m2) Standard deviation (%)

Figure 3.16 a) P90 of the mean annual sum of SIS averaged over the period 1983-2010. **b**) Relative standard deviation of the annual sum expressed as a percentage of average over the 1983-2010 period.

The spatio-temporal characteristics of SIS across the UK is mostly a result of the cloud circulation altered by local terrain characteristics. In the next step an analysis will be performed to simulate trends in SIS in inter-annual scale.

3.5.2 Trends

The approach introduced by Sanchez-Lorenzo and Wild (2012) in **Section 1.1.6** to derive trends in SIS over Europe for the period 1994-2005 using the SIS data from CMSAF is repeated in this study, but this time focusing over the UK domain for the period 1994-2010. For the 1994-2010 period the mean linear trend of SIS for the whole window (**Figure 3.17**) is 7.25 W/m^2/decade. It appears that the spatial characteristics of the mean decadal trends for the 1994-2010 correlates nicely with the result of Sanchez-Lorenzo and Wild (2012) based on the 1994-2005 period (**Figure 1.12**). Regarding the trends observed during spring for the whole window and during summer for the Scottish Highlands in particular as presented in the following figures (**Figures 3.18 b** & **3.18 c**).

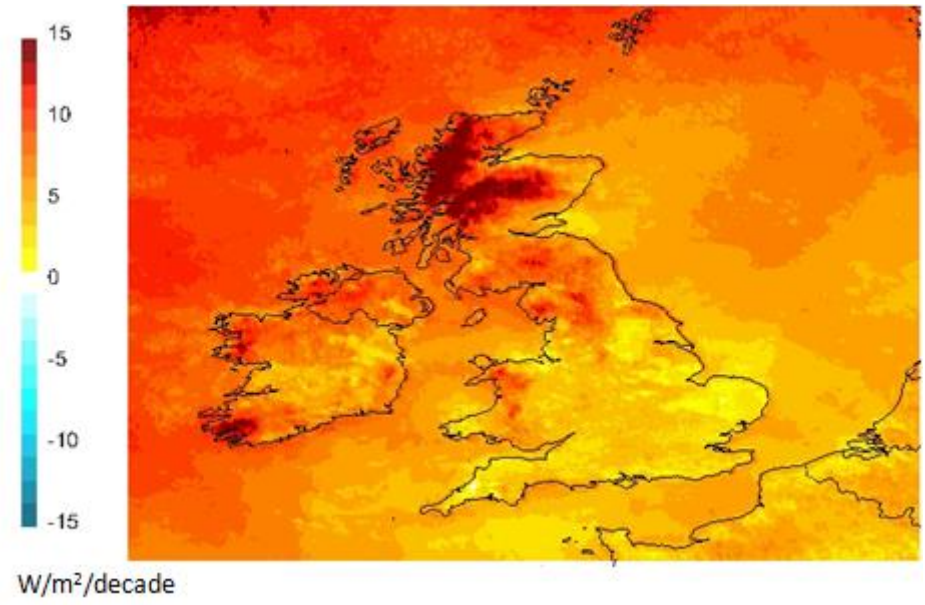

Figure 3.17 Linear trends (W/m^2/decade) of the satellite-derived SIS based on the annual series from the CMSAF over Europe during the period 1994-2010.

The seasonal trends over the period 1994-2010 appear in **Figure 3.18** and exhibit interesting variations from season to season and region to region.

The winter season (**Figure 3.18 a**) presents a mean trend value of + 0.72 W/m^2/decade over the whole domain with eastern parts of England facing small negative trends compared to western parts of Britain which present small positive trends.

Spring seasonal trends (**Figure 3.18 b**) exhibit positive trends for the same period over the whole domain leading to a spatially averaged trend of + 12.29 W/m^2/decade. It is noteworthy to mention that the largest increase of spring season SIS appears over the higher terrain UK areas such as the Pennines, the Welsh Mountains, the western hills of Ireland and the Scottish Highlands. One might hypothesize from this that, compared to long term averages, there has been less influence of Atlantic air masses during the period 1994-2010 in the spring season. It would be an interesting result to look at associated NAO behaviour to see if this is true, however this is beyond the scope of this research.

Trends for the summer season (**Figure 3.18 c**) present a similar spatial representation for the period 1994-2010 as for the 1994-2005 which was presented earlier in **Section 1.1.6.1** of this thesis, although with increasing positive trends when the record is extended to 2010. An interesting result is the fact that the whole of Wales along with central and southern parts of England observe negative trends compared to the northern parts of Britain which present "brightening". The mean field trend for the whole domain illustrated in **Figure 3.18 c** is in the order of + 7.77 W/m^2/decade for the summer season.

The autumn seasonal trends represent a general "brightening" over the 1994-2010 period across the whole domain illustrated in **Figure 3.18 d** with a mean positive trend of + 5.44 W/m^2/decade.

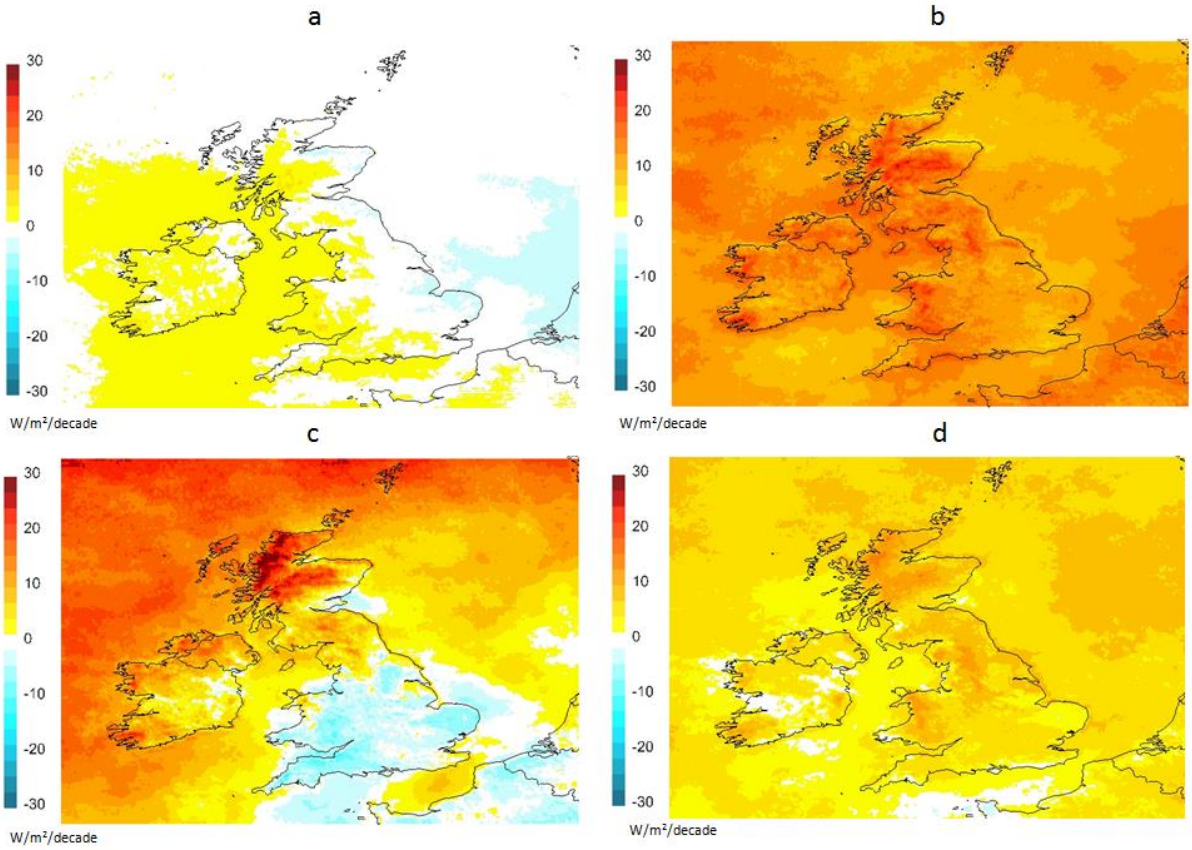

Figure 3.18 Linear trends (W/m^2/decade) of the satellite-derived SIS annual series from the CMSAF over Europe during the period 1994-2010 for winter (**a**), spring (**b**), summer (**c**) and autumn (**d**) series.

It is noteworthy that only monthly-varying climatological aerosol information has been used in the SIS algorithm and the trends can therefore be attributed to changes in clouds (changes in cloud physical/optical properties or changes in atmospheric circulation influencing the likelihood of cloud development). By working with high quality, daily satellite-sensed SIS data, period-specific surface solar radiation accumulations can be generated for applications to specific research problems. The effect of varying synoptic scale daily circulations is analysed in the following section.

3.6 The impact of weather typing

3.6.1 GrossWetterLagen (GWL)

The magnitude of the daily surface solar radiation flux follows a predictable seasonal cycle. However, superimposed on this cycle is the impact of day to day weather variability which, as a result of spells of particular synoptic weather types, can lead to anomalous periods of solar energy accumulation on the timescale of days-weeks with associated impact, for example, on agriculture when it coincides during crucial crop growth stages.

Through a combination of daily derived synoptic weather types [Grosswetterlagen; James, 2007] and satellite-based solar radiation monitoring, the extremes of surface solar radiation accumulation over the UK have been quantified in this thesis and the key associated atmospheric circulation patterns have been identified, as follows.

3.6.2 Case study - The impact of synoptic-scale weather variability on surface radiation accumulation

Weather pattern variability and persistence have the potential to strongly influence accumulations of surface solar radiation over periods of days to weeks. Such variability can have important impacts on electricity markets and on agricultural production when it coincides with critical crop growth phases. Here the focus is on the months of March 2012 (**Figure 3.19**) and June 2012 (**Figure 3.20**), which saw the strongest positive and negative solar radiation and sunshine duration anomalies in the year 2012 [Gkousarov et al., 2013; MetOffice (2013b)].

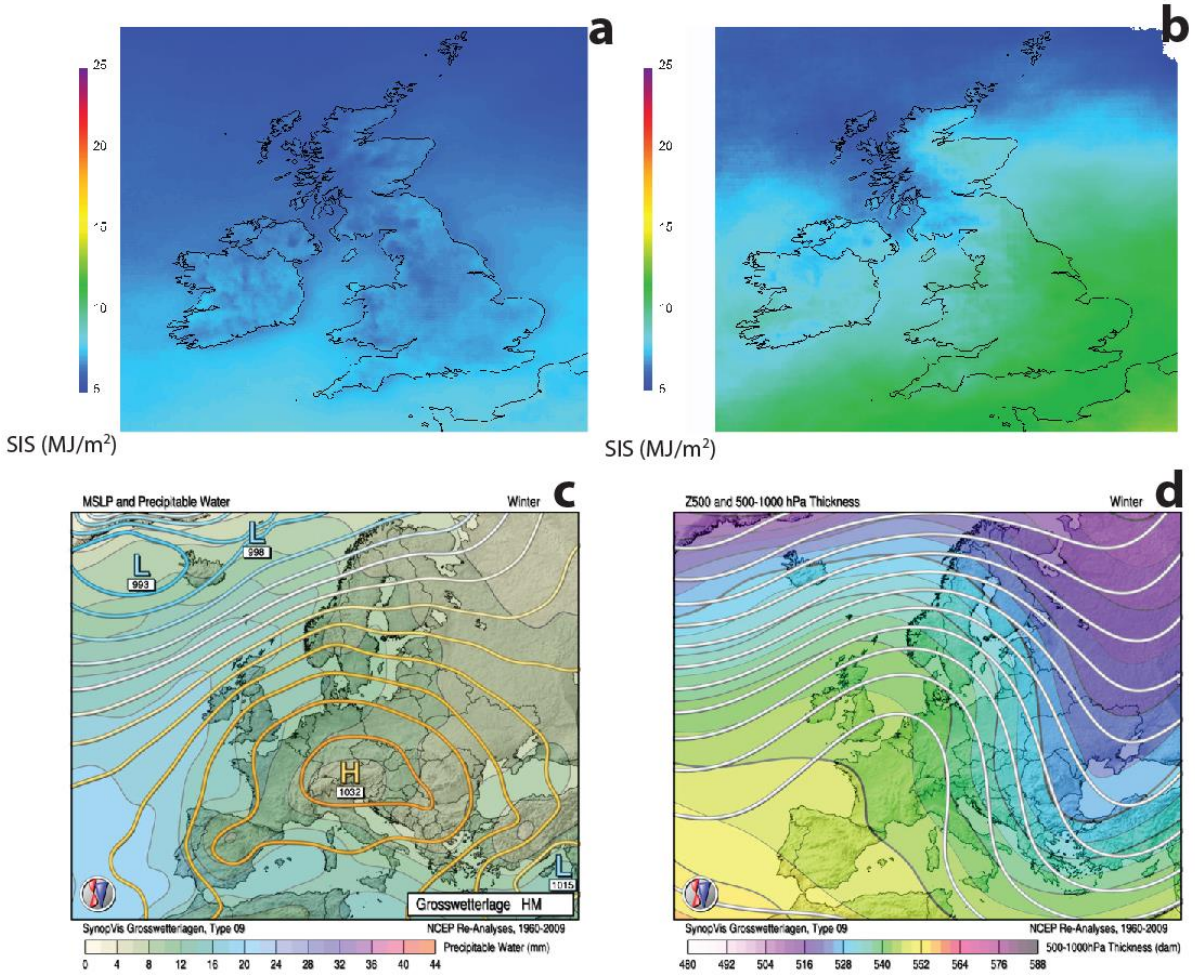

Figure 3.19 **a**) Average daily March SIS based on 1983-2010 data; **b**) the average March SIS for all those March days (48) over the 1983-2010 record classified as experiencing the HM GWL weather type; **c**) HM GWL weather type mean sea level pressure; **d**) HM GWL weather type mean 500hPa circulation).

The HM weather type (evident 48 days in total for the month of March based on the 1983-2010 period) is dominated by an area of surface high pressure centred over Central Europe (over the Alps) with an upper ridge extending across the British Isles and Western Europe leading to a south-westerly flow at surface. This blocking high steers Atlantic lows to the north of Scotland it leads to wetter weather conditions in the North. The HM weather type was the most dominant circulation pattern (14 days) in March 2012. It is worth mentioning that March 2012 was also within the long drought period starting in 2011 across much of southern, central and south-east England with these areas applying hose-pipe bans as early as

April 2012 [Met Office, 2013 b]. The impacts of drought lasted until early summer 2012 before an exceptional rainfall period followed from April to July [Met Office, 2013 b].

Droughts in the early growing stages of cereals, when associated with high temperatures, can affect photosynthetic efficiency limiting the potential yields. This could have also contributed to the low yields being observed during the harvest of 2012. The very wet summer of 2012, with June being an exceptionally wet month [Met Office, 2013 c], also set challenging weather conditions for the growers.

In contrast, to simulate a regime which leads to below average accumulations of SIS, the WS weather type was selected as it features an area of low pressure centred over northern Europe with a shortwave upper trough just over the UK. This pattern during summertime would be associated with wet conditions resulting mostly from convective showers with a northerly or north-westerly cool airflow over the relatively warm land of the UK. **Figures 3.20 a-d** show the equivalent information as for March 2012, but this time for June and for the Weather type WS, the most common individual weather type (8 days) in June 2012.

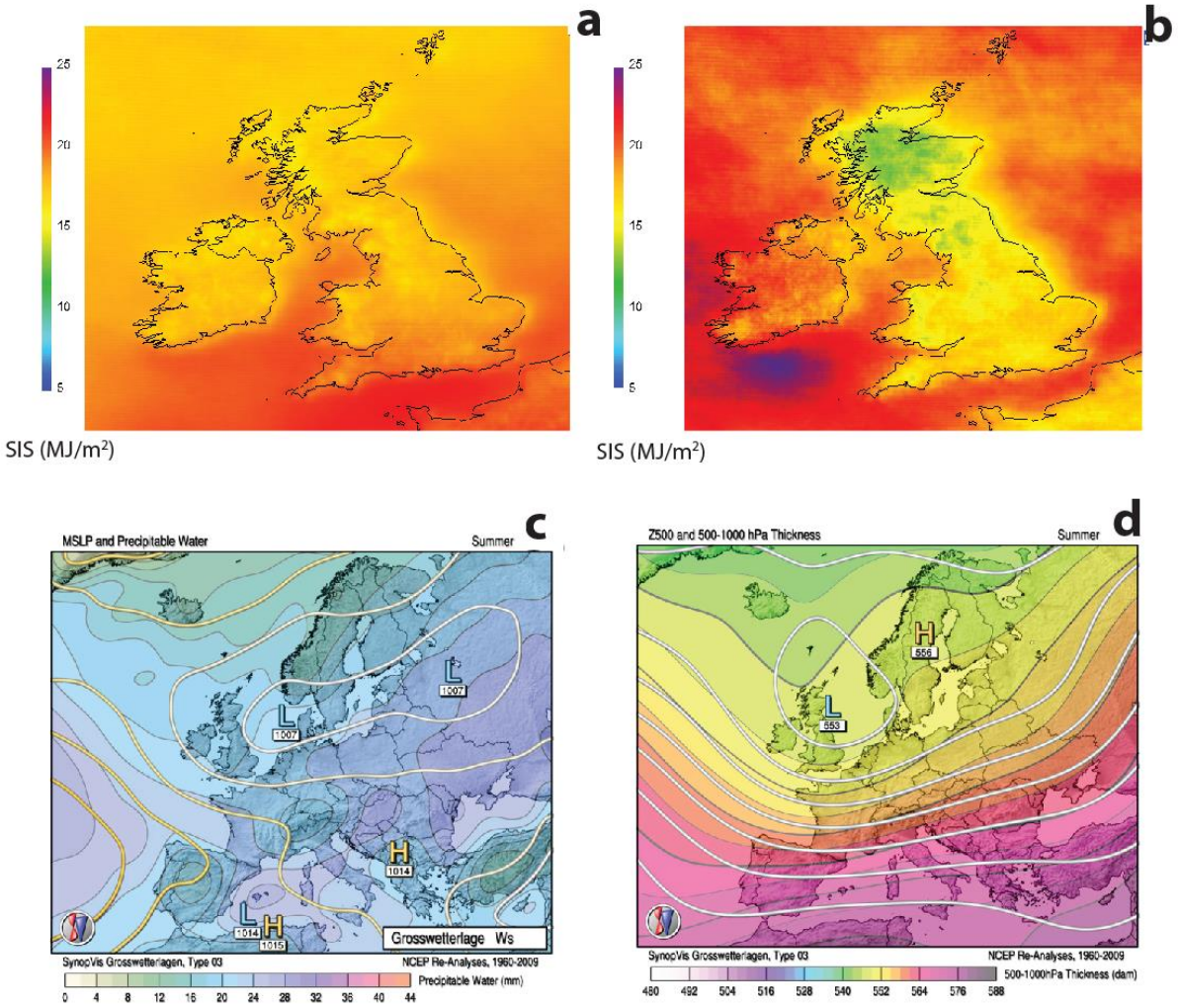

Figure 3.20 **a**) Average daily June SIS based on 1983-2010 data; **b**) the average June SIS for all those June days (8) classified as experiencing the WS GWL weather type; **c**) WS GWL weather type mean sea level pressure; **d**) HM GWL weather type mean 500hPa circulation.

To confirm the statement A:iv set in **Section 1.3** which states that high pressure leads to higher accumulations of SIS (positive anomaly), an analysis has been undertaken for a larger European domain (**Figure 3.21**), enabling a more comprehensive analysis. It is clearly shown that around the centre of the area of high pressure associated with weather pattern HM, due to vertically descending airflow, cloud formation is suppressed, therefore clearer skies lead to higher SIS accumulations. Only the CMSAF CDR of SIS for the period 1983-2005 has been used for this demonstration as the available data set for the whole 1983-2010 period covers only the UK domain. The manipulation of the satellite based data sets covering large domains

such as the one illustrated in **Figure 3.21** are time- and computationally expensive and this is the other reason for selecting only this period.

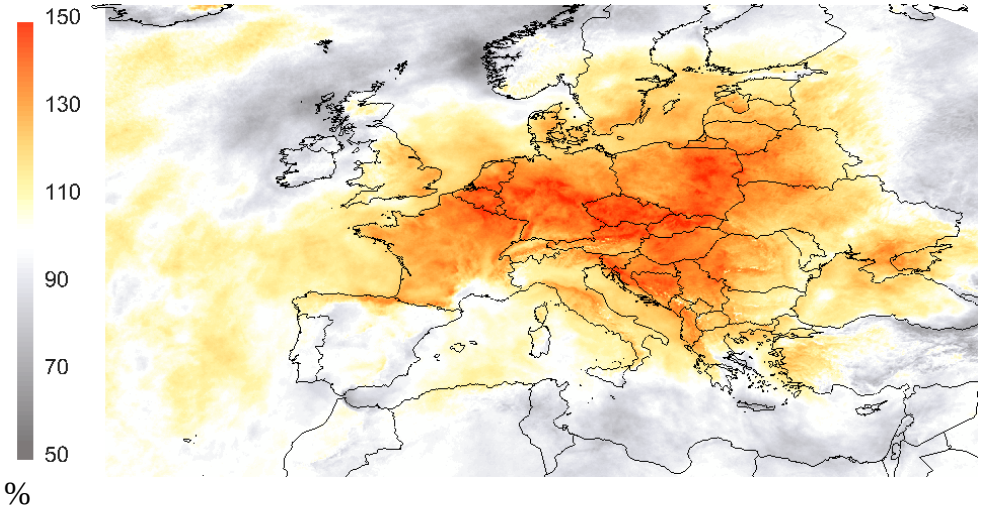

Figure 3.21 Solar radiation anomalies for the weather type HM during the month of March, expressed as a percentage of average, based on the 1983-2005 period over Europe.

Adopting the technique of the weather typing or monitoring and estimating SIS accumulations would have a distinct advantage over the alternative conventional ways such as the model analysis/ forecast or satellite based monitoring. The reason for this is the fact the NWP have difficulty in simulating cloud cover (verification results **Section 3.2**) which relates to the amount of solar radiation incoming on surface. However, NWP are much better to simulate synoptic scale patterns which, using results such as those shown in **Figure 3.21**, can now be correlated with anomalies in SIS accumulations.

The focus now is to relate the observed variability in cumulative surface solar radiation during the grain fill period to reported wheat yields. In order to achieve this, the aim is to try to quantify the contributory effect of the variable radiation climate to the 'yield plateau' in wheat which has been widely observed over the last twenty years [Brisson et al., 2010; Finger, 2010; Knight et al., 2012, Lobell et al., 2011]. The following chapter will focus on the climatology of SIS during the wheat grain fill period over the UK as well as the variability of the grain fill period length, which consequently drives the amount of SIS intercepted by the plants during one of the most important stages of the crop development.

4 Grain fill climatology and wheat grain yield correlation

In this chapter the benefit of using high resolution daily satellite based estimates of SIS is assessed through analysis of the climatology of SIS during the critical wheat growth stage of grain fill. The more solar radiation that is intercepted by the crop during that period, the higher the potential yield. However, it is not as simple as that because, as described in **Section 1.2.1,** there are many other important factors which can impact the crop yield. It should also be noted that some of the final yield results from accumulated growth prior to flowering, therefore, solely measuring yield gain as a function of radiation during grain fill will underestimate the overall effect of solar radiation variability on the final yield. In order to understand better and provide a meaningful interpretation of the results, it is important to know the spatial distribution of the main wheat growing areas in the UK. **Figure 4.1** shows the percentage of total area occupied by wheat crops per region in the UK.

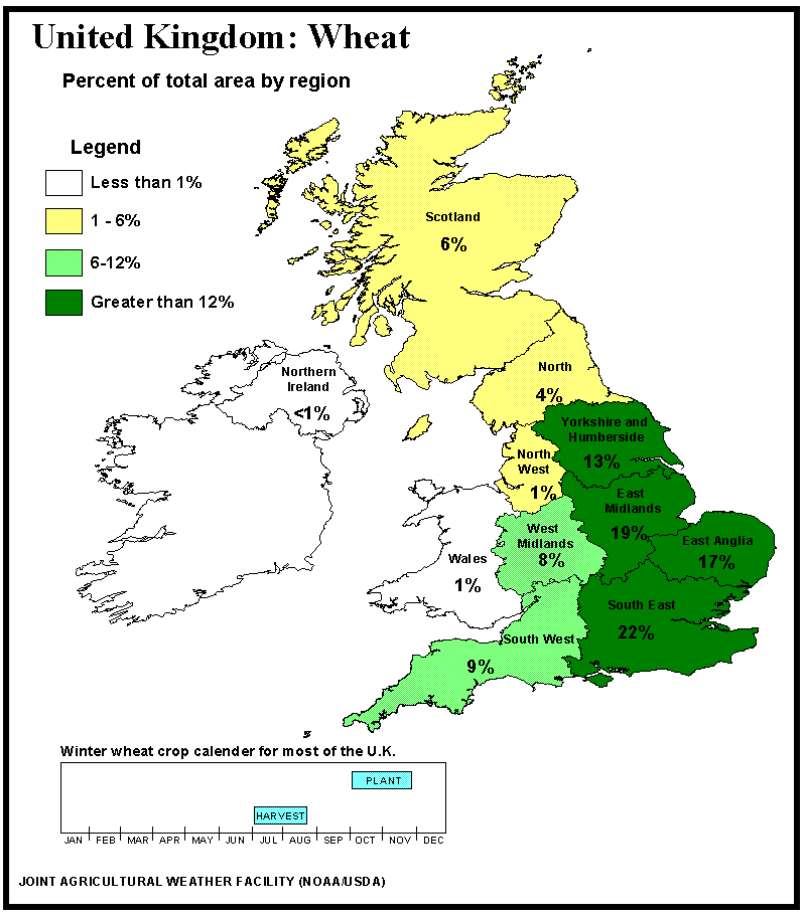

Figure 4.1 Wheat growing regions coloured by the percentage of the total region area occupied by wheat crops. [Source: Spectrumcommodities.com (2014)]

4.1 A climatology of SIS over the UK during the 'standard' grain fill period

Ignoring in the first instance the temperature effect on the length of the grain fill period, **Figure 4.2** shows the mean of SIS accumulations during 10th June -21st July over the 1983-2010 period. The spatial distribution of total accumulations presents a similar spatial pattern when compared to the mean annual SIS over the 1983-2010 record as illustrated in **Figure 3.10.** North-western Scotland presents the lowest mean SIS totals with about 660 MJ/m^2 received on average during the 'standard'grain fill period compared to southern coasts of England which present a mean of up to 910 MJ/m^2. In this case the topography (**Figure 4.2 b**) also plays an important role in the spatial distribution of the SIS during this specific grain fill period.

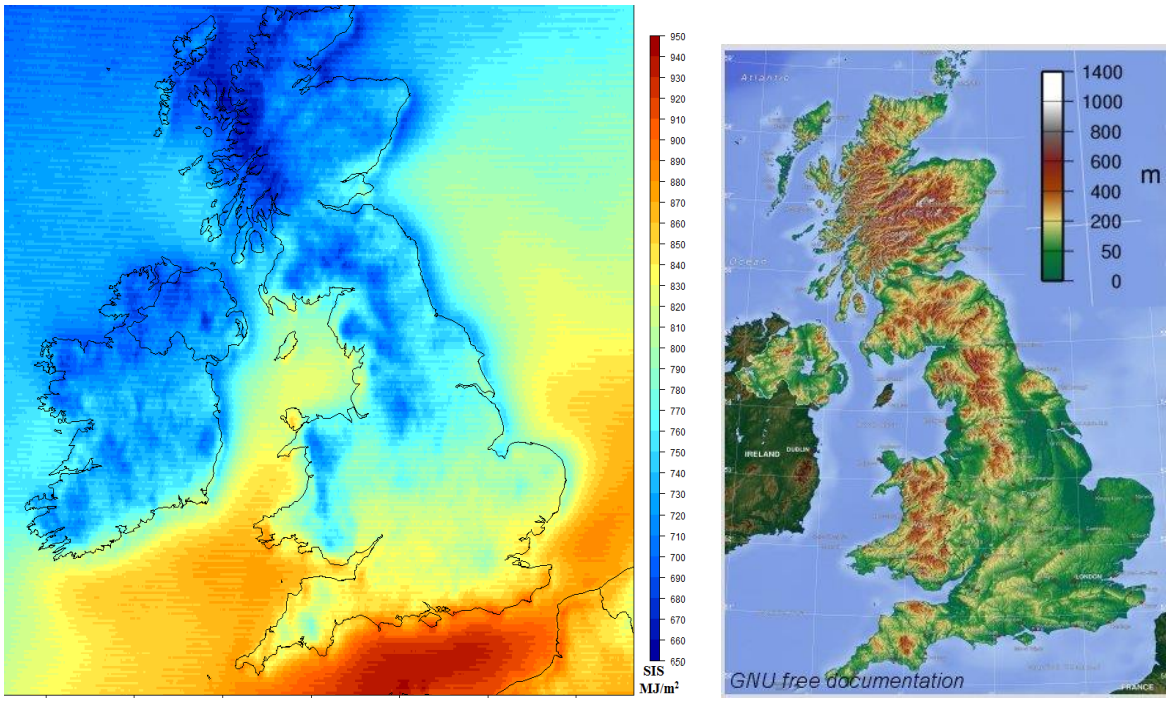

Figure 4.2 a) Mean sum of SIS during the 'standard'grain fill period (MJ/m^2) based on MVIRI+SEVIRI (1983-2010) **b**) UK terrain [Source: www.withnature.co.uk, 2014]

Interestingly Anglesey, an island off the north-west coast of Wales, exhibits a mean sum of SIS during grain fill of about 840 MJ/m^2 which is higher than any other part of the UK at the

same latitude and can even be compared with parts of England further south. The penetration of the solar radiation through the atmosphere to the Earth's surface depends greatly on cloud cover. During the summer season when grain fill occurs, clouds are increasingly developing as a result of convection which is partly driven by the more extensive daytime surface heating over land. Since large water bodies are cooler than the land (during spring and summer daytime), there is a relative lack of developing cloud over the sea. With westerlies or south-westerlies being the prevailing winds during summertime over the UK, clouds start to gradually build up a few miles inland of western coasts, aided by forced ascent over terrain, further developing as they move eastwards, reducing the incoming solar radiation reaching the surface. This partly explains why south-western areas of England exhibit higher mean SIS values in **Figure 4.2** compared to areas further east.

The mean pressure pattern during the 'standard'grain fill period (**Figure 4.3**) indicates an area of high pressure (H) dominating over the Azores and an area of low pressure (L) over the north-Atlantic. This setup leads to a mean west to south-westerly air flow over the mid-Atlantic and to the west of Ireland. Wind direction across the UK depends on the storm track with storms originating over north-eastern America and moving eastwards as these die in the mid-Atlantic they create secondary depressions (Dacre and Gray 2009).These depressions are then moving eastwards towards Ireland and diverting north-eastwards towards north-western Scotland before heading to Scandinavia. As a result this contributes to the north-west to south-east SIS distribution pattern presented in **Figure 4.2**.

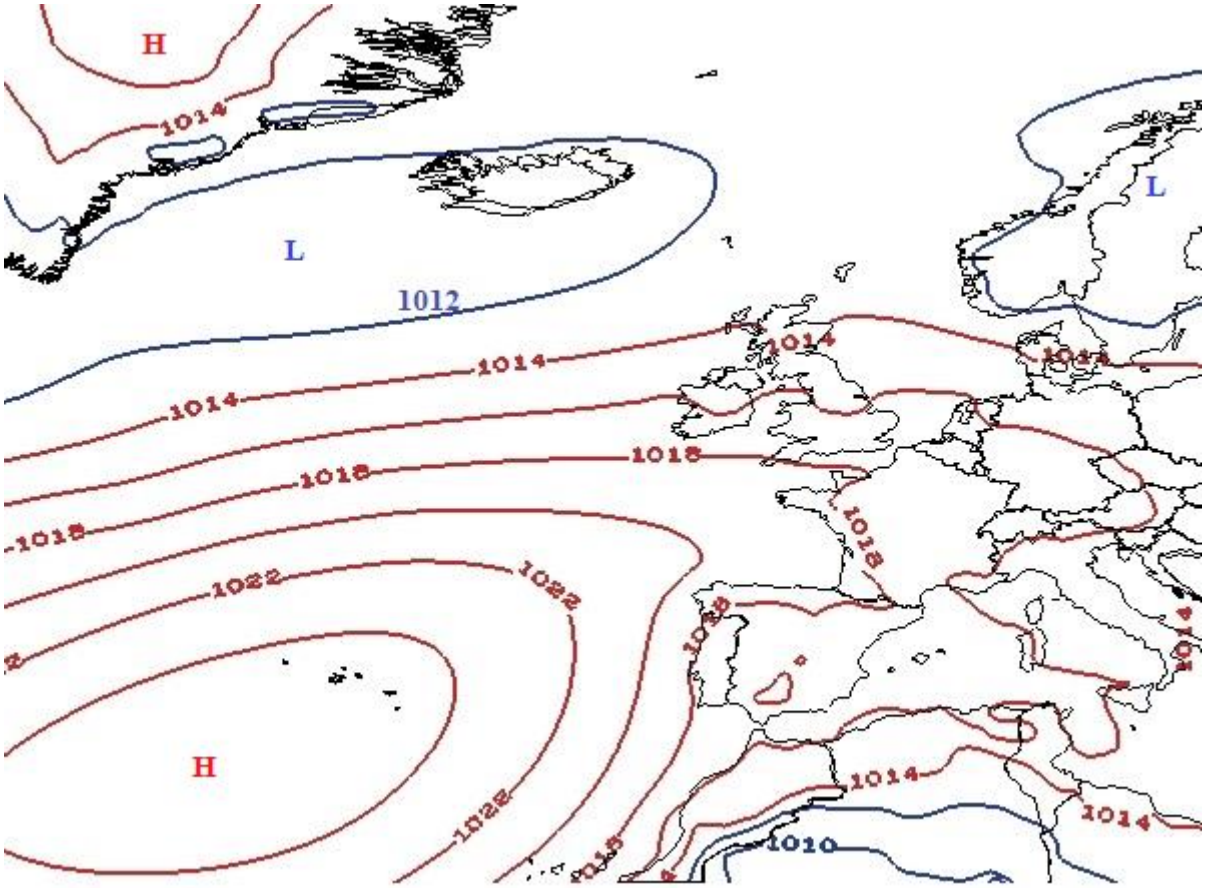

Figure 4.3 Mean sea level pressure pattern from ECMWF ERA Interim reanalysis data, over the June 10th – July 21st 1983-2010 period valid for 1200GMT. Contours are shown in millibars.

An analysis of the standard deviation of SIS during the standard grain fill period over the period 1983-2010 across the UK (**Figure 4.4**) highlights the areas which exhibit the lowest and the highest variability. In general it appears that coastal areas are experiencing lower variation in SIS (6-10%) compared to the inland counterparts and the elevated areas such as the Pennines, the Welsh and the Scottish mountains (10-14%). However, although not included in the scope of this analysis, parts of the Netherlands (low-lands) also present relatively high variability (up to 14%), therefore this effect cannot be solely associated with altitude. These variations can in fact be also associated again with cloud cover variability driven by convection processes.

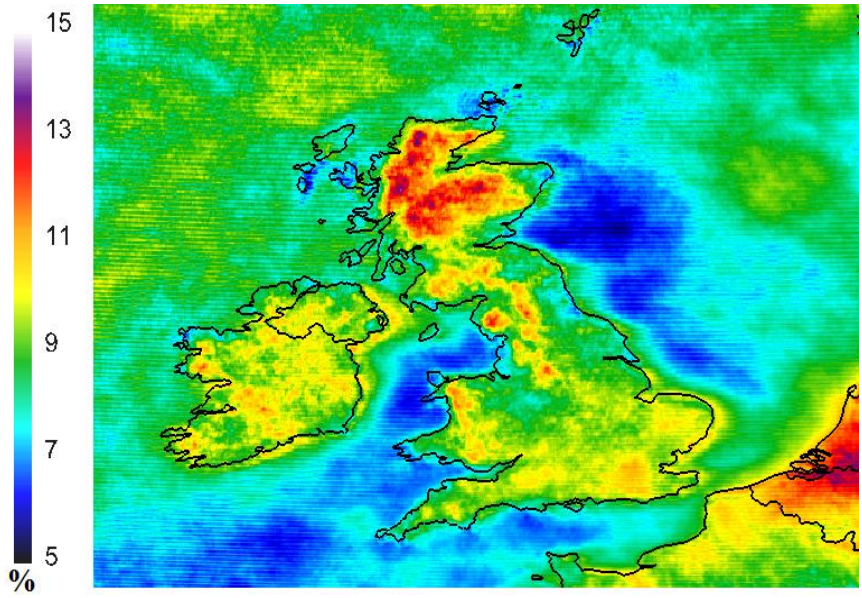

Figure 4.4 Standard deviation of SIS during the ‘‘standard’grain fill period based on the total accumulations each individual year over the period 1983-2010.

Based on **Figure 4.4**, one can speculate that the western coasts of England and Wales, Anglesey and parts of north-eastern England (Lincolnshire and Yorkshire) as well as south-eastern coasts of Scotland are more reliable locations for crop growing. It is worth highlighting that western coasts of England benefit particularly from a combination of high mean SIS totals during the grain fill period and relatively low variability. This result can be particularly useful in applied agronomics since it can determine the type of crops or wheat varieties which can be grown. Some wheat varieties may be able to produce high yields when solar radiation is in abundance, but during cloudy and dull growing seasons the same varieties may have difficulty in reaching their average. It is preferable that varieties grown in areas with high SIS variability during the growing season are relatively tolerant to solar radiation variability, able to produce average yields even when SIS is a limiting factor.

Weather pattern variability and persistence during the grain fill season can lead to anomalous accumulations of SIS which, as a result, can have a significant impact on yields and grain quality. **Figure 4.5** presents how total SIS has varied spatially and temporally in each of the last 12 years of the grain fill season. Only the most recent 12 years are presented in this example as, firstly, these are still relatively fresh in the farmer’s memory regarding yield variations. Secondly, it is possible to compare the ‘standard’against the ‘temperature adjusted’ grain fill SIS accumulations over this 2002-2012 period, as explained in **Section**

2.6. The year 2013 was added as a further option, since the data for this year recently became available, but it will not be analysed further in this study. Interestingly, significant year-to-year spatial variations in grain-fill SIS magnitude are observed over this relatively short record highlighting the usefulness of the high resolution daily satellite based data. Using a visual approach it is possible to distinguish 'good' years (2003; 2006; 2010) and 'bad' years (2007; 2008; 2012) for total SIS accumulation during the standard grain fill season.

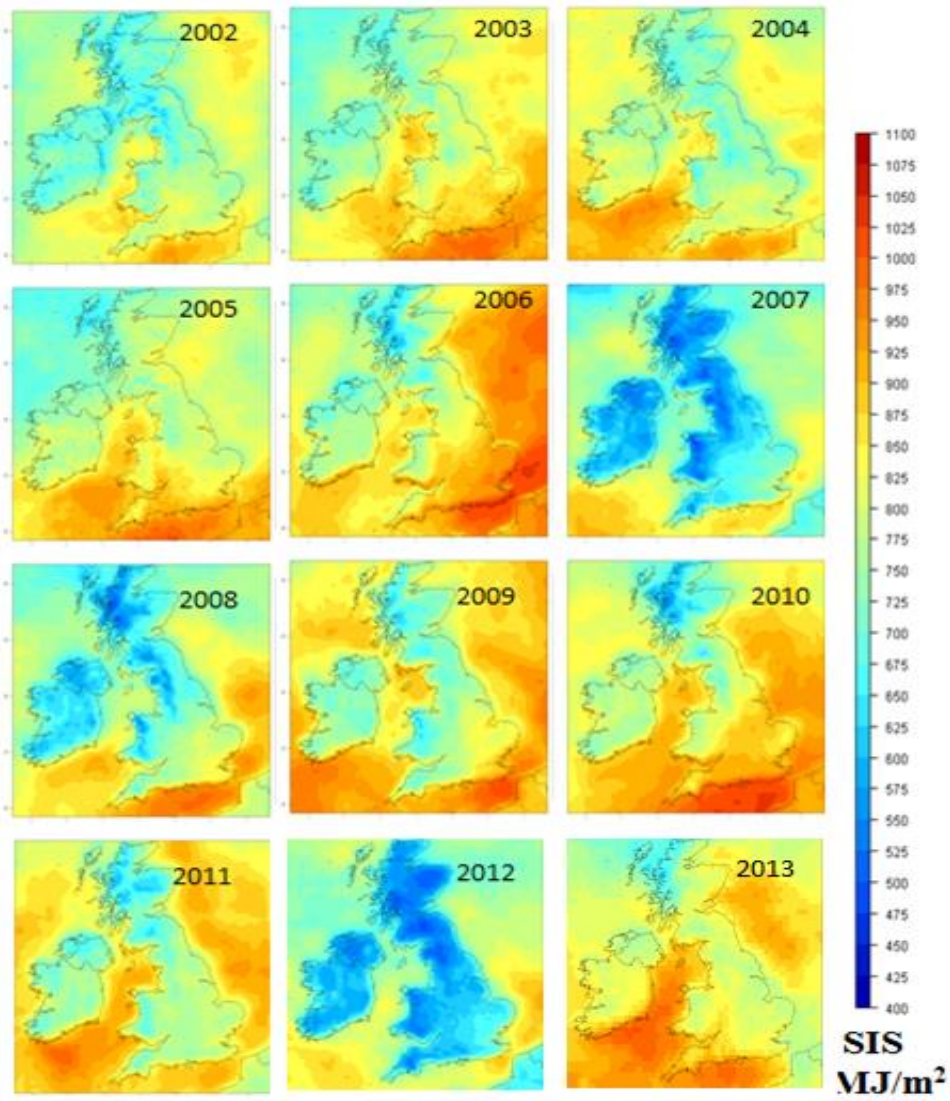

Figure 4.5 Total accumulated SIS (MJ/m^2) during the 'standard'grain fill season, for each year in the period 2002-2013, based on MVIRI+SEVIRI.

An initial coarse scale analysis suggests a relationship between SIS during the 'standard' grain fill season and the magnitude of average wheat yields in the UK. For example, in 2006,

8.0 tonnes per hectare was achieved on average over the UK in a year of high grain fill SIS (**Table 4.1**), especially over parts of Eastern England which is the main wheat growing region in the UK (**Figure 4.1**). On the other hand, wheat yields for 2012 appear to be the lowest in the recent record (**Table 4.1**), as low as 6.7 tonnes per hectare average production in a year when surface solar radiation accumulations during the grain fill period were among the lowest in the recent record (**Figure 4.5).** Low yields coinciding with low SIS during the grain fill season are also noticeable in 2007 with average production of wheat limited to 7.2 tonnes per hectare. Meanwhile wheat yields for 2008 are not corresponding with the observed magnitude of grain fill SIS and this is not a surprise since there are numerous other factors which can determine the final yields, including the variable length of the grain fill season. An interesting point which can be derived from **Table 4.1** is the fact that wheat yields are undergoing higher variations compared to other cereals and this is providing some hints that solar radiation variability can have a more significant impact on wheat than on other cereals.

Table 4.1 Average cereal yields in tonnes per hectare over the UK. [Source: DEFRA (2014)]

Year [(a)]	Wheat	Barley	Oats	Rye	Mixed Corn	Triticale	Oilseed Rape
2002	8.0	5.6	6.0	5.8	4.7	4.7	3.4
2003	7.8	5.9	6.2	5.8	4.3	4.1	3.3
2004	7.8	5.8	5.8	5.7	4.3	4.1	2.9
2005	8.0	5.9	5.8	6.7	4.4	4.2	3.2
2006	8.0	5.9	6.0	6.1	4.5	4.3	3.3
2007	7.2	5.7	5.5	5.7	3.9	3.9	3.1
2008	8.3	6.0	5.8	6.1	4.4	4.4	3.3
2009	7.9	5.8	5.8	6.6	4.1	4.1	3.4
2010	7.7	5.7	5.5	6.3	4.1	4.0	3.5
2011	7.7	5.7	5.6	5.4	3.9	4.1	3.9
2012	6.7	5.5	5.1	5.2	4.2	3.5	3.4
2013	7.4	5.8	5.5	5.6	4.2	3.9	3.0

A more detailed, site-specific analysis of the relationship between the final wheat yields and the solar radiation intercepted by the crop during the UK grain fill period is presented in **Section 4.4** of this thesis.

4.2 Trends of Surface Incoming Shortwave (SIS) solar radiation during the 'standard'UK grain fill period.

The high spatial resolution and the long record of the homogeneous daily satellite based estimates of SIS enable trend analysis for specific periods such as the grain fill season,

building on the seasonal trends presented in **Section 3.5.2**. Using only the homogeneous period of the combined MVIRI+SEVIRI dataset the surface solar radiation trend has been derived for the period of 10th June to 21st July from 1994-2010 and the results compared with the observed yield plateau. Trends for the 'standard'grain fill season over the 1994-2010 period (**Figure 4.6 a**) present a somewhat similar spatial representation to the observed trends during the whole summer season (JJA) as shown in **Figure 3.13 c (**also repeated in **Figure 4.6 b).**

a

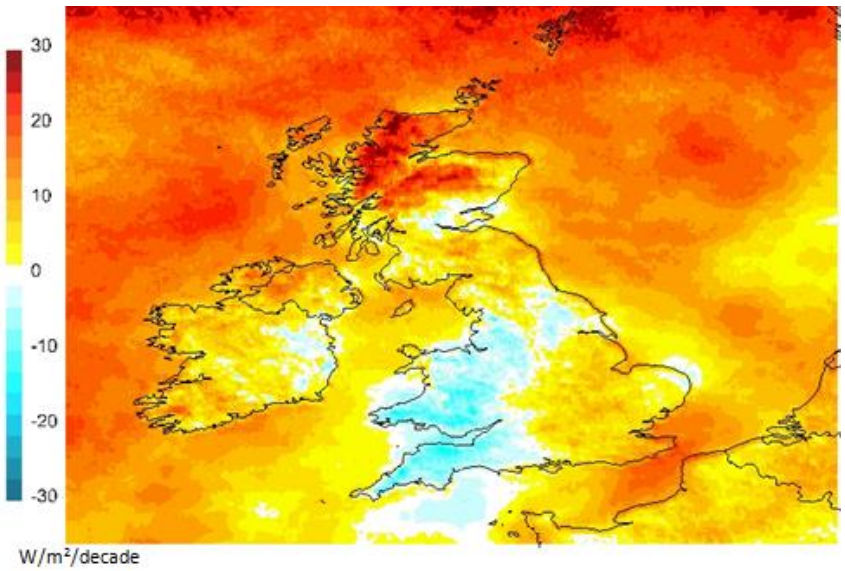

b

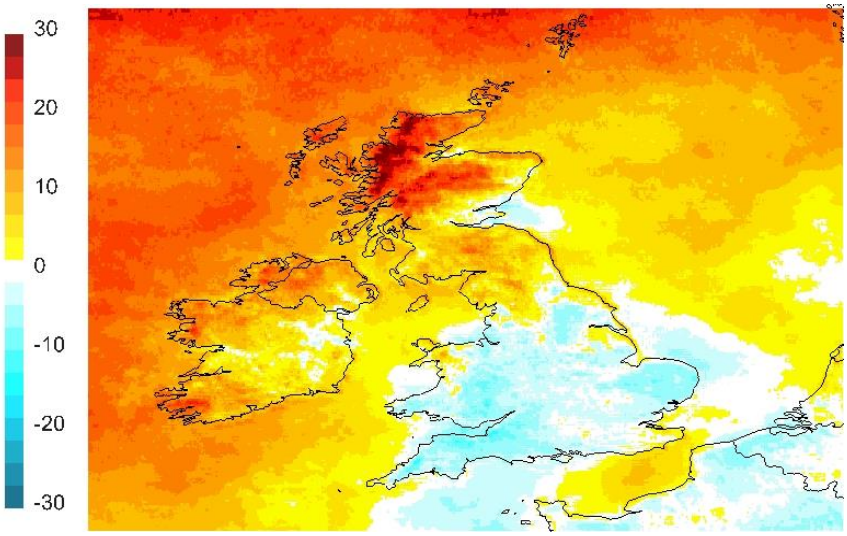

W/m^2/decade

Figure 4.6 Linear trends (W/m^2/decade) of the satellite-derived SIS based on the CMSAF dataset during **a**) the standard grain fill period; **b**) the summer season (JJA) for the years 1994-2010.

An interesting difference however is the fact that although the summer season revealed a small negative or no trend over the 1994-2010 across the whole of southern England and Wales, the analysis for the standard grain fill period indicates a positive trend over much of eastern and south-eastern England, key wheat growing areas in the UK (**Figure 4.1**). The mean trend for the whole domain illustrated in **Figure 4.6a** is in the order of + 10.27 W/m^2/decade for the standard grain fill season over the analysis period (compared to +7.77 W/m^2/decade for the summer season). Meanwhile, **Figure 4.7** shows the relative trends expressed as percentage change. It appears that Wales and western parts of England suffer from a decrease of SIS of the order of 5% over the 1994-2010 standard grain fill period, while eastern areas of England benefit by about a 3-5% SIS increase.

More noticeable changes occur in the far north of Scotland and over the Northern Isles where the solar radiation seems to have increased by about 10-15% over the 1994-2010 grain fill period. Solar radiation trends derived in this analysis can only be attributed to change in cloud cover or cloud thickness/optical properties. Perhaps the reason behind the contrasting results in the south and the north reflect a small southward change in storm track (jet stream) during this period. As a result of this shift, the effect of a modest change in wind direction during the grain fill season is possible, leading to a more south to south-westerly rather than south-westerly flow. This may lead to Cornwall, Devon and Wales experiencing more cloud/orographic rain. Further analysis is needed to understand the exact reasons for this interesting pattern and more sensitivity tests should be carried out to quantify the SIS trends during the grain fill period with different start and end dates. It would be interesting to examine the trends of SIS during the 'temperature adjusted' grain fill period also taking into account flowering start dates at each individual location.

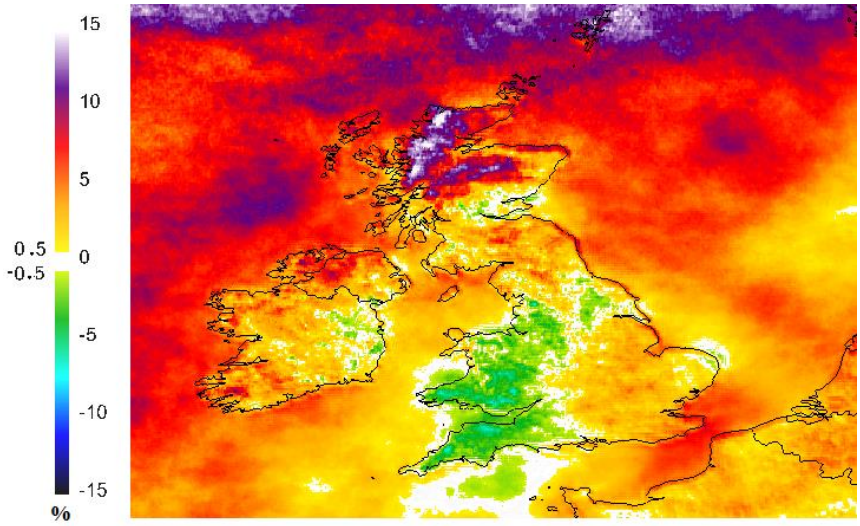

Figure 4.7 Relative trend of SIS (%) during the grain fill season over the 1994-2010 period.

The analysis of the 'standard'grain fill SIS trends does not at first sight support the hypothesis set in **Section 1.3** (ii) that the observed yield plateau may be partly explained by solar radiation variability, taking a coarse national perspective Although there is a small decrease of SIS during the summer season over much of England, the main wheat growing area of England exhibits a general increase of SIS accumulations over the 1994-2010 grain fill period of about 3-5%. Without this observed increase, it is possible that a decline in yields might actually have been recorded.

A suggestion that arises from this result is that the analysis should be repeated for the same period, but only taking into account specific wheat growing areas. Unfortunately, this analysis was not possible in this research due to a) software limitations and b) the fact that a high resolution gridded database of wheat growing areas was not available. CMSAF is planning to release in November 2014 an updated version of SIS which will be covering the whole 1983-2013 period with high quality satellite based estimates and homogeneous throughout [Trentmann, 2013]. This will give an opportunity to perform the trend analysis for the whole period during which the yields stopped increasing and started to plateau. Meanwhile, a detailed site-specific analysis will be presented in **Section 4.4** of this thesis to investigate whether there is a direct relationship of SIS during the grain fill with actual yields, using trial site data.

4.3 The effect of temperature on grain fill duration -WRF simulations

As discussed in **Section 1.2.1**, temperature influences the duration of the grain fill season and can therefore also affect final yields. The exact grain fill start date and end date naturally varies on a spatial basis according to the local temperature climate in each location, region or country. Furthermore, according to Todd (2013) the grain fill start date and end date vary temporally from year to year. In a typical year in East Anglia, the date of anthesis (which is hours before the start of grain fill) is 3-5 days after wheat ear emergence. The date of ear emergence varies by approximately 2-3 weeks each year across the UK, according to Todd (2013), in a typical year, for example in East Anglia grain fill can start from 30th May for early varieties, to 7th June for late varieties. However, the equivalent dates could be as early as 25th May and 4th June or as late as 2nd and 11th June depending on weather conditions. Knight et al. (2012) in their study used a value of 42 (days) as an average grain fill period length over Central England with a start date of 10th of June for each year. In this study, model simulations are used to calculate, each year, in each location, the number of days taken to accumulate the 660 grain fill period degree days, starting 10th June (one day with an average temperature of 15^{0}C is 15 degree days) (**Figure 4.8)**.

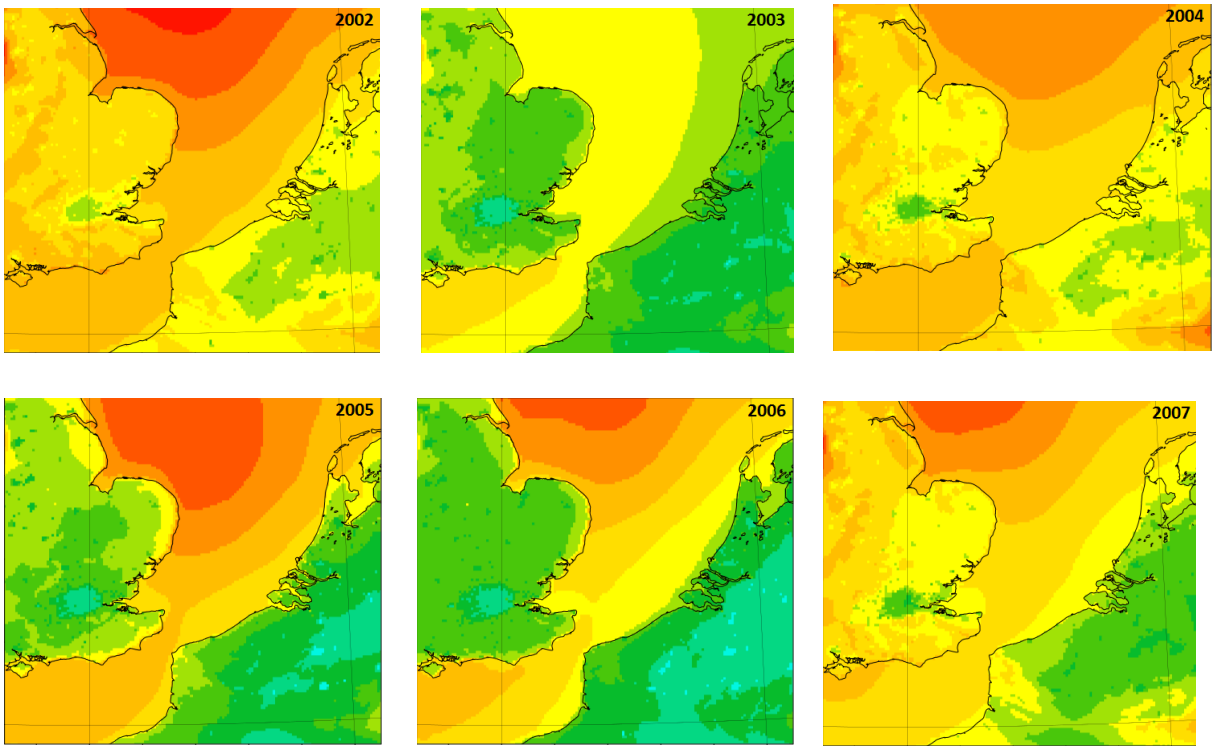

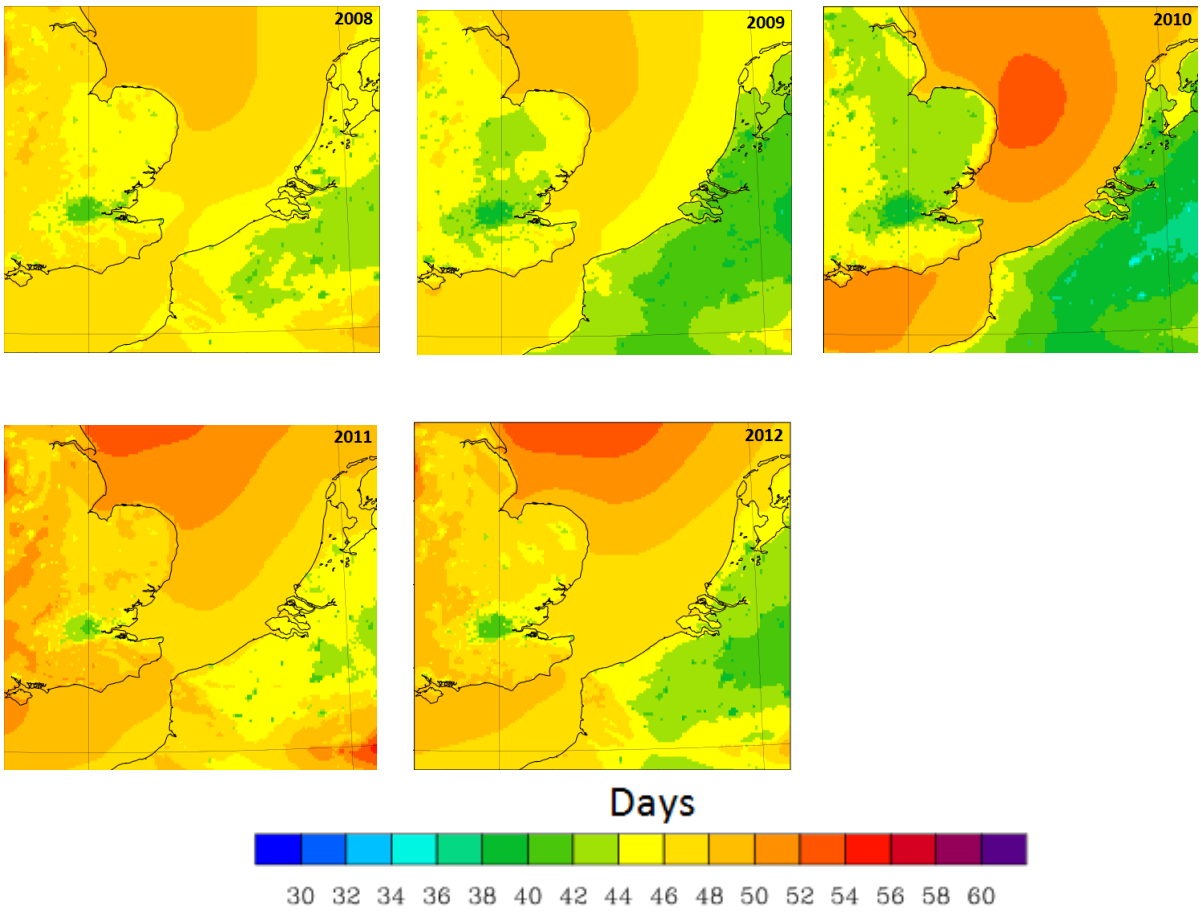

Figure 4.8 The duration of grain fill (days) starting on the 10th June for each year. The length of the period is estimated using 660 degree day accumulations at each individual grid point.

Results reveal an expected spatiotemporal variation in the duration of the grain fill period in the southeast of the UK. Although not relevant to this study, the effect of the London urban heat island is also very clear. The length of the grain fill period is ranging from 38 days in 2003 and 2006 to 50 days in 2011 and 2012 (**Figure 4.8**), as a result of the temperature effect, depending on the location, confirming the statement 5 set in **Section 1.4.** The next step is to calculate the total amount of solar radiation accumulated during these days and to relate the temperature-adjusted grain-fill accumulated SIS to actual yields.

4.4 Site-specific analysis of yields against grain-fill Surface Incoming Shortwave solar radiation (unadjusted and temperature-adjusted) using RL trials data

The total number of data entries in the variety trial Excel spreadsheet lists kindly provided by HGCA consisted of 49,102 rows over the period 1992-2012. These include data from trials in different locations, with a range of previous crop regimes, alternative soil types, and variable sowing and harvesting dates. Some trials involve fungicide treatments and others not. Philpott [personal communication, 2013] suggested that the Claire variety presents the longest record of cultivation among all the varieties listed in the RL spreadsheet file and is therefore selected for the purposes of this study, limiting the available number of winter wheat RL data to 935. To ensure that yields are not affected by fungi or fungal spores which can also limit yields, only fungicide treated fields are used, further limiting the available data to 597 entries. The records for the Claire variety start in 1996 and are then separated based on different trial soil types and on previous crop regimes (**Table 4.2**). Deep clay and Medium soil types dominate most of the RL trial records with 150 and 207 entries, respectively. The locations of the sites where the Claire variety was grown over the 1996-2012 period are shown in **Figure 4.9** and this reveals a good spatial distribution across most of the arable growing regions.

Table 4.2 Number of entries for fungicide treated Claire variety based on different soil types and previous crops. Green cells highlight those combinations which have more than 4 entries. The following Figures 4.10-4.13 refer to the data presented in this Table.

-	Soil Type								
Previous Crop	Deep Clay	Deep Silt	Light Sand	Medium	Organic	Peaty	Shallow	Unknown	Grand Total
Forage maize							1		1
Garden peas	7	1		1					9
Grass	1		1	8	4		2		16
Linseed	3	3	2	4		1	2	1	16
Mustard	1	1							2
Other		7		6			4		17
Pea	12	10	4	11		3	4		44
Potato	5		7	10	2	1	1		26
Set aside				4	2		1	1	8
Spring barley	5		6	4					15
Spring bean	1	2		3	1		1		8
Sugar beet		1	14	9		2			26
Spring oats	1								1
Spring rape	3	1	2	4			4		14
Unknown	11	4	3	13	2		2	12	47
Veg		19	3	9					31
Vining peas	5	3		2					10
Winter barley				1					1
Winter bean	19	3		10	2				34
Winter oat	3	4	1	10	3				21
Winter rape	37	8	6	55	7		28		141
Winter wheat	36	6	12	43	3		9		109
Grand Total	**150**	**73**	**61**	**207**	**26**	**7**	**59**	**14**	**597**

Figure 4.9 RL sites where fungicide-treated Claire winter wheat variety is grown.

An analysis is performed for the four main combinations of 'previous crop' and soil types which dominate the charts with more than 30 records. The four main combinations are Medium soil type – Winter wheat, Medium soil type - winter rape, Deep clay soil type – Winter wheat, Deep clay soil type – Winter rape). The daily mean SIS (MJ/m^2) is calculated as the sum of total SIS intercepted during the 42 days of the 'standard' grain fill period, divided by the number of days of that grain fill period. Results are presented in **Figures 4.10** to **4.13**.

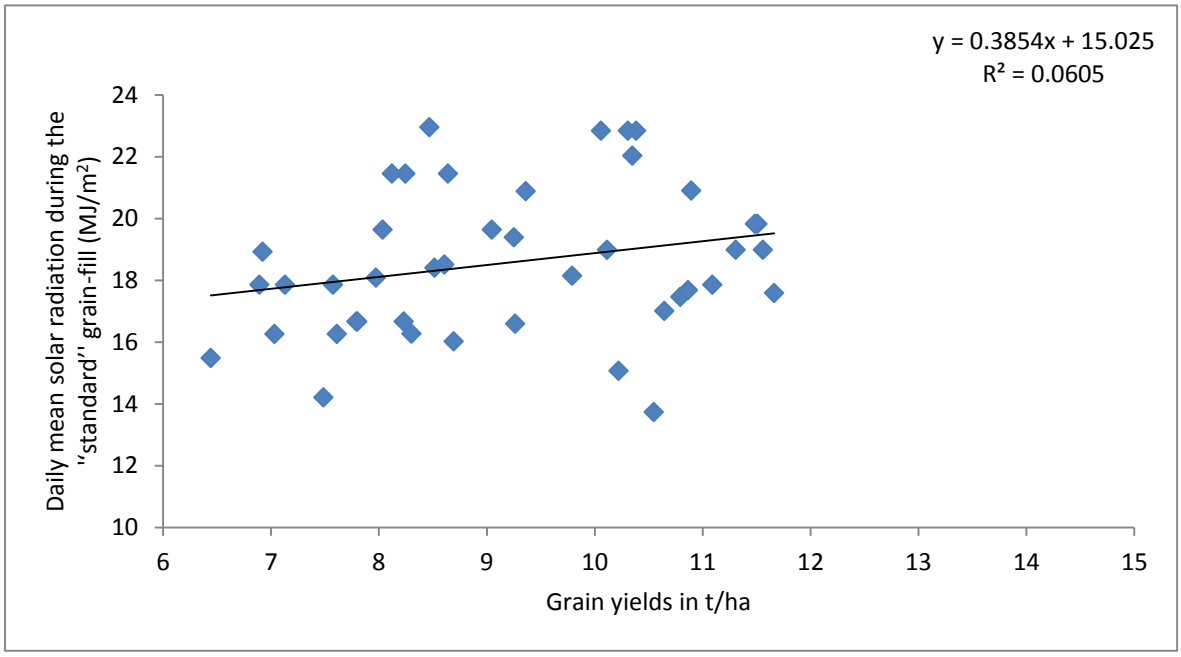

Figure 4.10 Correlation of wheat yields (t/ha) against daily mean SIS (MJ/m^2/day) during the standard grain fill period at all trial locations in the UK where Previous Crop was Winter wheat and Soil Type was Medium (n=43). R^2 = 6% and correlation coefficient = 0.25

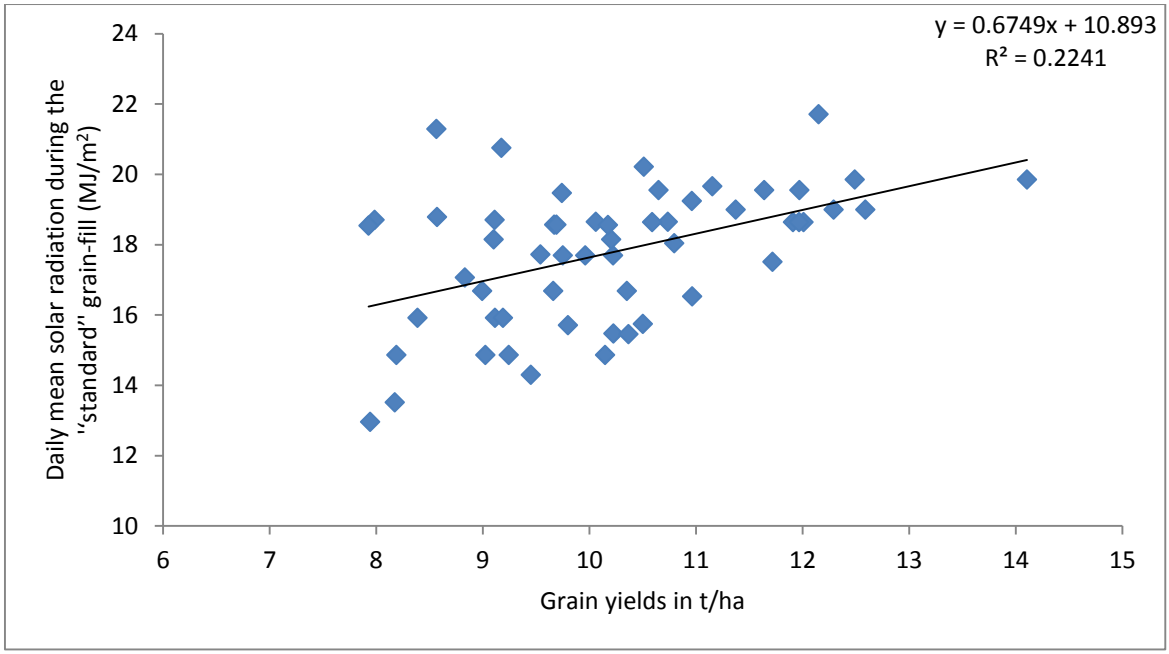

Figure 4.11 Correlation of wheat yields (t/ha) against daily mean SIS (MJ/m^2/day) during the standard grain fill period at all trial locations in the UK where Previous Crop is Winter rape and Soil Type is Medium (n=55). R^2 = 22% and correlation coefficient = 0.47

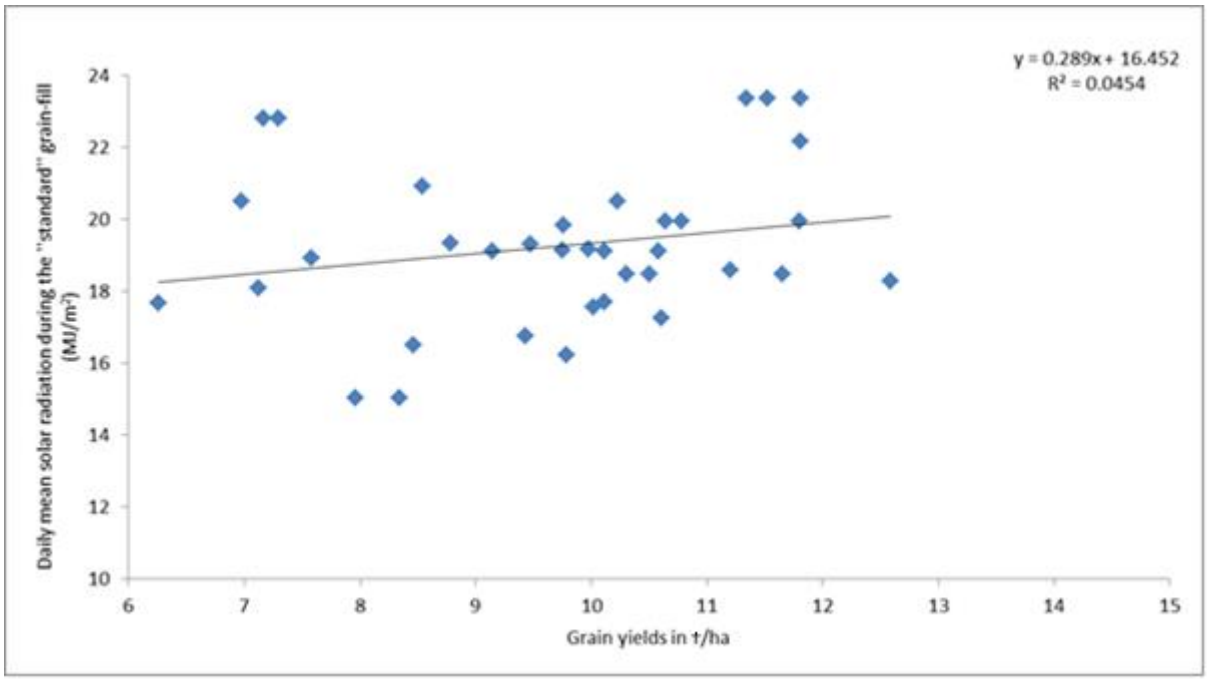

Figure 4.12 Correlation of wheat yields (t/ha) against daily mean SIS (MJ/m^2/day) during the standard grain fill period at all trial locations in the UK where Previous Crop was Winter wheat and Soil Type was Deep clay (n=36). R^2 = 4.5% and correlation coefficient = 0.21

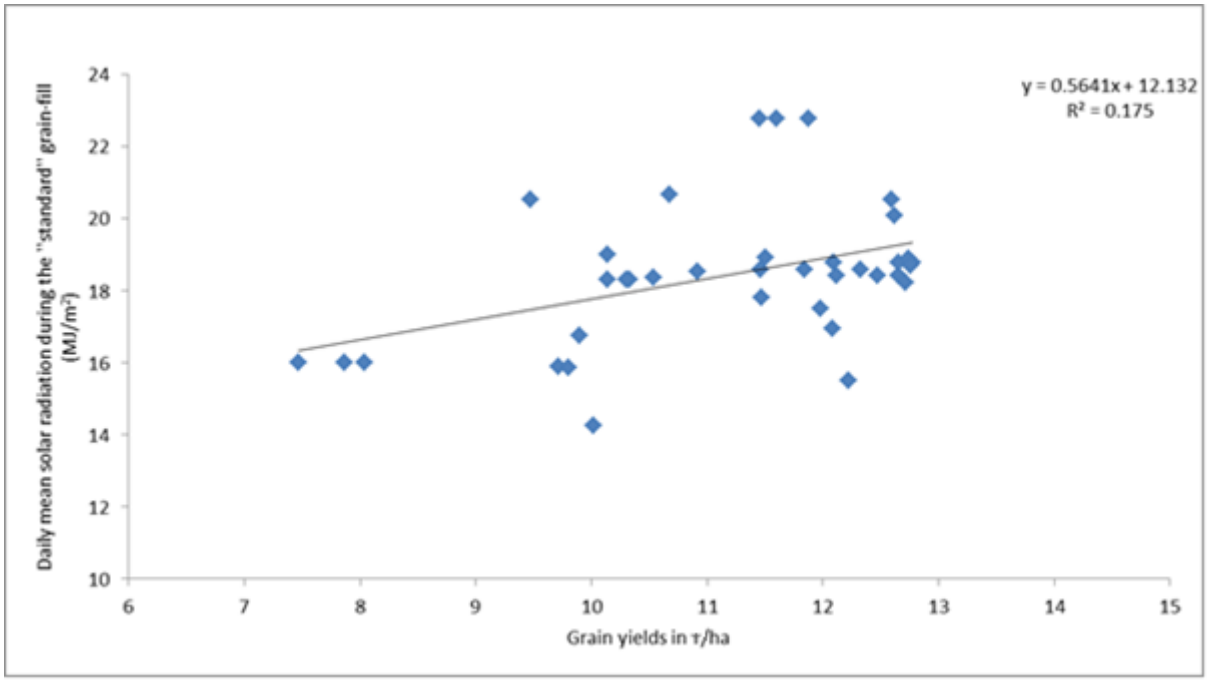

Figure 4.13 Correlation of wheat yields (t/ha) against daily mean SIS (MJ/m^2/day) during the standard grain fill period at all trial locations in the UK where Previous Crop was Winter rape and Soil Type was Deep clay (n=37). R^2 = 17.5% and correlation coefficient = 0.42

It appears that the R^2 is lower in **Figure 4.10** and **Figure 4.12** where previous crops were Winter wheat compared to **Figure 4.11** and **Figure 4.13** where Winter rape was previously grown and this can be partly caused due to monoculture. It is known that growing wheat in the same field year after year (2nd wheats, 3rd wheats) leads to a yield penalty, partly due to the development of soil-borne diseases such as the 'take-all', a soil fungal disease [Knight et al., 2012; Gutteridge et al. (2003)]. In addition, growing the same crop year after year reduces the nutrients in the soil, therefore a crop rotation needs to be applied. Crop rotation can also minimize and reverse the development of pathogens and pests which often develop as a result of monoculture.

The analysis of the combination of Medium-soil type with winter rape as previous crop (**Figure 4.11**) revealed a positive correlation R^2 = 22% and correlation coefficient = 0.47 which allows to use regression modelling approach to try to estimate yields based on this combination. Although, it should be noted that due to the small sample of examples, these results should be treated carefully. Estimating wheat yields prior to harvesting is a useful skill for a number of reasons ranging from insurance assessment to harvest management. Farmers

can plan their activities and manage their resources most effectively by having a good estimate of the expected yields just after the end of the grain fill period. However, predicting yields only as a function of SIS during the grain fill and using soil types and previous crops can be a very challenging task in real life as this approach does not take into account several other equally important factors such as water deficiency or waterlogging, diseases, variable sowing and harvesting dates and the impact of extreme temperatures during grain fill over the different years.

The relationship between yields and SIS during the 'standard' grain fill period is not a perfect one, and this is something to be expected since apart from all the other confounding factors affecting final yields, the assumed grain fill period was fixed as 42 days. To proceed one step further, a sensitivity test has been applied to demonstrate the effect of the varying length of the grain fill period with a fixed starting date of 10th June for each individual year, while acknowledging that this varies both spatially and temporally. The hypothesis iii from **Section 1.3** which states that the relationship between the 'temperature adjusted' grain fill SIS accumulations and final yields from RL trials is expected to be stronger than that associated with the 'standard' grain fill period SIS accumulations will now be tested. Among all the entries of the fungicide-treated Claire variety trials (597), only 2 locations (**Figure 4.9**) could be chosen since these are under the same 'previous crop' type (Winter rape) and same soil type (Medium) and also are at some distance from each other while falling within the domain and the time record covered by the WRF model to calculate the length of the grain fill period and consequently the 'temperature adjusted' grain fill SIS. After applying those filters, the results revealed only 6 entries which became available and would give a step to test the hypothesis iii. **Table 4.3** includes the important parameters linked to these locations, while **Figure 4.14** and **Figure 4.15** show the results in the form of scatter plots.

Table 4.3 Summary of the data used to correlate total SIS (MJ/m2) with yields for both 'adjusted' and 'standard' grain fill period.

Year	Location & Yield (T/ha)	'Standard GF SIS" (MJ/m2)	Temperature adjusted grainfill duration (Days)'	Temperature adjusted grainfill SIS (MJ/m2)
	Ragnall			
2004	9.54	724	46	792
2005	8.57	770	43	779
2006	9.17	855	38	762
	Fowlemere			
2009	10.51	823	45	878
2010	12.15	886	43	904
2012	9.8	638	46	746

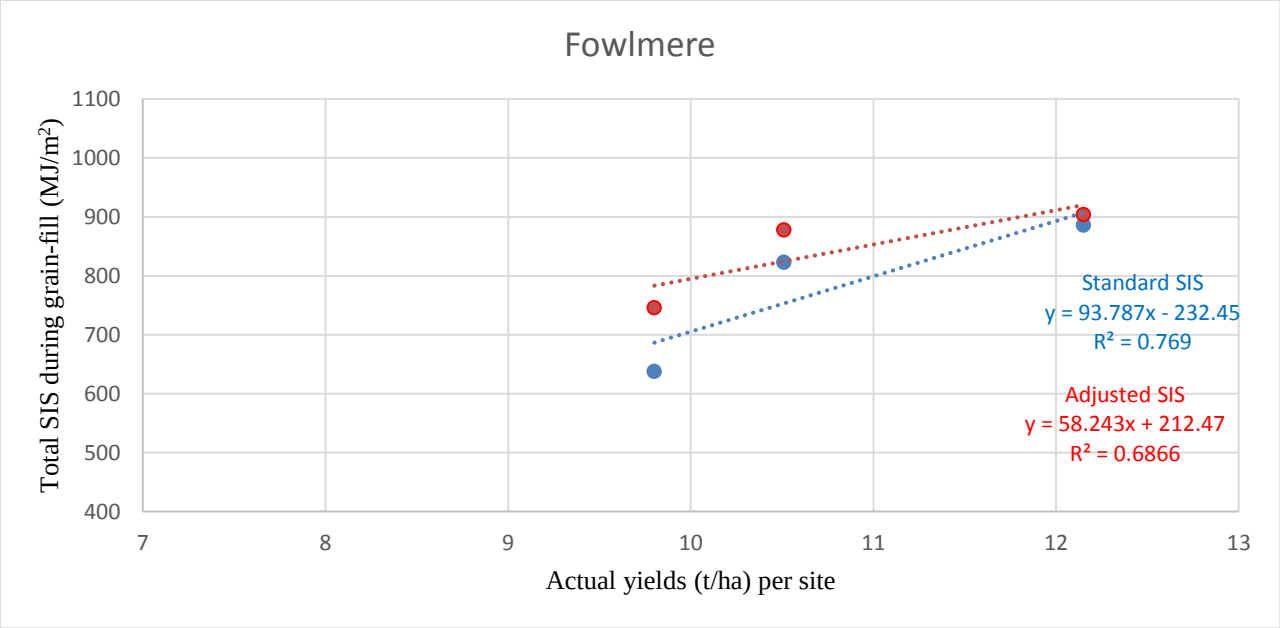

Figure 4.14 Correlation of wheat yields (t/ha) against total SIS (MJ/m^2) during the 'standard' (blue) and also during the 'temperature adjusted' (red) grain fill period in Fowlmere (52.9N 0.06E) where Previous Crop was Winter rape and Soil Type was Medium (n=3). R^2 = 77% and correlation coefficient = 0.87, R^2 = 69% and correlation coefficient = 0.83.

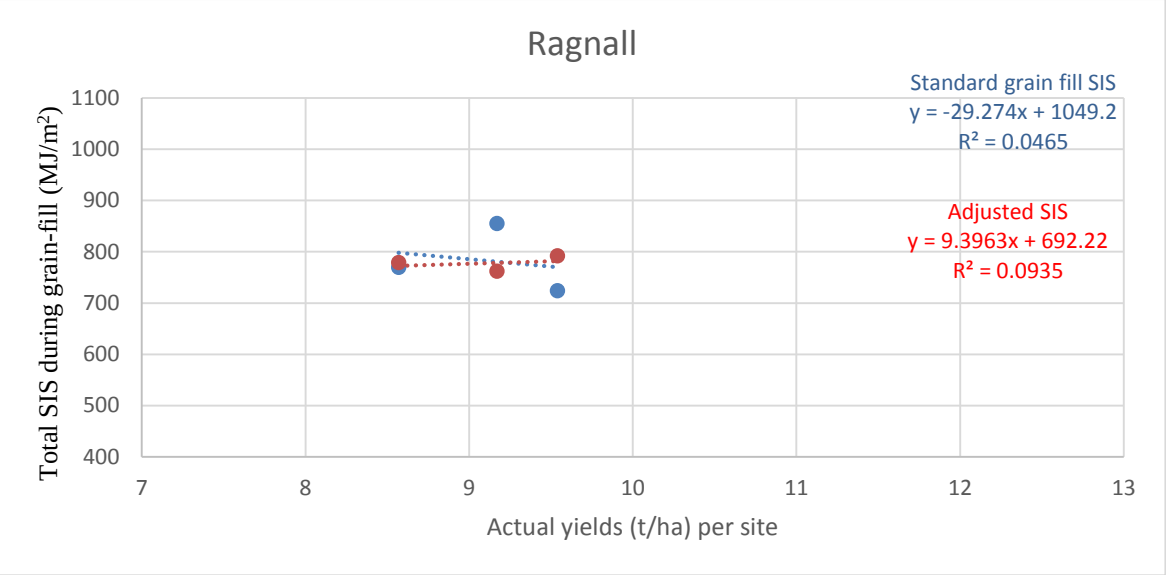

Figure 4.15 Correlation of wheat yields (t/ha) against total SIS (MJ/m^2) during the 'standard' (blue) and also during the 'temperature adjusted' (red) grain fill period in Ragnall (53.25N 0.79W) where Previous Crop was Winter rape and Soil Type was Medium (n=3). R^2 = 4.6% and correlation coefficient = -0.21, R^2 = 9.3% and correlation coefficient = 0.30.

The analysis in terms of scatter plots for single locations derives mixed results. In **Figure 4.14** for Fowlmere one can observe a strong statistical relationship between yields (t/ha) and the total SIS intercepted during the grain fill stage (MJ/m^2). It appears that the 'temperature adjusted' grain fill period SIS derives a weaker correlation (R^2 = 69% and correlation coefficient = 0.83) than the 'standard' grain fill period (R^2 = 77% and correlation coefficient = 0.87), although it should be noted that the analysis is only based on three points. However, in **Figure 4.15** for Ragnall although at first the results look disappointing, with a low correlation and a negative coefficient of correlation for the 'standard' grain fill period (R^2 = 4.6% and correlation coefficient = -0.21). On the other side, the 'temperature adjusted' SIS appears to bring a better correlation and a positive correlation coefficient (, R^2 = 9.3% and correlation coefficient = 0.30). This result hinting to the fact that yields are affected by something else rather than solely the grain fill SIS or the chosen grain fill period start and end dates are not the ideal for the proposed locations during these specific years. Potential reasons for low or even negative correlation in a single-site analysis could well be the fact that Ragnall and Fowlmere sites have a different grain fill start and/or end date. It should be noted that for the sites in Ragnall the SIS estimates are for the period of 'standard' grain fill for the years 2004, 2005 and 2006 while for Fowlmere is for 2009, 2010 and 2012. Both years 2006

and 2012 have seen noticeable variations as far as the total SIS accumulations during the' standard' grain fill period (**Figure 4.5).** Both 2006 and 2012 summer periods experienced unusual weather conditions with much below the seasonal average daily mean temperatures and extreme precipitation respectively and such extreme weather events can impact crop performance. Another factor which can also play an important role is if the crop is well-established or if the crop hasn't developed well, partly due to earlier weather conditions. Sufficient earlier growth of the crop canopy is also essential for the effective interception of solar radiation, as is sufficient moisture in the soil. The number of the RL trial sites and entries chosen for this analysis were quite limited and therefore this result cannot be considered very reliable. This creates a good incentive to repeat this process for a larger number of sites under different combinations of previous crop regimes and soil types with different grain fill start/end dates for each individual location described in the RL trial list.

The recommended approach following this result would be to run the WRF model simulations for the whole 1992-2012 period (the RL trial data availability) covering the whole of the UK domain. This would provide more opportunities to find the right combination of entries to test the above hypothesis in a way which could provide more meaningful and statistically reliable results.

5 Conclusions and Recommendations

5.1 SIS datasets performance

The results of the inter-comparison of satellite based SIS against the surface solar radiation output from the WRF model revealed that the satellite based SIS has a better performance when compared with station based observations. Therefore only satellite based SIS was subsequently used for the purposes of this study. A change in WRF model physics configuration could possibly improve the accuracy of the output, however this would require the regeneration of the model climatology (which was beyond the scope of this study). It is recommended that any future work performed using the WRF model climatology of SIS should first require testing of different boundary layer and cloud parameterizations schemes to potentially enable better results.

5.2 SIS climatology over the UK

The high spatial resolution of the satellite based data from CMSAF enabled the generation of a smooth, high-resolution climatology of SIS over both land and sea allowing a better interpretation of the influence of topographic features than could have been achieved by simple interpretation between the stations in the Met Office observing network. The climatology of the mean annual sum of SIS over the UK for the period 1983-2010 (**Figure 3.10**) revealed that the south-western parts of the UK, Anglesey in north-west Wales, and the Channel Islands not only yield high annual totals, but also experience the lowest inter-annual variability (**Figure 3.16 b**). However, these areas are not significant wheat growing areas (**Figure 4.1**), therefore this inbuilt advantage is not especially relevant to agriculture. Current main wheat growing areas that experience a good solar radiation climate on a yearly basis are the south and the south-east of England. Nevertheless, this result is particularly useful for the renewable energy sector as it demonstrates which locations across the UK can yield a higher and more reliable income potential as a result of a PV investment.

5.3 Synoptic weather typing and potential applications

The impact of synoptic scale weather typing on SIS accumulations was analysed using a combination of daily satellite based data from CMSAF and daily weather types from the

GrossWetterLagen classification (GWL). This research addressed two contrasting weather types, HM weather type (Anti-cyclonic) during the month of March 2012 proved to bring positive SIS anomalies across the whole of UK for all these March days classified as experiencing the HM GWL weather type. On the other side, the cyclonic WS weather type for the month of July proved to result below average SIS accumulations for all these days classified as experiencing the WS GWL weather type during the month of July 2012. By working with high quality, daily satellite-sensed SIS data, period-specific surface solar radiation accumulations can be generated for applications to specific research problems. One obvious application is the verification of Numerical Weather Prediction (NWP) forecasts of SIS. NWP models are more reliable in their simulations of atmospheric circulation than of cloud coverage. The next step is therefore to use synoptic weather typing as a forecasting tool in order to better estimate solar radiation accumulations over user-defined periods based on the inverse approach demonstrated in this study, for renewable energy and agricultural research applications. A recommendation arising from these results is to create the respective anomalies for all the months for all the weather types (29 for summer and 29 for winter season) where there are sufficient cases.

5.4 Trends on SIS accumulations - quantifying the impact on yield plateau

This thesis followed the yield-plateau recommendation of the Knight et al. (2012) study to use high resolution daily surface solar radiation estimates instead of coarse scale monthly sunshine hour data for weather-yield analyses. The assessment of annual SIS data over the 1994-2010 period showed a general positive trend of 7.25 W/m^2/decade across the whole of the UK domain with most parts experiencing increasing trends (**Figure 3.17**). This result contradicts the findings of Sanchez-Lorenzo and Wild (2012), which showed that much of England was experiencing a slight negative trend (**Figure 1.12**) although their analysis was limited to the 1994-2005 period. At the seasonal scale (**Figure 3.18**), analyses revealed a negative trend across most of England and Wales (including the main arable growing region) during the summer season (JJA).

A sensitivity test was applied to investigate the trends during a sub-period of the summer season which is regarded as the 'standard' grain-fill season in the UK (10th June – 21st July). Results show that the spatial distribution and characteristics of trends remain similar to those derived for the summer season as a whole (JJA) across most areas, however an obvious

increase ranging from about 2-5% was found (**Figure 4.7**) across the main arable growing regions of the UK (mainly south-east and Eastern England, south-east Scotland). This result does not therefore, by itself, account for the wheat yield-plateau observed across the UK since the mid-1990s. Therefore, the initial hypothesis (ii) that SIS trends will be stable or negative during the grain-fill period is not supported.

A recommendation that arises from this result is that the analysis should be repeated for the same period, but only taking into account specific wheat growing areas using spatially aggregated data on a regional scale as defined by DEFRA (e.g. Eastern England, Midlands etc). It is recommended that the analysis is performed again after the release of the 'updated' version of the CMSAF SIS which will be available in autumn 2014 and will cover homogeneously the whole 1983-2013 period.

5.5 Grain fill climatology - Simulating the grain fill period length.

WRF model output was used to generate the climatology of the length of the grain fill period with a starting date of 10th June and a threshold of 660 degree days for the end point for each individual year over the 2002-2012 period across eastern England. Results showed that the length of the 'temperature adjusted' grain fill period significantly varies both spatially and temporally. The length of the grain fill period ranges from 36 days in warm years/areas to 54 days in cooler years/areas varying significantly from the 42 day period suggested by Knight et al. (2012). It should also be noted that the 10th of June start date is just an approximation of the average starting date of the grain fill process across England and that this varies based on weather conditions before the flowering stage. A recommendation which arises from this result is to calculate the variable length of the grain fill period over the whole of the UK, based on actual grain fill start dates for individual areas.

5.6 SIS - Yields correlations analysis.

Based on the hypothesis (i) that grain yield has a positive relationship with the mean daily sum of SIS intercepted by the crop during the grain fill period, a correlation analysis was performed for both the 'standard' and the 'temperature adjusted' grain fill period SIS using RL trial data. The correlation analysis was performed for a single variety under three different combinations of soil types and 'previous crop' regimes and revealed a positive relationship when incorporating several RL trial locations (for example r=0.47 for Claire variety on

‘Medium’ soil and following Winter rape, n=55). These results provide some encouragement for using end of grain-fill cumulative SIS as a predictor variable for final yield.

Individual site analyses of the Claire variety grown in ‘medium’ soil type with previous crop being Winter rape for two different locations each with only three SIS-yields points only revealed contrasting results. For one of the locations (Fowlmere) the correlation appears good for the ‘standard’grain fill period SIS comparison (R^2 = 77% and correlation coefficient = 0.87) although slightly worse for the ‘temperature adjusted’ (R^2 = 69% and correlation coefficient = 0.83). However, for the other location (Ragnall) the correlation was very low and with a negative correlation coefficient (R^2 = 4.6% and correlation coefficient = -0.21) for the ‘standard’grain fill period and slightly better for the ‘temperature adjusted’ although it should be noted that the coefficient of correlation turns back to positive (R^2 = 9.3% and correlation coefficient = 0.30). This can lead to the conclusion that a single-site analysis is too simplified to reveal any meaningful results since there are also other factors influencing yields which can be averaged out when the analysis is performed over a larger number of samples. Another potential reason for not achieving a strong correlation is the fact that the starting date for both the ‘standard’ and the ‘temperature adjusted’ grain fill periods was set by default as the 10th of June, while in reality this date could vary from site to site and even more substantially from year to year.

It would also be useful to test the sensitivity of the analysis to different grain fill period start and end dates. It should also be noted that some of the final yield is as a result of accumulated growth prior to flowering, so solely measuring yield gain as a result of radiation during grain fill will underestimate final yield. Therefore the next approach should be to also consider the impact of SIS variability prior to the grain fill stage. Another recommendation is to focus on using only the portion of surface incoming solar radiation which is actually absorbed by the plants and which is known as FAPAR (Fraction of Absorbed Photosynthetically Active Radiation).

Another recommendation arising from this research is to perform a correlation analysis between SIS and yield for all the varieties included in the RL trial data, for as many locations as possible, under all the combinations of soil types and previous crop regimes. For this purpose it would be ideal to generate the site-specific climatology of the grain fill period length based on actual start dates with the end date being the last day when the 660 degree

days are accumulated. As a result, hypothesis iii cannot be fully tested to derive trustworthy conclusions due to limited data resources.

Solar radiation plays an important role in crop growth as it is a key ingredient in photosynthesis. However there are many other also important factors both from the weather point of view (extreme temperatures during crucial crop growth stages, water availability, strong winds which can damage canopy) as well as from the agronomic perspective (disease treatment, correct use of chemicals, compacted soil due to heavy machinery) which can affect yields. Therefore more extensive research is required in order to help faithfully account for the combined impact of multiple variables on wheat yields in the UK. It is hoped that the findings reported in this thesis help to account for one of the important factors.

6 References

Ahmed, M., Fayyaz-ul-Hassan, M. A. Aslam, M. N. Akram and M. Akmal (2011). Regression model for the study of sole and cumulative effect of temperature and solar radiation on wheat yield. African Journal of Biotechnology **10**(45): 9114-9121.

Araki, H., A. Hamada, M. A. Hossain and T. Takahashi (2012). Waterlogging at jointing and/or after anthesis in wheat induces early leaf senescence and impairs grain filling. Field Crops Research **137**(0): 27-36.

Archbold, H. (1945). Some factors concerned in the process of starch storage in the barley grain. Nature **156**: 70-73.

Beyer, H. G., C. Costanzo and D. Heinemann (1996). Modifications of the heliosat procedure for irradiance estimates from satellite images. Solar Energy **56**(3): 207-212.

Bidinger, F., R. B. Musgrave and R. A. Fischer (1977). Contribution of stored pre-anthesis assimilate to grain yield in wheat and barley. Nature **270**(5636): 431-433.

Briffa, K. R., P. D. Jones and P. M. Kelly (1990). Principal Component Analysis of the Lamb-Catalog-of-Daily-Weather-Types .2. Seasonal Frequencies and Update to 1987. International Journal of Climatology **10**(6): 549-563.

Brisson, N., P. Gate, D. Gouache, G. Charmet, F. X. Oury and F. Huard (2010). Why are wheat yields stagnating in Europe? A comprehensive data analysis for France. Field Crops Research **119**(1): 201-212.

Cano, D., J. M. Monget, M. Albuisson, H. Guillard, N. Regas and L. Wald (1986). A method for the determination of the global solar radiation from meteorological satellite data. Solar Energy **37**(1): 31-39.

Clark, B. (2013). Getting off the yield plateau –Lessons from 2012 and future prospects for wheat production. Norfolk Farming Conference, Norfolk.

Dacre, H. F. and S. L. Gray (2009). The Spatial Distribution and Evolution Characteristics of North Atlantic Cyclones. Monthly Weather Review **137**(1): 99-115.

DEFRA. (2014). Cereal production Survey. Retrieved 20 May, from https://www.gov.uk/government/uploads/system/uploads/attachment_data/file/267314/structure-june-ukcerealoilseed-19dec13.xls.

EUMETSAT. (2013). A decontamination of the SEVIRI instrument onboard Meteosat-10 is scheduled from 1 to 9 July., from http://www.eumetsat.int/website/home/News/DAT_2045911.html.

Farmers Weekly. (2012). Wheat yields lowest for 25 years from http://www.fwi.co.uk/articles/10/10/2012/135658/wheat-yields-lowest-for-25-years.htm. Retrieved 5 November, 2012.

Finger, R. (2010). Evidence of slowing yield growth - The example of Swiss cereal yields. Food Policy **35**(2): 175-182.

Gilgen, H., Wild, M., Ohmura, A., (1998). Means and trends of shortwave irradiance at the surface estimated from Global Energy Balance Archive (GEBA) data. Journal of Climate, 11, pp 2042-2061.

Gkousarov, T., S. Dorling and A. Lovett (2013). Combining synoptic-scale weather typing and satellite-based surface solar radiation monitoring for the assessment of extremes of solar radiation accumulation. 2nd International Conference on Energy Meteorology, Toulouse, France.

Gueymard, C. A. (2004). The sun's total and spectral irradiance for solar energy applications and solar radiation models. Solar Energy **76**(4): 423-453.

Gutteridge, R. J., G. L. Bateman and A. D. Todd (2003). Variation in the effects of take-all disease on grain yield and quality of winter cereals in field experiments. Pest Manag Sci **59**(2): 215-224.

Hakuba, M. Z., D. Folini, A. Sanchez-Lorenzo and M. Wild (2013). Spatial representativeness of ground-based solar radiation measurements. Journal of Geophysical Research D: Atmospheres **118**(15): 8585-8597.

Hammer, A., D. Heinemann, C. Hoyer, R. Kuhlemann, E. Lorenz, R. Muller and H. G. Beyer (2003). Solar energy assessment using remote sensing technologies. Remote Sensing of Environment **86**(3): 423-432.

Herbek, J. and L. Chad (2009). A Comprehensive Guide to Wheat Management in Kentucky. Section 2. Growth and Development. University of Kentucky Cooperative Extension..

Hess, P. and H. Brezowsky (1952). Katalog der Grosswetterlagen Europas, Bibliothek des Deutschen Wetterdienstes in der US-Zone 33.

James, P. M. (2007). An objective classification method for Hess and Brezowsky Grosswetterlagen over Europe. Theoretical and Applied Climatology **88**(1-2): 17-42.

Journée, M., R. Müller and C. Bertrand (2012). Solar resource assessment in the Benelux by merging Meteosat-derived climate data and ground measurements. Solar Energy **86**(12): 3561-3574.

Karlsson, K. G., A. Riihelä, R. Müller, J. F. Meirink, J. Sedlar, M. Stengel, M. Lockhoff, J. Trentmann, F. Kaspar, R. Hollmann and E. Wolters (2013). CLARA-A1: A cloud, albedo, and radiation dataset from 28 yr of global AVHRR data. Atmospheric Chemistry and Physics **13**(10): 5351-5367.

Kniffka, A. (2012). Operational Products on Clouds and Radiation http://training.eumetsat.int/pluginfile.php/7578/mod_resource/content/2/08_OperationalProducts_Kniffka.pdf.

Knight, S., S. Kightley, I. Bingham, S. Hoad, B. Lang, H. Philpott, R. Stobart, J. Thomas, A. Barne and B. Ball (2012). Desk study to evaluate contributory causes of the current yield plateau in wheat and oilseed rape. HGCA Project Report 502, HGCA.

Large, E. C. (1954). Growth stages in cereals illustration of the feeks scales Plant Pathology **3**(4): 128-129.

Lobell, D. B., W. Schlenker and J. Costa-Roberts (2011). Climate Trends and Global Crop Production Since 1980. Science **333**(6042): 616-620.

Met Office. (2012). Summer 2012 was the wettest in 100 years. Retrieved 8 January, 2014, from http://www.metoffice.gov.uk/news/releases/archive/2012/second-wettest-summer.

Met Office. (2013a). Solar Radiation maps of the UK. Retrieved 8 October, from http://www.metoffice.gov.uk/renewables/solar

MeteoSwiss. (2013a). Baseline Surface Radiation Network (BSRN) monitoring sites. from http://www.meteoschweiz.admin.ch/web/en/meteoswiss/international_affairs/gcos/uebersicht_klimabeobachtung/nationales_klimabeobachtungssystem/BSRN.html.

MeteoSwiss. (2013b). CMSAF Global Radiation Datasets. from http://www.meteoschweiz.admin.ch/web/en/research/current_projects/climate/cmsaf.html

MetOffice. (2013b). June 2012. Retrieved 8 December, 2013, from http://www.metoffice.gov.uk/climate/uk/2012/june.html.

Mueller, R. W., C. Matsoukas, A. Gratzki, H. D. Behr and R. Hollmann (2009). The CM SAF operational scheme for the satellite based retrieval of solar surface irradiance - A LUT based eigenvector hybrid approach. Remote Sensing of Environment **13**: 1012-1024.

NASA. (2003). Solar constant intensities Retrieved 8 November, from http://science.nasa.gov/media/medialibrary/2003/01/14/17jan_solcon_resources/beat_lg.gif

NOAA. (2007). Global Surface Station Network figure taken from. from http://www.goes-r.gov/education/comet/satmet/remote_sensing/media/graphics/global_surface_obs_mar2007.gif.

Ohmura, A. and H. Lang (1989). Secular variation of global radiation in Europe. Abstracts, International Radiation Symposium, Lille.

Orson, J. (2013). Personal Communication.

Pandey, C. K. and A. K. Katiyar (2013). Solar Radiation: Models and Measurement Techniques. Journal of Energy **2013**: 8.

Perez, R., R. Seals, A. Zelenka and P. Ineichen (1990). Climatic Evaluation of Models That Predict Hourly Direct Irradiance from Hourly Global Irradiance - Prospects for Performance Improvements. Solar Energy **44**(2): 99-108.

Philpott, H. (2013). Personal Communication.

Posselt, R., R. Mueller, R. Stöckli and J. Trentmann (2011). Spatial and Temporal Homogeneity of Solar Surface Irradiance across Satellite Generations. Remote Sensing **3**(5): 1029-1046.

Posselt, R., R. W. Mueller, R. Stockli and J. Trentmann (2012). Remote sensing of solar surface radiation for climate monitoring - the CM-SAF retrieval in international comparison. Remote Sensing of Environment **118**: 186-198.

PVGIS. (2013). Solar radiation and photovoltaic electricity potential

country and regional maps for Europe. from http://re.jrc.ec.europa.eu/pvgis/cmaps/eur.htm.

Reddy, K. S. (2008). Environmental and Cultural Factors

Limiting Potential Yields from. from http://www.spar.msstate.edu/class/EPP-2008/Chapter%201/Solar%20Radiation.pdf.

Russak, V. (1990). Trends of solar radiation, cloudiness and atmospheric transparency during recent decades in Estonia. Tellus B **42**(2).

Sanchez-Lorenzo, A. and M. Wild (2012). Validation of the means and trends in the CM-SAF high-resolution surface solar radiation product over Europe against a homogenized surface dataset (1983-2005). A. Sanchez-Lorenzo, ETH**:** 50.

Solargis. (2013). What is Global Horizontal Irradiance/Irradiation (GHI)? Retrieved 12 November, from http://solargis.info/doc/103

Spectrumcommodities.com. (2014). United Kingdom Wheat growing areas. from http://www.spectrumcommodities.com/education/commodity/maps/wheat/ukgw_wht.gif

Stanhill, G. (1995). Solar Irradiance, Air-Pollution and Temperature-Changes in the Arctic. Philosophical Transactions of the Royal Society a-Mathematical Physical and Engineering Sciences **352**(1699): 247-258.

Stanhill, G. and S. Cohen (1997). Recent changes in solar irradiance in Antarctica. Journal of Climate **10**(8): 2078-2086.

Stanhill, G. and S. Cohen (2001). Global dimming: a review of the evidence for a widespread and significant reduction in global radiation with discussion on its probable causes and possible agricultural consequences. Agric. For. Meteorol **107**: 255-278.

Stanhill, G. and J. D. Kalma (1995). Solar Dimming and Urban Heating at Hong-Kong. International Journal of Climatology **15**(8): 933-941.

Steele, C. J. (2013). Simulating sea breeze type climatologies: Implications for wind energy, weather forecasting and sailing in the southern North Sea. Norwich, UEA. **PhD:** 21-275.

Todd, M. (2013). Personal Communication.

Travis, D. M. (1992). Growth Stages of Wheat: Identification and Understanding Improve Crop Management. Better Crops **76**(3): 12-17.

Trentmann, J. (2013). Personal Communication.

Trentmann, J., C.-T. Chatterje, R. Mueller, R. Posselt and R. Stöckli (2010). Product User Manual Meteosat (MVIRI) Solar Surface Irradiance and effective Cloud Albedo Climate Data Sets. Remote Sensing. CMSAF. **3:** 1029-1046.

UKMO. (2012). UK Meteorological Office. Met Office Integrated Data Archive System (MIDAS) Land and Marine Surface Stations Data (1853-current), NCAS British Atmospheric Data Centre, 2012, Available from http://badc.nerc.ac.uk/view/badc.nerc.ac.uk__ATOM__dataent_ukmo-midas

Retrieved 14 November.

Weatherquest (2013). EUMETSAT Satellite imagery provided by Weatherquest. School of Environmental Sciences, University of East Anglia, Norwich.

Wikipedia. (2013). Solar Radiation Spectrum figure. Retrieved 12 November, from http://en.wikipedia.org/wiki/Sunlight

Wild, M. (2009). Global dimming and brightening: A review. Journal of Geophysical Research-Atmospheres **114**.

Wild, M., D. Folini, C. Schär, N. Loeb, E. Dutton and G. König-Langlo (2013). The global energy balance from a surface perspective. Climate Dynamics **40**(11-12): 3107-3134.

Wild, M., H. Gilgen, A. Roesch, A. Ohmura, C. N. Long, E. G. Dutton, B. Forgan, A. Kallis, V. Russak and A. Tsvetkov (2005). From dimming to brightening: decadal changes in solar radiation at Earth's surface. Science **308**(5723): 847-850.

Withnature.co.uk. (2014). Topographic map of the UK, image taken from. Retrieved 7 June, from http://www.withnature.co.uk/countryside/Uk_topo_en.jpg.

WMO. (2003). Guidelines on Climate Observation Networks and Systems. Retrieved 10 October, from http://www.wmo.int/pages/prog/wcp/wcdmp/documents/WCDMP-52_000.pdf.

Zempleni, M., Davison, A., (2010), PV Solar Power Generation Projects, Moody's investors service, Report 125811.